Enhancing the Performance of Dye-Sensitized Solar Cells by Nanoscale Interface and Structure Control

Chohui Kim

June 2015

WCU Hybrid Materials Program,

Department of Materials Science and Engineering,

Seoul National University

Abstract

Dye-sensitized solar cells (DSSCs) have become one of the most promising candidates for next generation of photovoltaic cells, due to low-cost process, flexibility, and ease of changing colors of cells. Despite their emergence with a relatively high efficiency of ~8%, the efficiency is still remained early ten percent over twenty years. To improve the performance of the DSSC, all components of the cell should be extensively investigated. The dye should be developed to have the smaller bandgap to increase the light absorption in visible region. The semiconductor should reduce the recombination loss at a metal oxide/electrolyte interface and be able to utilize a scattering effect efficiently. Lastly, the electrolyte should have lower redox potential to reduce a voltage loss and be non-volatile for long-term use.

In chapter 1, the current state and recent improvements of three major components (dye, metal oxide, and electrolyte) are demonstrated. Especially, achievements in developing metal oxides are discussed in detail to emphasize the importance of nanoscale interface and structure control, which are main objective of this research.

In chapter 2, the effect of TiO_2-coating on the ZnO-based DSSCs performance is systematically investigated with various TiO_2-coating thicknesses. The TiO_2 layer plays an important role in the suppression of the formation of Zn^{2+}/dye complexes and the recombination at ZnO/dye/electrolyte interfaces. As a result, both the open-circuit voltage (V_{oc}) and short-circuit current (J_{sc}) are improved, and the power-conversion efficiency is consequently enhanced by a factor of three.

In chapter 3, the scattering layer is optimized by varying mixture ratios of

nanoporous ZnO spheres (NS) and ZnO nanoparticles (NP). Nanoporous ZnO spheres in the scattering layer provide not only the effective light scattering but also a large surface area. Furthermore, added ZnO nanoparticles to the scattering layer facilitate the charge transport and increase the surface area by filling-up large voids of nanoporous ZnO sphere composite. The bilayer structure using the optimized scattering layer improves the solar cell efficiency by enhancing both the short-circuit current (J_{sc}) and fill factor (FF), compared to the non-mixed scattering layer.

In chapter 4, expected synergy effects of topic 1 (TiO_2 coating) and topic 2 (mixed scattering layer) are theoretically demonstrated. When the optimized nanostructure is coated with TiO_2, the open-circuit voltage (V_{oc}) higher than that of topic 2 (~0.56 V) is expected from the increased photo-generated current (J_{ph}) and reduced recombination rate (k_{rec}). The fill factor (FF) is expected to be enhanced more than that of topic 1 (~60%) due to the decreased series resistance (R_s) by improved electron transport. The short-circuit current (J_{sc}) is considered to be most enhanced, because all factors relevant to J_{sc} (light harvesting (η_{LHE}), electron injection (η_{inj}), and charge collection (η_{cc}) efficiency) are improved by adding nanoparticles and TiO_2-coating layer. Therefore, it is concluded that the collaboration of two topics (TiO_2 coating on optimized nanostructure) is essential for highly efficient DSSCs.

Keywords: Dye-Sensitized Solar Cell, ZnO Photoelectrode, Titanium Dioxide Coating, Nanoparticle, Nanoporous Sphere, Light Trapping, Mixed Electrode

Student Number: 2012-30727

Table of Contents

List of Figures

Chapter 1.

Chapter 2.

Chapter 3.

Chapter 4.

List of Tables

Chapter 2.

Chapter 3.

Chapter 1. Overview

1.1. General Introduction of Dye-Sensitized Solar Cells

Dye-sensitized solar cells (DSSCs), invented by Michael Grätzel and O'Regan in 1991 with power conversion efficiency of ~8%, have been regarded as potential candidates for the next-generation solar cells due to their low cost, high durability, large flexibility in shape, and transparency [1-3]. In spite of these advantages, the efficiency of DSSC is remained in early ten percent over ten years, with the maximum reported efficiency of approximately 12% [4]. To overcome the efficiency limitation, each component of DSSC should be improved.

1.2. Light Absorber in Dye-Sensitized Solar Cells

DSSC is composed of transparent conducting oxide, nanostructured metal oxide, absorber dye, iodide/iodine redox couple electrolyte, and catalyst deposited on counter electrode as illustrated in Fig. 1-1 [5]. Among other things, a dye is the most important component for high efficiency because it plays a role of light absorber and electron generator. When the dye absorbs the light which has higher energy than the difference between the lowest unoccupied molecular orbital (LUMO) and the highest occupied molecular orbital (HOMO) of the dye, it generates carriers and transports them to the metal oxide where it is attached on. A ruthenium-based dye (N719) shows the highest efficiency with bandgap of approximately 1.7 eV, which is much wider than that of a silicon (~1.1 eV). Therefore a ruthenium-based dye cannot absorb the light efficiently above 700 nm wavelength, as demonstrated in Fig. 1-2 [6]. Since DSSCs use limited light from sun, it is urgent to develop a dye which has smaller bandgap to absorb the long wavelength and generate more carriers. In addition, acidity of the dye from carboxyl proton limits the use of various metal oxides such as ZnO dissolved in acidic environment [7]. When the DSSC is exposed for long period of time under the sun, the performance of DSSC is degraded. The reason of decrease in cell efficiency is the exchange of a dye ligand with iodine in electrolyte [8]. The ligand-exchanged dye loses the ability of regeneration, and then the current and efficiency are reduced. Therefore, it is necessary to develop a nonacidic dye having a new ligand which does not react with iodine in electrolyte.

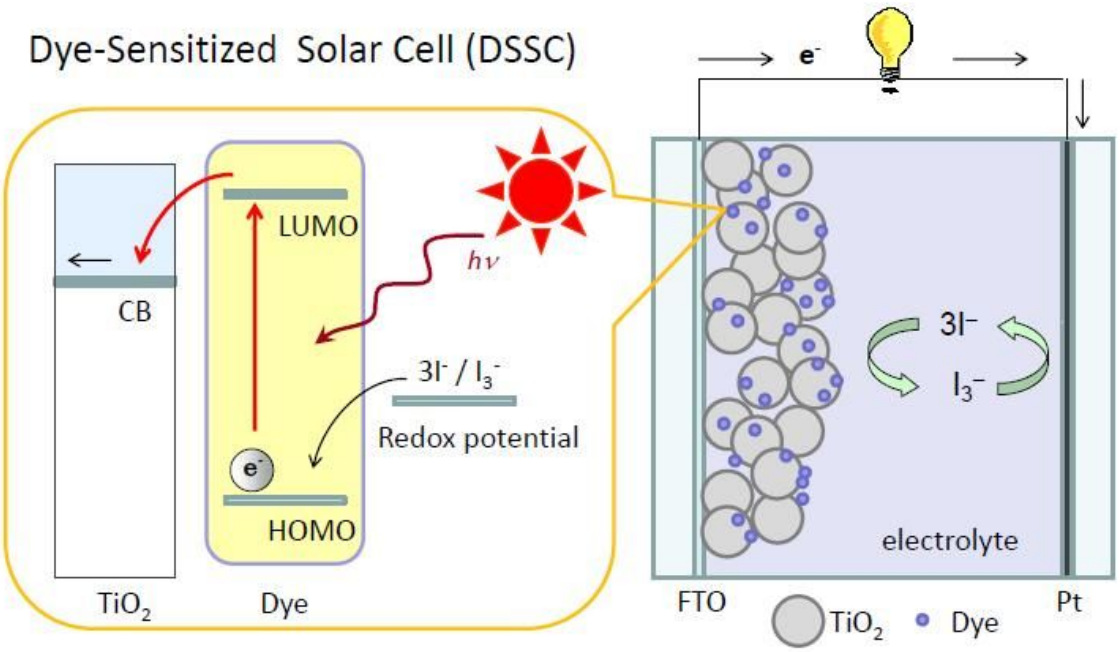

Fig. 1-1. (Color) Schematic illustration of dye sensitized solar cell. From Ref. [5].

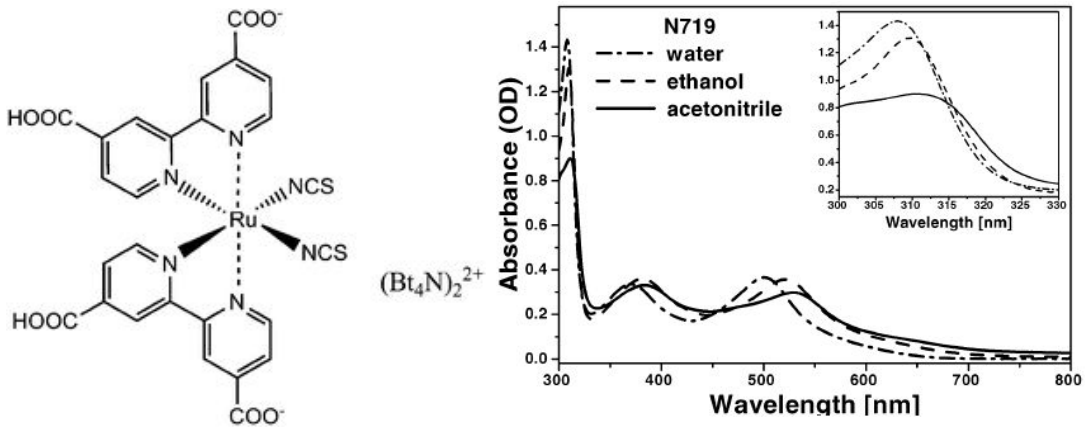

Fig. 1-2. Chemical structure and absorption spectra of N719 in different solvents. From Ref. [6].

1.3. Metal Oxides in Dye-Sensitized Solar Cells

The nanostructure metal oxide is another important component in DSSC. A metal oxide affords the place where dye is attached on and transports electrons to a working electrode from the dye. Therefore, a metal oxide should have suitable energy band position with the dye. For instance, their conduction band edge is located lower than the LUMO level of the dye to allow the electron injection from the dye to the semiconductor. And also the high electron mobility and large surface area are demanded.

1.3.1 Various Metal Oxides Candidates

Wide bandgap semiconductors such as titanium dioxide (TiO_2), zinc oxide (ZnO), and tin oxide (SnO_2) are commonly used metal oxides having properties mentioned above. A barium tin oxide ($BaSnO_3$) which has perovskite structure is also considered as a probable candidate for the high efficiency. As shown in Fig. 1-3, the various nanostructures having a large surface area are reported, such as branched ZnO nanowires, TiO_2 nanobamboos, and SnO_2 nanosheets [9-11].

Among various semiconducting materials, much attention has been given to TiO_2. Because of the wide bandgap of TiO_2 (3.2 eV), no visible light is absorbed directly in the metal oxide, so that the dye can absorb the light effectively. Furthermore, TiO_2 has high mobility of 1-4 cm^2/Vs in single crystal, chemical stability in acidic environment, and non-toxicity [12]. From these advantages, the DSSC using nanostructured TiO_2 has achieved highest efficiency of 12% [4].

ZnO is also considered as a potential candidate and actively researched for DSSCs. The energy bandgap of ZnO (~3.2 eV) and the position of conduction band are similar with that of TiO_2 (ZnO: -0.2 V versus NHE at pH = 1, TiO_2: -0.28 V versus NHE at pH = 2), as demonstrated in Fig. 1-4 [13]. ZnO has mobility of 2 orders of magnitude higher than that of the TiO_2 and is easy to synthesize in various nanostructures with simple and low-cost methods [14,15]. Nevertheless, ZnO has been showing limited performance on account of instability in acidic environment of a ruthenium-based dye and low electron-injection kinetics from dye [16].

In case of SnO_2, it has wider bandgap of 3.6 eV and lower position of conduction band than that

of ZnO or TiO_2 [17,18]. In spite of higher carrier mobility of 250 cm^2/Vs, SnO_2-based DSSCs exhibit the relatively lower open-circuit voltage and fill factor due to the high recombination kinetics with electrolyte and lower position of conduction band [19]. The possible strategies to overcome these problems are doping with gallium or zinc to elevate the conduction band position and surface modification (e.g. TiO_2, Al_2O_3, and MgO) to reduce the interface recombination, as illustrated in Fig. 1-5 [20,21].

To replace commonly used TiO_2, ternary metal oxides have been explored. Among various ternary metal oxides, the DSSC fabricated with a barium tin oxide ($BaSnO_3$) shows the highest efficiency for reported ternary oxide-based DSSCs [22]. $BaSnO_3$ which has perovskite structures is an intrinsic n-type semiconductor with indirect bandgap between 3.1 eV and 3.4 eV. The efficient electron injection from the dye to the conduction band of the $BaSnO_3$ nanoparticles is proved by the valence-band spectra and superior charge collection is observed in a thick film of ~40 μm [23]. The other ternary metal oxides, such as Zn_2SnO_4 or $Bi_4Ti_3O_{12}$ are also studied with the possibility of high efficiency [24,25].

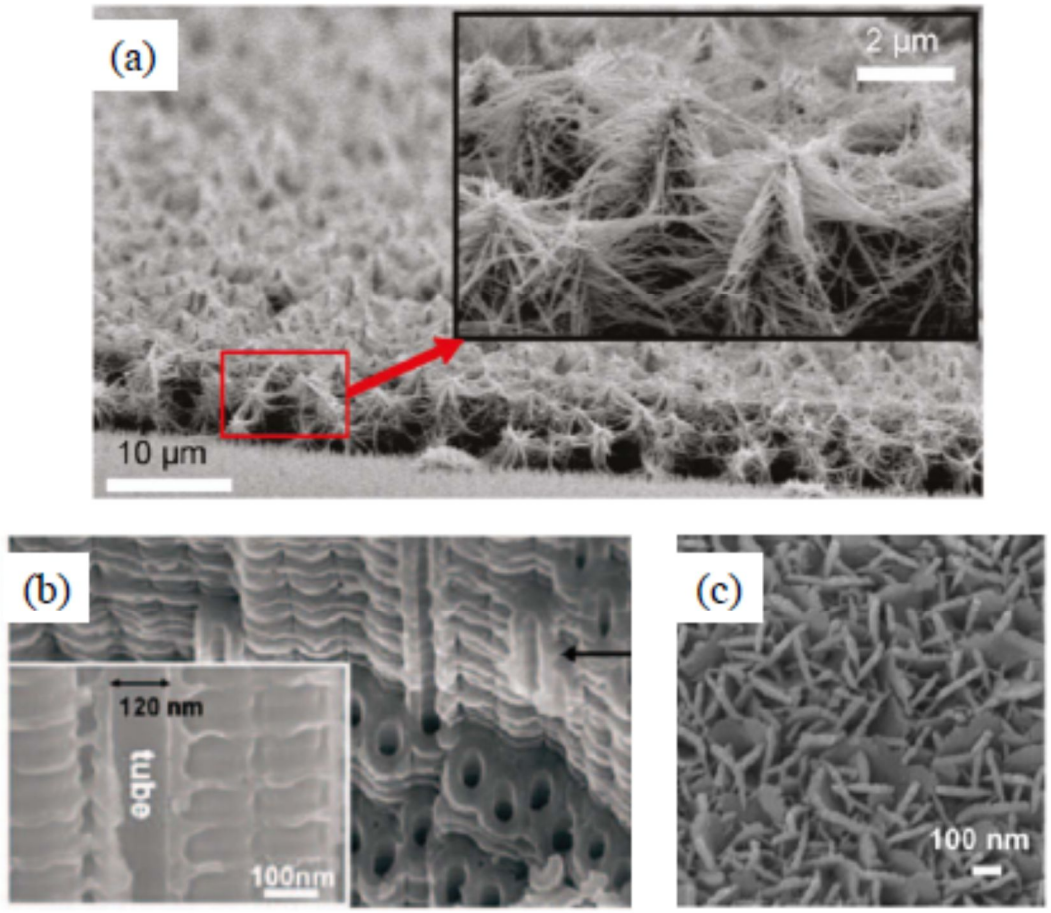

Fig. 1-3. Various nanostructures of metal oxides. (a) branched ZnO nanowires, (b) TiO_2 nanobamboos, and (c) SnO_2 nanosheets. From Ref. [9-11].

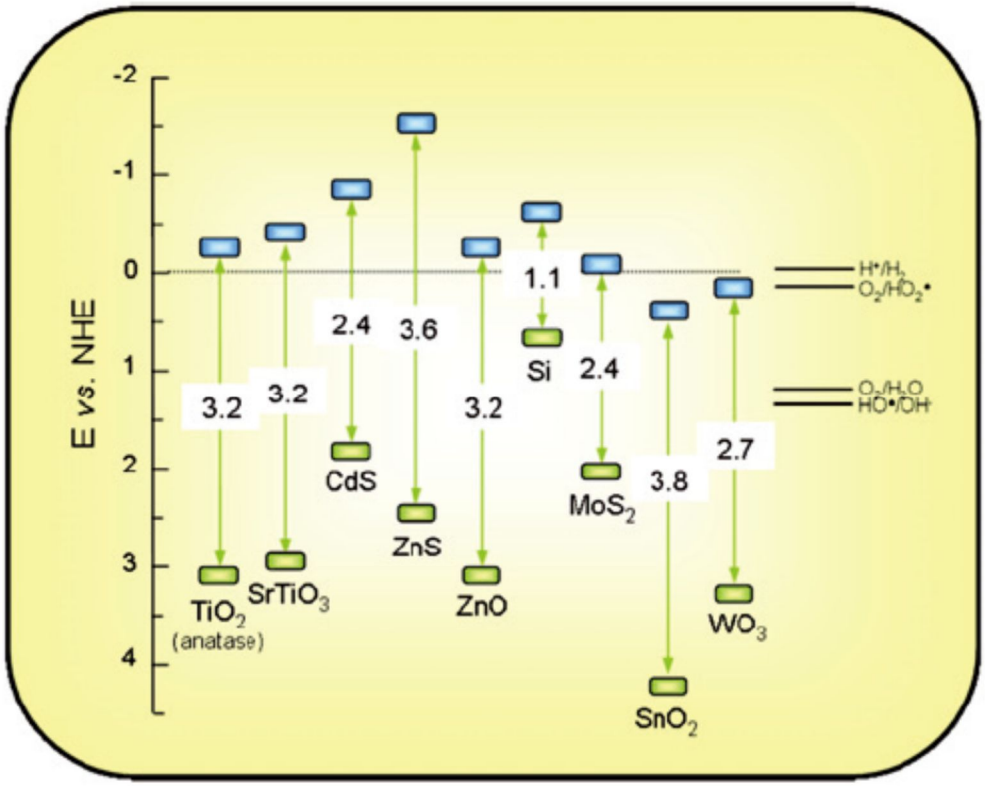

Fig. 1-4. (Color) Bandgap energies and redox potentials for several semiconductors using the normal hydrogen electrode (NHE) as a reference. From Ref. [13].

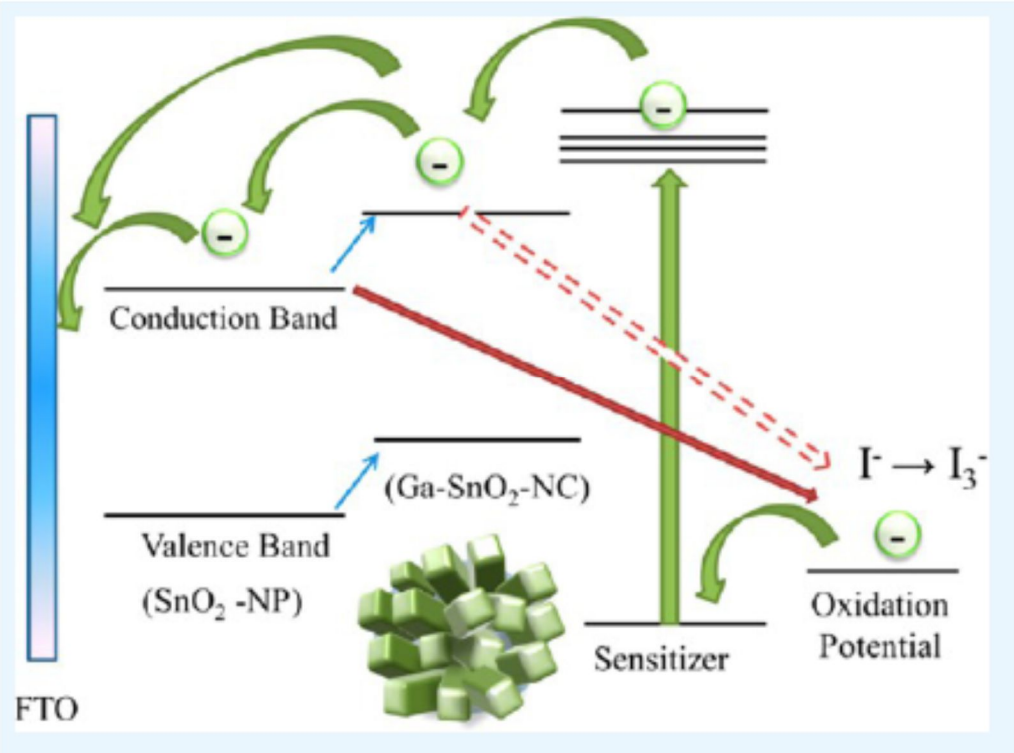

Fig. 1-5. (Color) Illustration of band structures and electron transfers of gallium-doped SnO_2 DSSCs. From Ref. [20].

1.3.2. Interface Recombination

Not all of electrons generated from dyes can arrive to the electrode because of the interface recombination. Therefore, reducing the interface recombination is one of main factors for improving efficiency. The recombination occurs from differences in kinetic properties at each interface, as shown in Fig. 1-6. The recombination takes place in the excited dye between generated electrons and holes directly (k_{-1}), injected electrons in the metal oxide with oxidized dyes (k_4), and between electrons in metal oxide or FTO and triiodide ions (I_3^-) in the electrolyte (k_5) [26]. The major recombination reaction occurs between a metal oxide/electrolyte interface, because metal oxide has lot of electrons by the fast electron injection from dye in a few femto seconds and electrolyte has empty states due to fast dye regeneration in micro seconds [27].

The most efficient way to reduce the interface recombination is energy barrier formation between metal oxide/electrolyte interfaces, and many studies about interface control using various metal oxides have been actively reported. $TiCl_4$ treatment is the most commonly used interface control method, especially in TiO_2-based DSSCs [28-30]. The reasons of $TiCl_4$ treatment on efficiency improvement have been reported that the recombination is reduced by deposition on defect sites presents on TiO_2 nanoparticles, TiO_2 condenses at the interparticle neck to help electron transport, or downward shift of conduction band increases the quantum efficiency of charge separation at the interface. Although downward shift of conduction band would decrease cell voltage, V_{oc} value is remained or increased from greater concentration of electrons by reduction in the recombination. Wide bandgap of metal oxides such as Al_2O_3, ZrO_2, and SiO_2 are used for energy barrier formation [31-34]. From their insulating property having bandgap of higher than ~5 eV, they can restraint the interface recombination effectively. When the coating is thicker than several monolayers, however, it blocks the electron injection from a dye and decreases the current. Furthermore, various semiconductors are utilized for surface treatment. Nb_2O_5 which is used for nanostructured film in DSSC is also utilized for interface control [35,36]. Nb_2O_5 has conduction band position that is lower than LUMO of a dye and higher than conduction band of TiO_2 or SnO_2 (approximately < ~0.1 eV for TiO_2 and < ~0.7 eV for SnO_2), therefore, efficient barrier formation can be expected as shown in Fig. 1-7 [37].

Surface coating with $CaCO_3$ on TiO_2 nanoparticles shows the reduced recombination, however, it decreases J_{sc} from its insulating property of wide bandgap (~5.6 eV) [38]. In case of Li_2CO_3 which is one of the electrolyte components, it forms the passivation layer on TiO_2 and the conducting substrate. The passivation layer suppresses the rate of the main recombination reaction between the photoinjected electrons and the oxidized ions in the electrolyte solution [39]. Surface coating using $SrTiO_3$ increases the cell voltage by negative shift of TiO_2 conduction band from dipole formation on TiO_2 surface, not the barrier formation [40].

The proper band position, chemical stability, and transport property should be considered for surface coating material. To establish an energy barrier at the metal oxide/electrolyte interface, proper band position of coating material, lower than LUMO level of dye molecule and higher than conduction band of nanostructured metal oxide, is needed. Otherwise, it can block both the recombination from metal oxide to electrolyte and transport from dye to metal oxide. That is why wide bandgap materials, for instance Al_2O_3, are hard to control their properties on the metal oxide and cause decrease in current [31-33]. It blocks the electron transport from dye to nanostructured metal oxide due to their much higher position of conduction band than LUMO level of dye, thus it should be thin enough to transport electrons through electron tunneling. Because surface coating material contacts directly with dyes, as a shell in nanostructured film, it should have fast kinetic property of electron injection from dye and improve the insufficient surface property of inner metal oxide, for instance weak chemical stability of ZnO. Although $TiCl_4$ treatment has been shown efficient effect on reduced recombination, their acidic environment can dissolve the ZnO electrode and change the morphology [41]. Surface coating material is required to have fast mobility because it is possible that injected electrons transport through surface coating layer, when coating layer cover all surfaces of nanostructured metal oxide or form their own network. In addition, when bandgap of coating material is much smaller ($< \sim 2$ eV), it can absorb the light before dyes absorb and generate another recombination site of hole in valance band. If coating material has better absorption ability than a dye molecule, it can be considered as a little different type of solar cell, such as quantum-dot-sensitized solar cell (QDSCs) [42-44].

Although various metal oxide materials are reported with the enhanced efficiency, regarding mechanisms are still uncertain in inconsistency of literatures. This is probably because of the difficulty of finding optimum thickness, coverage and crystallinity in different experimental condition. Thus, researchers on this topic should continue making an effort on both scientific and technical aspects.

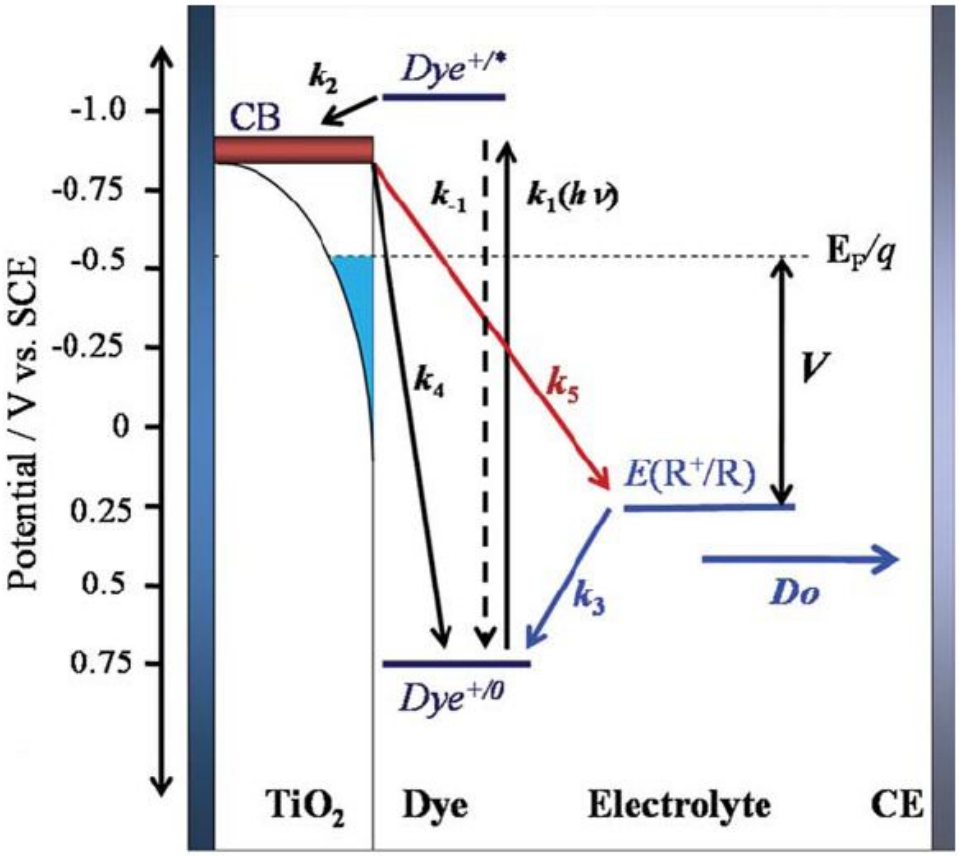

Fig. 1-6. (Color) Recombination reactions in dye sensitized solar cell. From Ref. [26].

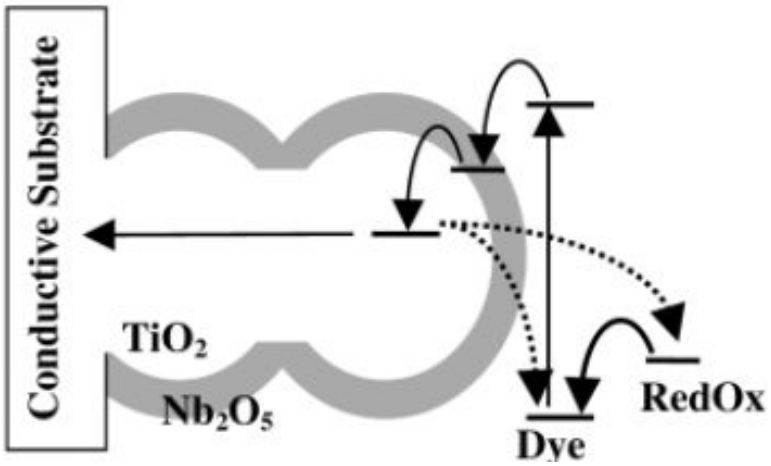

Fig. 1-7. Schematic diagram with energy levels of Nb_2O_5-coated TiO_2-based DSSCs. From Ref. [37].

1.3.3. Scattering Effects for Light Harvesting

To generate more carriers, more amount of dye is required, because dyes absorb the light and generate electrons in DSSCs. As dyes are adsorbed on metal oxide as a monolayer, the surface area of metal oxide should be increased through reducing in particle size or increasing film thickness to increase the amount of dyes. But there is a limitation on particle size reduction or increasing film thickness. When the particle size is too small, generally less than 10 nanometers, or film thickness becomes greater than electron diffusion length, the electron losses from interface recombination exceed the increased electrons from more dye adsorption [45]. Also from the nonlinear relation between light absorption and film thickness, the average electron density in metal oxide decreases as the film thickens, because back side of metal oxide film cannot absorb the light sufficiently compared to absorption of the front part, reducing the cell voltage consequently [46,47].

This is why the efficient use in incident light is greatly important for increase of carrier generation in limited thickness or metal oxide particle size. The efficient use of light can be performed with scattering effect that increases light-path length passed through the film. Theoretically, the scattering effect depends on both the size of the scattering centers and the wavelength of the incident light. The maximum of scattering effect occurs when the diameter of scatterers is about $k\lambda$ and k means a constant and λ is the wavelength and this indicates that several hundreds-nanometer-sized scatterers have efficient scattering effect for DSSCs that mainly use visible light [48]. The scattering layer for DSSC is proposed based on theoretical examination for the first time by Usami's group in 1997 [49]. It has been shown that the theoretical scattering effects of several hundreds-sized TiO_2 nanoparticles as the light scatterers on the film consisting of 40 nm-sized small particles. The scattering effects of large sized nanoparticles have been experimentally verified by many groups [50-54]. They showed the enhanced efficiency by scattering effect using from 100 to 500 nm-sized scatterers on nanostructured film composed of nanoparticles, nanotubes, and nanorods. But the introduction of large-sized particle leads to a significant decreased surface area to volume ratios due to their large size. To overcome the drawback, various hierarchical nanostructures which provide both the large surface area and efficient light scattering effect are considered. There

are various hierarchical nanostructures: aggregates composed numerous nanoparticles, nanoflowers consisted nanosheets or nanorods, and hollow spheres [55-64]. They show comparable surface area (80 ~ 100 m^2/g) to that of the nanoparticles film (~90 m^2/g) with efficient scattering effect. Apart from morphologies of scatterers, the film structures with scattering particles are investigated to enhance the scattering effect more effectively [65,66]. These studies try to optimize the scattering effect by tuning the film structure: embedding scattering particles in the nanocrystalline film or forming scattering layer with monolayer or multilayer, as shown in Fig 1-8. They propose that scattering layers acting as the back reflector and multilayer with gradually increased scatterer size from the most-inner layer provide the largest achievable light harvesting efficiencies.

As the demonstrated effects of scattering on efficiency, scattering becomes indispensable for high efficiency in DSSCs. I think size, morphology and position of scatterers should be considered for efficient scattering effect. As mentioned above, scatterers are of several hundreds of nanometers that scatter the visible wavelength, and they should be composed of smaller particles for not to sacrifice the total specific surface area of films. Thus, the use of hierarchical nanostructured scatterers is inevitable. I consider aggregates composed of nanoparticle are most efficient scatterers among various hierarchical nanostructured scatterers. Although all aggregate morphologies have sufficient scattering effect, aggregates composed of nanowires or nanosheets have smaller surface area than nanoparticles and counteract their fast transport property because they are synthesized in all directions not to straight on the electrode [56,59,60]. Hollow structure also has smaller surface area even though it shows more efficient scattering effect from multiple reflections inside hollow spheres, as shown in Fig. 1-9 [58,63]. Aggregates which consist of nanoparticles have the largest surface area and highest configuration density. In case of size of scattering particle size, scatterers sized of 300~500 nm are generally known to be efficient for visible light, and scattering layer composed with various sizes of scatterers are more efficient to scatter the various wavelength of light [51,67]. For the electrode structure with scatterers, I consider the bilayer or multilayer more desirable to optimize the scattering effect, because scatterers near the conducting glass can reflect the incident light before dyes absorb. Furthermore, large voids and unfavorable transport among large sized scatterers should

be improved. These problems can be solved by adding nanoparticles in scattering layer [68-70]. The added nanoparticles provide additional surface area and short electron transport path by filling large voids. For this concept, the balance between surface area and scattering effect should be considered through various ratios of nanoparticles and scattering particles.

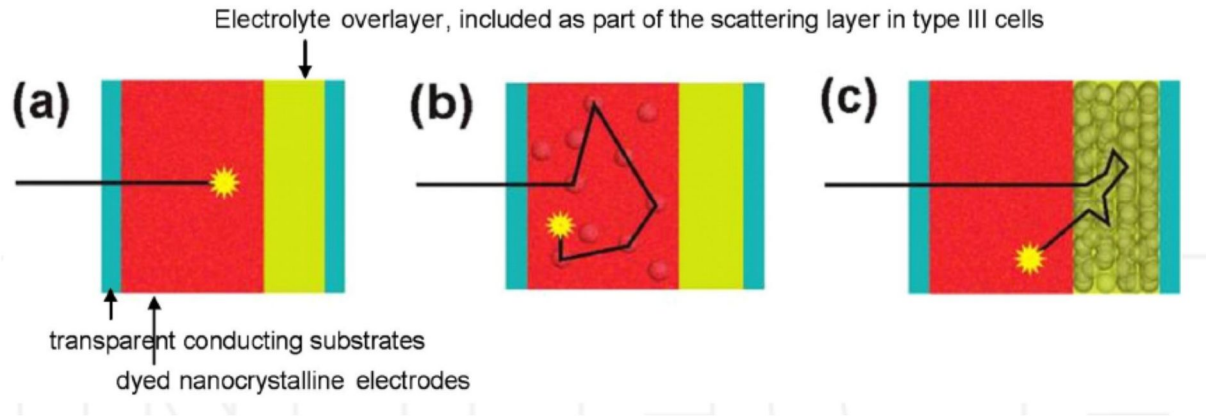

Fig. 1-8. (Color) Schematic figures of scattering effect in a) standard nanoparticles film, b) electrode embedding diffuse scattering particles, and c) film with a scattering layer. From Ref. [65].

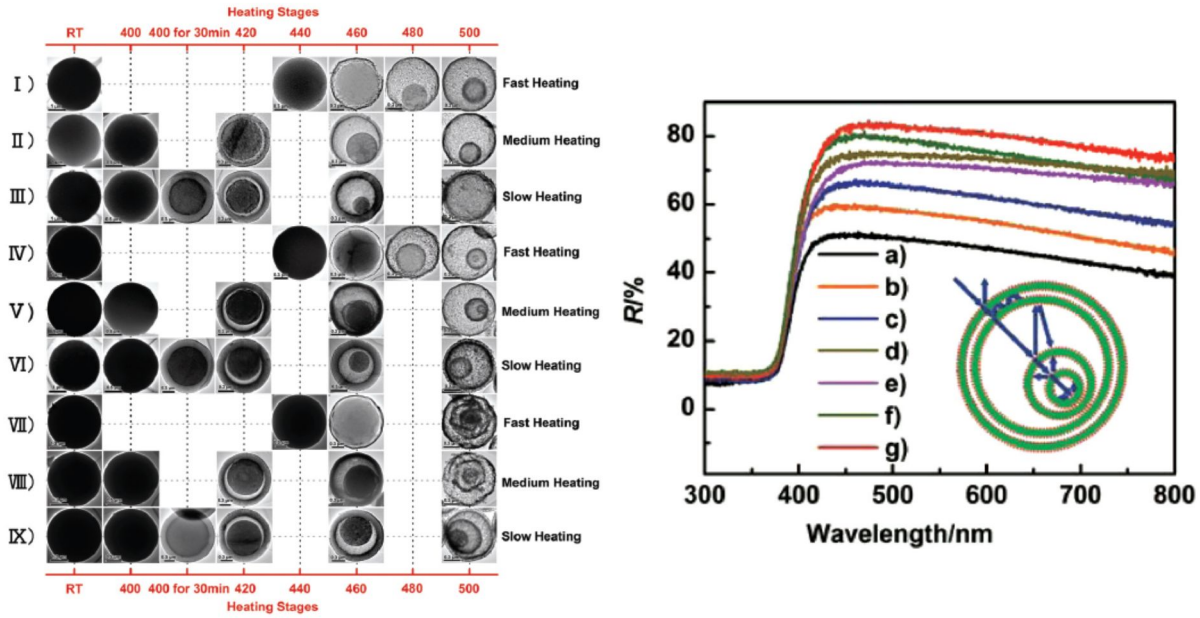

Fig. 1-9. Evolution process of the multi-shelled ZnO hollow microspheres (left) and diffuse reflectance spectra of ZnO hollow spheres with single to quadruple shells (right). From Ref. [63].

1.4. Electrolyte in Dye-Sensitized Solar Cells

The last major component of DSSC is electrolyte. Electrolyte transports the electrons from a counter electrode to the dye and regenerate the dye using the redox reaction. The most widely used redox mediator is iodide/tri-iodide (I^-/I_3^-) and the oxidation-reduction reaction is as below:

$$\mathbf{3I^- - 2e \leftrightarrow I_3^-} \quad (1)$$

three iodides release two electrons and form one tri-iodide. The redox potential of mediator has a significant effect on efficiency because the open-circuit voltage is determined with the difference between redox potential and metal oxide Fermi level. To regenerate the dye, the redox potential of mediator should be higher than dye HOMO level. The iodide/tri-iodide (I^-/I_3^-) redox potential is approximately 0.5 eV higher than N719 HOMO level, therefore there is the possibility of increased open-circuit voltage using newly developed mediator with lower redox potential, as shown in Fig. 1-10 [71]. For instance, DSSC having ~12% efficiency uses the cobalt-based electrolyte (Co^{2+}/Co^{3+}), which has lower redox potential of ~ 0.2 eV than that of the iodide, and shows the high open-circuit voltage of 0.94 eV [3].

Volatility of electrolyte is another problem generated in long-term use under sunlight exposure. To minimize this problem, solid-state hole-transport materials (HTM) are developed such as spiro-OMeTAD (2,2′,7,7′-tetrakis-(N,N-di-p-methoxyphenylamine)9,9′-spirobifluorene) or P3HT (Poly(3-hexylthiophene-2,5-diyl) [72]. But solid-state DSSCs show lower efficiency than the DSSCs used liquid type of electrolyte because it is difficult to permeate into the pores of nanostructured electrodes due to their high viscosity and has low hole mobility (10^{-4} cm^2/Vs) [73]. The p-type direct bandgap semiconductor, $CsSnI_3$, is developed for new HTM. This HTM material is solution-processable and has high mobility of 585 $cm^2/V\,s$, and shows conversion efficiencies of up to 10% [74]. As mentioned above, nonvolatility electrolyte having fast mobility and lower redox potential should be developed to enhance the efficiency.

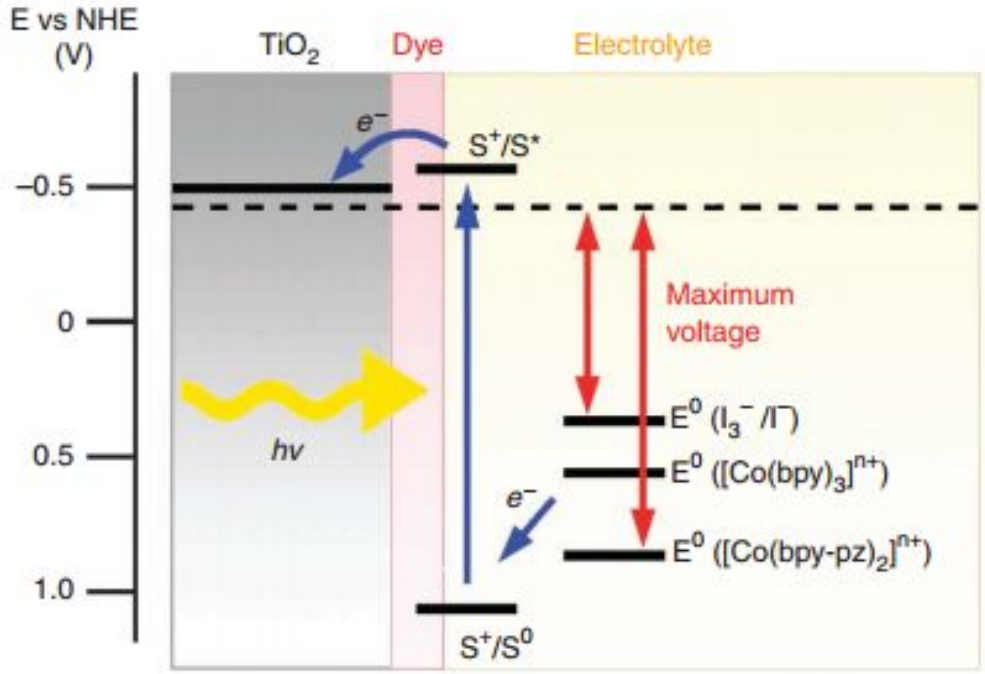

Fig. 1-10. (Color) (a) Schematic energy diagram for dye-sensitized solar cell using iodide/tri-iodide (I^-/I_3^-) and cobalt (Co^{2+}/Co^{3+}) based electrolyte. From Ref. [52].

1.5. Objective of Research

The main components of DSSCs are a dye which absorbs the light and generates electron, metal oxide which provides surface where dye can attach and transports generated electrons, and electrolyte that regenerates the dye by the redox reaction itself. Large bandgap of dye (~1.7 eV) and low molar absorption coefficient (~10^4 /cm M) results in insufficient light absorption and then low efficiency [6]. To overcome this, synthesis of new organo-metal ruthenium-based dye are attempted with various ligands for sufficient absorption of the long wavelength light and inorganic-organic hybrid perovskite absorbers, such as methyl ammonium lead iodide ($CH_3NH_3PbI_3$), are used as a new absorber in established DSSC system and have shown the high efficiency of ~17% [75]. In case of electrolyte, redox potential is directly related to open-circuit voltage of the cell, so the lower redox potential is needed to increase the voltage and volatility issue should be answered for long-term use of the cell in sunlight exposure. To overcome these problems, electrolytes with new redox mediator, having lower redox potential such as cobalt-based electrolyte (Co^{2+}/Co^{3+}), are developed and sol-gel type of non-volatile electrolytes, for instance spiro-OMeTAD, are used instead of liquid type of electrolyte [3,43]. High viscosity of sol-gel type of electrolyte remains a challenge because of the difficulty of penetration into the nanostructured metal oxide. And electron losses at metal oxide surfaces by interface recombination occur from different kinetic properties of each component. Limited metal oxide film thickness by relatively short electron diffusion length of approximately ~8 μm is also a problem and should be solved in metal oxide part [76].

This study focuses on the main problems of the metal oxide component. As mentioned above, electron losses from interface recombination between metal oxide/electrolyte are considerable because oxides form nanostructures which allow more dye to attach with, thus surface of nanostructure involves large portion in whole architecture. Therefore, interface of metal oxide should be controlled to reduce interface recombination. And also, there is a limitation of increase in film thickness because recombination occurs more when metal oxide film gets thicker than electron diffusion length, and average electron density decreases due to the nonlinear relationship of absorption and film thickness [46,47]. To generate more carriers, nanostructure of metal oxide film

should be optimized to absorb the light sufficiently in the limited film thickness. The most important things to be improved are reduction of interface recombination and efficient use of the light in metal oxide. Therefore, this study focuses on two experiments, first interface control to reduce the recombination and second optimization of nanostructure for efficient light absorption, respectively.

The interface control of metal oxide is significant and necessary to reduce the recombination at the metal oxide/electrolyte interfaces [31,35,36]. The surface coating using metal oxide which is one of the interface control methods can be performed by easy, low-cost techniques, and takes advantages of both inner and outer materials. ZnO is chosen for inner metal oxide due to the fast mobility of electron and suitable conduction band position to obtain increased voltage among commonly used metal oxides, ZnO, TiO_2, and SnO_2, etc., however, it has unfavorable surface property that dissolves in acidic N719 dye solution and forms Zn^{2+}/dye complex [77]. Thus, the materials for surface treatment of ZnO must have strong stability against acidic environment and fast electron injection property from dye, because coating material contact directly with the dye instead of inner metal oxide, ZnO. Among the various metal-oxide candidates, I select TiO_2 as a surface coating material. TiO_2 has strong stability against acidic environment and faster kinetic property of electron injection from dye to TiO_2 than dye to ZnO [78]. When comparing the conduction band position of each in the bulk, ZnO has a similar electron affinity with that of the TiO_2 so barrier formation might be difficult from TiO_2 to ZnO. But the conduction band position with increased bandgap is expected when the expected coating thickness of TiO_2 layer is lower than Bohr radius of ~2 nm [13,35,79]. When the size of the semiconductor particle decreases from the bulk to that of Bohr radius, bandgap increases due to the spatial confinement of charge carriers [80,81]. C. P. Hang's group reports that the bandgap change of TiO_2 is approximately 0.12 eV when the particle size decreased from 17 nm to 3.8 nm and M. R. Hoffmann's group reports blue shift of the absorption edge by 0.156 eV when the particle size is less than 12 nm [82,83]. In this study, much more increase of TiO_2 bandgap is expected, because bandgap increase of more than 0.1 eV is observed even in larger particle size than Bohr radius. Thus, TiO_2 is considered as the appropriate material as a barrier to reduce recombination and also transport electron to ZnO. ZnO coated with TiO_2 can have both advantages,

first high mobility from ZnO and second from TiO_2, strong stability in acidic and fast electron injection from dye, at the same time. The effect of surface treatment on efficiency as mentioned above will be discussed in chapter 2.

The efficient use of sun light is extremely important due to insufficient absorption of the dye and limited film thickness. The dye has molar absorption coefficient of only ~10^4 /cm M and even much lower in the long wavelength region, as shown in Fig. 1-2. To increase the amount of the dye, film thickness of metal oxide can be increased. Otherwise, this gives rise to decrease in voltage because of the electron losses from increased interface recombination and the insufficient light absorption toward the film end. The light-path length passed through the film should be increased with the nanostructure having the efficient scattering effect. Several hundred-nanometer-sized particles are known as most effective scatterers for visible wavelength but they have very small surface area from their large particle size [50-54]. Hierarchical nanostructures having efficient scattering effect with the large surface area should be used for scatterers, such as nanoaggregates or nanoflowers structure, etc. [56,59,60]. But the hierarchical nanostructures dissipate the spaces forming the voids among them and transport the carriers with point contact from their large particle sizes. And also, the film structure with scatterers should be contemplated because the loss of the light can occur from scatterers near the glass where the light is incident. The optimized nanostructure that has large surface area in bottom layer and sufficient scattering effect in upper layer should be designed. Thus, I would like to suggest the bilayer structure that bottom layer consists of nanoparticles which provide large surface area but no scattering effect and upper layer consists of mixture of nanoparticles and nanoporous spheres that help facile carrier transport and efficient scattering (in chapter 3).

1.6. References

1. B. O'Regan and M. Grätzel, "A Low-Cost, High-Efficiency Solar Cell Based on Dye-Sensitized Colloidal TiO_2 Films," *Nature* **353**, 737 (1991).
2. J. M. Kroon, N. J. Bakker, H. J. P. Smit, P. Liska, K. R. Thampi, P. Wang, S. M. Zakeeruddin, M. Grätzel, A. Hinsch, S. Hore, U. Würfel, R. Sastrawan, J. R. Durrant, E. Palomares, H. Pettersson, T. Gruszecki, J. Walter, K. Skupien, and G. E. Tulloch, "Nanocrystalline Dye-Sensitized Solar Cells Having Maximum Performance," *Prog. Photovoltaics* **15(1)**, 1 (2007).
3. A. Yella, H. W. Lee, H. N. Tsao, C. Yi, A. K. Chandiran, M. K. Nazeeruddin, E. W. G. Diau, C. Y. Yeh, S. M. Zakeeruddin, and M. Grätzel, "Porphyrin-Sensitized Solar Cells with Cobalt (II/III)–Based Redox Electrolyte Exceed 12 Percent Efficiency," *Science* **334**, 629 (2011).
4. National Center for Photovoltaics, Nat. Renewable Energy Lab., Golden, CO, USA. "Chart of Best Research-Cell Efficiencies" (2014). [Online]. Available: http://www.nrel.gov/ncpv.
5. Y. Ooyama, and Y. Harima, "Molecular Designs and Syntheses of Organic Dyes for Dye-Sensitized Solar Cells Nanostructured Photoelectrodes for Dye-Sensitized Solar Cells," *Eur. J. Org. Chem.* 2903 (2009).
6. C. P. Leon, L. Kador, B. Peng, and M. Thelakkat, "Characterization of the Adsorption of Ru-bpy Dyes on Mesoporous TiO_2 Films with UV-Vis, Raman, and FTIR Spectroscopies," *J. Phys. Chem. B* **110**, 8723 (2006).
7. T. P. Chou, Q. Zhang, and G. Cao "Effects of Dye Loading Conditions on the Energy Conversion Efficiency of ZnO and TiO_2 Dye-Sensitized Solar Cells," *J. Phys. Chem. C* **111**, 18804 (2007).
8. H. Greijer, J. Lindgren, and A. Hagfeldt. "Resonance Raman Scattering of a Dye-Sensitized Solar Cell: Mechanism of Thiocyanato Ligand Exchange," *J. Phys. Chem. B* **105**, 6314 (2001).
9. S. H. Ko, D. Lee, H. W. Kang, K. H. Nam, J. Y. Yeo, S. J. Hong, C. P. Grigoropoulos, H. J. Sung, "Nanoforest of Hydrothermally Grown Hierarchical ZnO Nanowires for a High Efficiency Dye-Sensitized Solar Cell," *Nano Lett.* **11(2)**, 666 (2011).

10. D. Kim, A. Ghicov, S. P. Albu, and P. Schmuki, "Bamboo-Type TiO_2 Nanotubes: Improved Conversion Efficiency in Dye-Sensitized Solar Cells," *J. Am. Chem. Soc.* **130**, 16454 (2008).
11. L. Zhang, H. B. Wu, and X. W. Lou, "Growth of SnO_2 Nanosheet Arrays on Various Conductive Substrates as Integrated Electrodes for Lithium-Ion Batteries," *Mater. Horiz.* **1**, 113 (2014).
12. H. Tang, K. Prasad, R. Sanjinès, P. E. Schmid, and F. Lévy, "Electrical and Optical Properties of TiO_2 Anatase Thin Films," *J. Appl. Phys.* **75**, 2042 (1994).
13. M. D. Hernandez-Alonso, F. Fresno, S. Suareza and J. M. Coronado, "Development of Alternative Photocatalysts to TiO_2: Challenges and Opportunities," *Energy Environ. Sci.* **2**, 1231 (2009).
14. E. M. Kaidashev, M. Lorenz, H. Wenckstern, A. Rahm, H. C. Semmelhack, K. H. Han, G. Benndorf, C. Bundesmann, H. Hochmuth, and M. Grundmann, "High Electron Mobility of Epitaxial ZnO Thin Films on c-Plane Sapphire Grown by Multistep Pulsed-Laser Deposition," *Appl. Phys. Lett.* **82**, 3901 (2003).
15. E. Hendry, F. Wang, J. Shan, T. F. Heinz, and M. Bonn, "Electron Transport in TiO_2 Probed by THz Time-Domain Spectroscopy," *Phys. Rev. B* **69**, 081101 (2004).
16. T. P. Chou, Q. Zhang, and G. Cao "Effects of Dye Loading Conditions on the Energy Conversion Efficiency of ZnO and TiO_2 Dye-Sensitized Solar Cells," *J. Phys. Chem. C* **111**, 18804 (2007).
17. M. Grätzel, "Photoelectrochemical Cells," *Nature* **414**, 338 (2001).
18. R, Bhattacharjeez, and I.-M. Hung, "A SnO_2 and ZnO Nanocomposite Photoanodes in Dye-Sensitized Solar Cells," *ECS Solid State Lett.* **2**, Q101 (2013).
19. Z. Jarzebski and J. Marton, "Facile Synthesis of Au–SnO_2 Hybrid Nanospheres," *J. Electrochem. Soc.* **123**, 299 (1976).
20. J. J. Teh, S. L. Ting, K. C. Leong, J. Li, and P. Chen, "Gallium-Doped Tin Oxide Nano-Cuboids for Improved Dye Sensitized Solar Cell," *ACS Appl. Mater. Interfaces* **5**, 11377 (2013).
21. J. Liu, T. Luo, T. S. Mouli, F. Meng, B. Sun, M. Li and J. Liu, "A Novel Coral-Like Porous SnO_2 Hollow Architecture: Biomimetic Swallowing Growth Mechanism and Enhanced

Photovoltaic Property for Dye-Sensitized Solar Cell Application," *Chem.Commun.* **45**, 472 (2010).

22. D. W. Kim, S. S. Shin, S. Lee, I. S. Cho, D. H. Kim, C. W. Lee, H. S. Jung, and K. S. Hong, "$BaSnO_3$ Perovskite Nanoparticles for High Efficiency Dye-Sensitized Solar Cells," *ChemSusChem* **6**, 449 (2013).
23. Y. Zhang, H. Zhang, Y. Wang, and W. F. Zhang, "Efficient Visible Spectrum Sensitization of $BaSnO_3$ Nanoparticles with N719," *J. Phys. Chem. C* **112**, 23 (2008).
24. B. Tan, E. Toman, Y. Li, and Y. Wu, "Zinc Stannate (Zn_2SnO_4) Dye-Sensitized Solar Cells," *J. Am. Chem. Soc.* 1**29**, 4162 (2007).
25. Z. Chen, S. Li, and W. Zhang, "Dye-Sensitized Solar Cells Based on $Bi_4Ti_3O_{12}$," *International Journal of Photoenergy* (2011).
26. T. W. Hamann and J. W. Ondersma, "Dye-Sensitized Solar Cell Redox Shuttles," *Energy Environ. Sci.* **4**, 370 (2011).
27. A. Hagfeldt, G. Boschloo, L. Sun, L. Kloo, and H. Pettersson, "Dye-Sensitized Solar Cells," *Chem. Rev.* **110**, 6595 (2010).
28. N. Fuke, R. Katoh, A. Islam, M. Kasuya, A. Furube, A. Fukui, Y. Chiba, R. Komiya, R. Yamanaka, L. Han, and H. Harima, "Influence of $TiCl_4$ Treatment on Back Contact Dye-Sensitized Solar Cells Sensitized with Black Dye," *Energy Environ. Sci.* **2**, 1205 (2009).
29. C. J. Barbe, F. Arendse, P. Comte, M. Jirousek, F. Lenzmann, V. Shklover, and M. Gratzel, "Nanocrystalline Titanium Oxide Electrodes for Photovoltaic Applications," *J. Am. Ceram. Soc.* **80**, 3157-3171 (1997).
30. Brian C. O'Regan, J. R. Durrant, P. M. Sommeling, and N. J. Bakker, "Influence of the $TiCl_4$ Treatment on Nanocrystalline TiO2 Films in Dye-Sensitized Solar Cells. 2. Charge Density, Band Edge Shifts, and Quantification of Recombination Losses at Short Circuit," *J. Phys. Chem. C* **111**, 14001-14010 (2007).

31. M. Law, L. E. Greene, A. Radenovic, T. Kuykendall, J. Liphardt, and P. Yang, "ZnO-Al_2O_3 and ZnO-TiO_2 Core-Shell Nanowire Dye-Sensitized Solar Cells," *J. Phys. Chem. B* **110**, 22652 (2006).

32. G. R. R. A. Kumara, K. Tennakone, V. P. S. Perera, A. Konno, S. Kaneko, and M. J. Okuya, "Supperssion of Recombinations in a Dye-Sensitized Photoelectrochemical Cell Made from a Film of Tin IV Oxide Crystallites Coated with a Thin Layer of Aluminium Oxide," *Phys. D: Appl. Phys.* **34**, 868 (2001).

33. E. Palomares, J. N. Clifford, S. A. Haque, T. Lutz, and J. R. Durrant, "Control of Charge Recombination Dynamics in Dye Sensitized Solar Cells by the Use of Conformally Deposited Metal Oxide Blocking Layers," *J. Am. Chem. Soc.* **125**, 475 (2003).

34. H. Alarcon, G. Boschloo, P. Mendoza, J. L. Solis, and A. Hagfeldt, "Dye-Sensitized Solar Cells Based on Nanocrystalline TiO_2 Films Surface Treated with Al^{3+} Ions: Photovoltage and Electron Transport Studies," *J. Phys. Chem. B* **109**, 18483 (2005).

35. R. A. Rani, A. S. Zoolfakar, J. Subbiah, J. Z. Ou, and K. Kalantar-zadeh, "Highly Ordered Anodized Nb_2O_5 Nanochannels for Dye-Sensitized Solar Cells," *Electrochem. Commu.* **40**, 20 (2014).

36. S. G. Chen, S. Chappel, Y. Diamant, and A. Zaban, "Preparation of Nb_2O_5 Coated TiO_2 Naanoporous Electrode and Their Application in Dye-Sensitiezed Solar Cells," *Chem. Mater.* **13**, 4629 (2001).

37. A. Zaban, S. G. Chen, S. Chappel, and B. A. Gregg, "Bilayer Nanoporous Electrodes for Dye Sensitized Solar Cells," Chem. Commun. 2231 (2000).

38. Z.-S. Wang, M. Yanagida, K. Sayama, and Hideki, "Electronic-Insulating Coating of $CaCO_3$ on TiO_2 Electrode in Dye-Sensitized Solar Cells: Improvement of Electron Lifetime and Efficiency," *Chem. Mater.* **18**, 2912 (2006).

39. J. Zhang and A. Zaban, "Efficiency Enhancement in Dye-Sensitized Solar Cells by In Situ Passivation of the Sensitized Nanoporous Electrode with Li_2CO_3," *Electrochim. Acta* **53**, 5670 (2008).

40. Y. Diamant, S. Cheppel, S. G. Chen, O. Melamed, and A. Zaban, "Core-Shell Nanoporous Electrode for Dye Sensitized Solar Cells: the Effect of the $SrTiO_3$ Shell on the Electronic Properties of the TiO_2 Core," *Coord. Chem. Rev.* **248**, 1271 (2004).

41. P. Atienzar, T. Ishwara, B. N. Illy, M. P. Ryan, B. C. O'Regan, J. R. Durrant and J. Nelson, "Control of Photocurrent Generation in Polymer/ZnO Nanorod Solar Cells by Using a Solution-Processed TiO_2 Overlayer," *J. Phys. Chem. Lett.* **1**, 708 (2008).

42. H Lee, M. Wang, P. Chen, D. R. Gamelin, S. M. Zakeeruddin, M. Grätzel, and M. K. Nazeeruddin, "Efficient CdSe Quantum Dot-Sensitized Solar Cells Prepared by an Improved Successive Ionic Layer Adsorption and Reaction Process," *Nano Lett.* **9**, 4221 (2009).

43. P. K. Santra and P. V. Kamat, "Mn-Doped Quantum Dot Sensitized Solar Cells: A Strategy to Boost Efficiency over 5%," *J. Am. Chem. Soc.* **134**, 2508 (2012).

44. Y. L. Lee and Y. S. Lo, "Highly Efficient Quantum-Dot-Sensitized Solar Cell Based on Co-Sensitization of CdS/CdSe," *Adv. Func. Mater.* **19**, 604 (2009).

45. K Zhu, N. Kopidakis, N. R. Neale, J. van de Lagemaat, and A. J. Frank, "Influence of Surface Area on Charge Transport and Recombination in Dye-Sensitized TiO_2 Solar Cells," *J. Phys. Chem. B*, **110**, 25174 (2006).

46. A. Mathewa, G. M. Raoa, and N. Munichandraiah, "Effect of TiO_2 Electrode Thickness on Photovoltaic Properties of Dye Sensitized Solar Cell Based on Randomly Oriented Titania Nanotubes," *Mater. Chem. Phys.* **127**, 95 (2011).

47. M. G. Kang, K. S. Ryu, S. H. Chang, N. G. Park, J. S. Hong, and K.-J. Kim "Dependence of TiO_2 Film Thickness on Photocurrent-Voltage Characteristics of Dye-Sensitized Solar Cells," *Bull. Korean Chem. Soc.* 25, 742 (2004).

48. W. C. Mundy, J. A. Roux, and A. M. Smith, "Mie Scattering by Spheres in an Absorbing Medium," *J. Opt. Soc. Am.* **64**, 1593 (1974).

49. A. Usami, "Theoretical Study of Application of Multiple Scattering of Light to a Dye-Sensitized Nanocrystalline Photoelectrichemical Cell," *Chem. Phys. Lett.* **277**, 105 (1997).

50. C. J. Barbe, F. Arendse, P. Comte, M. Jirousek, F. Lenzmann, V. Shklover, and M. Gratzel, "Nanocrystalline Titanium Oxide Electrodes for Photovoltaic Applica-tions," J. *Am. Ceram. Soc.* **80**, 3157 (1997).

51. H. J. Koo, J. Park, B. Yoo, K. Yoo, K. Kim, and N. G. Park, "Size-Dependent Scattering Efficiency in Dye-Sensitized Solar Cell," *Inorg. Chim. Acta* **361**, 677 (2008).

52. J.-K. Lee, B.-H. Jeong, S.-I. Jang, Y.-G. Kim, Y.-W. Jang, S.-B. Lee, and M.-R. Kim, "Preparations of TiO_2 Pastes and Its Application to Light-Scattering Layer for Dye-Sensitized Solar Cells," *J. Ind. Eng. Chem.***15**, 724 (2009).

53. Z. He, W. Que, P. Sun, and J. Ren, "Double-Layer Electrode Based on TiO_2 Nanotubes Arrays for Enhancing Photovoltaic Properties in Dye-Sensitized Solar Cells," *ACS Appl. Mater. Interfaces* **5**, 12779 (2013).

54. K. Shin, Y. Jun, J. H. Moon, and J. H. Park, "Observation of Positive Effects of Freestanding Scattering Film in Dye-Sensitized Solar Cells," *ACS Appl. Mater. Interfaces* **2**, 288 (2010).

55. K. Park, Q. Zhang, B. B. Garcia, X. Zhou, Y.-H. Jeong, and G. Cao, "Effect of an Ultrathin TiO_2 Layer Coated on Submicrometer-Sized ZnO Nanocrystallite Aggregates by Atomic Layer Deposition on the Performance of Dye-Sensitized Solar Cells," *Adv. Mater.* **22**, 1 (2010).

56. C. Y. Jiang, X. W. Sun, G. Q. Lo, D. L. Kwong, and J. X. Wang, "Improved Dye-Sensitized Solar Cells with a ZnO-Nanoflower Photoanode," *Appl. Phys. Lett.* **90**, 263501 (2007).

57. W. Yang, J. Li, Y. Wang, F. Zhu, W. Shi, F. Wan, and D. Xu, "A Facile Synthesis of Anatase TiO_2 Nanosheets-Based Hierarchical Spheres with Over 90% {001} Facets for Dye-Sensitized Solar Cells," *Chem. Commun.* **47**, 1809 (2011).

58. H.-J. Koo, Y. J. Kim, Y. H. Lee, W. I. Lee, K. Kim, and N.-G. Park, "Nano-Embossed Hollow Spherical TiO_2 as Bifunctional Material for High-Efficiency Dye-Sensitized Solar Cells," *Adv. Mater.* **20**, 195 (2008).

59. Y. J. Kim, M. H. Lee, H. J. Kim, G. Lim, Y. S. Choi, N.-G. Park, K. Kim, and W. I. Lee, "Formation of Highly Efficient Dye-Sensitized Solar Cells by Hierarchical Pore Generation with Nanoporous TiO_2 Spheres," *Adv. Mater.* **21**, 3668 (2009).

60. D. Chen, F. Huang, Y.-B. Cheng, and R. A. Caruso, "Mesoporous Anatase TiO_2 Beads with High Surface Areas and Controllable Pore Sizes: A Superior Candidate for High-Performance Dye-Sensitized Solar Cells," *Adv. Mater.* **21**, 2206 (2009).

61. W.-G. Yang, F.-R. Wan, Q.-W. Chen, J.-J. Li, and D.-S. Xu, "Controlling Synthesis of Well-Crystallized Mesoporous TiO_2 Microspheres with Ultrahigh Surface Area for High-Performance Dye-Sensitized Solar Cells," *J. Mater. Chem.* **20**, 2870 (2010).

62. J.-Y. Liao, H.-P. Lin, H.-Y. Chen, D.-B. Kuang, and C.-Y. Sua, "High-Performance Dye-Sensitized Solar Cells Based on Hierarchical Yolk–Shell Anatase TiO_2 Beads," *J. Mater. Chem.* **22**, 1627 (2012).

63. Z. Dong, X. Lai, J. E. Halpert, N. Yang, L. Yi, J. Zhai, D. Wang, Z. Tang, and L. Jiang, "Accurate Control of Multishelled ZnO Hollow Microspheres for Dye-Sensitized Solar Cells with High Efficiency," *Adv. Mater.* **24**, 1046 (2012).

64. J. Qian, P. Liu, Y. Xiao, Y. Jiang, Y. Cao, X. Ai, and H. Yang, "TiO_2-Coated Multilayered SnO_2 Hollow Microspheres for Dye-Sensitized Solar Cells," *Adv. Mater.* **21**, 3663 (2009).

65. F. E. Gálvez, E. Kemppainen, H. Míguez, and J. Halme, "Effect of Diffuse Light Scattering Designs on the Efficiency of Dye Solar Cells: An Integral Optical and Electrical Description," *J. Phys. Chem. C* **116**, 11426 (2012).

66. Z.-S. Wang, H. Kawauchi, T. Kashimab, H. Arakawa, "Dye Sensitized Solar Cells Review: Significant Influence of TiO_2 Photoelectrode Morphology on the Energy Conversion Efficiency of N719 Dye-Sensitized Solar Cell," *Coord. Chem. Rev.* **248**, 1381 (2004).

67. Q. Zhang, T. P. Chou, B. Russo, S. A. Jenekhe, and G. Cao, "Polydisperse Aggregates of ZnO Nanocrystallites: A Method for Energy-Conversion-Efficiency Enhancement in Dye-Sensitized Solar Cells," *Adv. Funct. Mater.* **18**, 1564 (2008).

68. X. Sun, Y. Liu, Q. Tai, B. Chen, T. Peng, N. Huang, S. Xu, T. Peng, and X.-Z. Zhao, "High Efficiency Dye-Sensitized Solar Cells based on a Bi-Layered Photoanode Made of TiO_2 Nanocrystallites and Microspheres with High Thermal Stability," *J. Phys. Chem. C* **116**, 11859 (2012).

69. F. Huang, D. Chen, X. L. Zhang, R. A. Caruso, and Y.-B. Cheng, "Dual-Function Scattering Layer of Submicrometer-Sized Mesoporous TiO_2 Beads for High-Efficiency Dye-Sensitized Solar Cells," *Adv. Funct. Mater.* **20**, 1301 (2010).

70. K. Fan, W. Zhang, T. Peng, J. Chen, and F. Yang, "Application of TiO_2 Fusiform Nanorods for Dye-Sensitized Solar Cells with Significantly Improved Efficiency," *J. Phys. Chem. C* **115**, 17213 (2011).

71. J-H. Yum, E. Baranoff, F. Kessler, T. Moeh, Sh. Ahmad, T. Bessho, A. Marchioro, E. Ghadiri, J.-E. Moser, C. Yi, Md. K. Nazeeruddin, and M. Grätzel, "A Cobalt Complex Redox Shuttle for Dye-Sensitized Solar Cells with High Open-Circuit Potentials," *Nature Commun.* **3**, 631 (2012).

72. L. Yang, U. B. Cappel, E. L. Unger, M. Karlsson, K. M. Karlsson, E. Gabrielsson, L. Sun, G. Boschloo, A. Hagfeldta, and E. M. J. Johansson, "Comparing Spiro-OMeTAD and P3HT Hole Conductors in Efficient Solid State Dye-Sensitized Solar Cells," *Phys. Chem. Chem. Phys* **14**, 779 (2012).

73. H. J. Snaith and L. Schmidt-Mende, "Advances in Liquid-Electrolyte and Solid-State Dye-Sensitized Solar Cells," *Adv. Mater.* **19**, 3187 (2007).

74. I. Chung, B. Lee, J. He, R. P. H. Chang, and M. G. Kanatzidis, "All-Solid-State Dye-Sensitized Solar Cells with High Efficiency," *Nature* **485**, 486 (2012).

75. N. R. E. L. (NREL), NREL, http://www.nrel.gov/ncpv/images/efficiency_chart.jpg.

76. F. Xu, J. Chen, X. Wu, Y. Zhang, Y. Wang, J. Sun, H. Bi, W. Lei, Y. Ni, and L. Sun, "Graphene Scaffolds Enhanced Photogenerated Electron Transport in ZnO Photoanodes for High-Efficiency Dye-Sensitized Solar Cells," *J. Phys. Chem. C* **117**, 8619 (2013).

77. H. Horiuchi, R. Katoh, K. Hara, M. Yanagida, S. Murata, H. Arakawa, and M. Tachiya, "Electron Injection Efficiency from Excited N3 into Nanocrystalline ZnO Films: Effect of ($N3\text{-}Zn^{2+}$) Aggregate Formation," *J. Phys. Chem. B* **107**, 2570 (2003).

78. N. A. Anderson, X. Ai, and T. Lian, "Electron Injection Dynamics from Ru Polypyridyl Complexes to ZnO Nanocrystalline Thin Films," *J. Phys. Chem. B* **107**, 14414 (2003).

79. X. H. Yang, Z. Li, G. Liu, J. Xing, C. Sun, H. G. Yang, and C. Li "Ultra-Thin Anatase TiO_2 Nanosheets Dominated with {001} Facets: Thickness Controlled Synthesis, Growth Mechanism and Water-Splitting Properties," *CrystEngComm* **13**, 1378 (2011).

80. L. Bras, "Electron–electron and electron-hole interactions in small semiconductor crystallites: The size dependence of the lowest excited electronic state," *J. Chem. Phys.* **80**, 4403 (1984).

81. L. Bras, "Electronic Wave Functions in Semiconductor Clusters: Experiment and Theory," *J. Phys. Chem.* **90**, 2555 (1986).

82. H. Lina, C. P. Huanga, W. Lib, C. Nib, S. I. Shahb, and Y.-H. Tsengd, "Size Dependency of Nanocrystalline TiO_2 on Its Optical Property and Photocatalytic Reactivity Exemplified by 2-Chlorophenol," *Appl. Catal. B* **68**, 1 (2006).

83. C. Kormann, D. W. Bahnemann, and M. R. Hoffmann, "Preparation and Characterization of Quantum-Size Titanium Dioxide," *J. Phys. Chem.* **92**, 5197 (1988).

Chapter 2.

* The Effect of TiO_2-Coating Layer on the Performance in Nanoporous ZnO-Based Dye-Sensitized Solar Cells

2.1. Introduction

Dye-sensitized solar cells (DSSCs) have been regarded as one of potential candidates for next-generation solar cells due to their low cost, high durability, large flexibility in shape, and transparency [1-3]. While TiO_2 is the most commonly used as a oxide semiconductor, ZnO has also been considered as a promising candidate for DSSCs. The main reasons of ZnO uses are carrier mobility of single-crystal ZnO (115 - 155 cm2 V^{-1} s^{-1}), which is two orders of magnitude higher than that of TiO_2 (1 - 4 cm2 V^{-1} s^{-1}), its direct bandgap (~3.2 eV), and the position of the conduction band similar to that of TiO_2 [4-8]. Furthermore, various ZnO nanostructures can be obtained by easy and low-cost techniques [9-18]. Despite these advantages, the performances of ZnO-based DSSCs are typically lower (7.5% as a world record) [19] than those of TiO_2-based DSSCs (12.3% as a world record) [3]. The limited performance may be explained by the formation of Zn^{2+}/dye complexes and recombination at the ZnO/dye/electrolyte interface [20,21]. The Zn^{2+}/dye complexes are attributed to the poor chemical stability of ZnO in acidic dye solution, and are responsible for the inefficient electron injection from dye to semiconductor [22].

To overcome the problem of Zn^{2+}/dye complexes formation, several metal-oxide materials such as Al_2O_3, MgO, Nb_2O_5, SiO_2, and TiO_2 have been reported as a coating layer on ZnO-based DSSCs [23-28]. Among those materials, TiO_2 has been drawing most attention owing to its high stability in an acidic environment and the best performance so far in an optimized system such as iodine/iodide electrolytes or organometallic dye.

---

*The work presented in Chapter. 2 was published in *J. Power Sources* **232**, 159 (2013) entitled,

"The Effect of TiO_2-Coating Layer on the Performance in Nanoporous ZnO-Based Dye-Sensitized Solar Cells"

Chohui Kim, Jongmin Kim, Hongsik Choi, Changwoo Nahm, Suji Kang, Sungjun Lee, Byungho Lee, and Byungwoo Park*

Cao's group reported that ZnO-TiO_2 core-shell structure deposited by atomic layer deposition (ALD), demonstrated enhancements in both the open-circuit voltage and fill factor [29]. However, ALD is not considered as a cost-effective method, and the correlations between photovoltaic properties and coating layer thickness have not been investigated. It was reported that the $TiCl_4$ treatment improved the conversion efficiency of DSSCs composed of ZnO nanorods or nanoparticles [30,31]. However, it is hard to achieve the desired coating thickness by dipping samples into the aqueous solution of $TiCl_4$ with ZnO dissolved. Therefore, I adopted thin layer of TiO_2 coated on the ZnO electrode by a wet-chemical method which is inexpensive, convenient, and not acidic, and photovoltaic properties are systematically identified with various TiO_2-coating times.

2.2. Experimental Section

For the fabrication of nanoporous ZnO spheres, zinc acetate dihydrate ($Zn(CH_3COO)_2 \cdot 2H_2O$: Sigma-Aldrich) was added to diethylene glycol ($(HOCH_2CH_2)_2O$: Sigma-Aldrich), stirred with a magnetic bar at 300 rpm at room temperature (RT) for 10 min and heated in an autoclave at 160°C for 6 h [32]. Then, the as-synthesized solution was cooled down to RT, centrifuged at 3000 rpm for 15 min to separate the nanoporous ZnO spheres from solution, redispersed in anhydrous ethanol two times to remove the supernatant, and dried in air oven at 60°C. 1 g of as-prepared ZnO powder, 0.45 g of cellulose ($(C_6H_{10}O_5)_n$: Aldrich), and 5 ml of terpineol ($C_{10}H_{18}O$: Aldrich) were mixed and stirred on hot plate at 150 rpm and 40°C for one day. Terpineol is an organic solvent with high boiling point of 219°C and cellulose acts as a binder, preventing cracks during heat treatment and increasing adhesion among the ZnO nanospheres [33]. The resulting paste was spread on a cleaned fluorine-doped tin oxide substrate (FTO, TEC 8: Pilkington) by a doctor-blade method. FTO glass was cleaned by acetone, ethanol, and deionized water and subsequently dried with nitrogen. The doctor-blade was performed with two layers of punched Scotch tape having 80 μm thickness and straight edge such as a razor blade. The as-deposited films were dried on hot plate at 60°C for 10 min and subsequently annealed at 350°C for 1 h.

The TiO_2-coating layer on ZnO was prepared by a facile wet-chemical method. The as-

prepared ZnO films were immersed in 10 mM titanium butoxide ($Ti[O(CH_2)_3CH_3]_4$: Aldrich) in 2-propanol ($(CH_3)_2CHOH$: Sigma-Aldrich) at RT. The thickness of the coating layer was controlled by changing the deposition time (30, 60, and 120 min). After deposition of TiO_2 layers, films were rinsed with 2-propanol, dried with nitrogen gas, and post-annealed at 450°C for 30 min. Additionally the bare film was also sintered as a control set. After annealing, the films were sensitized with 0.5 mM of N719 dye ($RuL_2(NCS)_2$:2TBA, L = 2,2′-bipyridyl-4,4′-dicarboxylic acid, TBA = tetrabutylammonium: Solaronix) for 6 h at RT, followed by rinsing with ethanol and drying under a nitrogen stream. To prepare the counter electrode, Pt thin film was deposited by rf-magnetron sputtering on the diagonally pre-drilled FTO substrate with two holes. The deposition was carried out at RT under Ar atmosphere with an operating pressure of 30 mTorr, and rf power of 100 W for 20 min. The sensitized electrode and platinized counter electrode were sealed with thermoplastic foil (25 μm: Dupont, U.S.A.) on hot plate at 100°C, and the gap between the two electrodes was filled with an iodide-based redox electrolyte (AN-50: Solaronix, Switzerland) using micropipette.

The crystal structure of the electrode was analyzed by x-ray diffraction (XRD, M18XHF-SRA: MAC Science, Japan). Field-emission scanning electron microscopy (FE-SEM, SU70: Hitachi, Japan) was carried out to observe the morphology of the nanostructures. Photocurrent-voltage (*J-V*) curves were obtained on a solar cell measurement system (K3000: McScience, Korea) under a solar simulator (Xenon lamp, air mass (AM) 1.5, 100 mW cm^{-2}). High-resolution transmission electron microscopy (HRTEM, JEM-3000F: JEOL, Japan) and a focused ion beam (FIB, SMI3050SE: SII Nanotechnology Inc., Japan) were used to identify the uniform coating of TiO_2 through the nanoporous ZnO spheres. The elemental compositions and distribution were examined using energy-dispersive x-ray spectroscopy (EDX, ISIS-300: Oxford Instruments). An inductively coupled plasma-atomic emission spectrometer (ICP-AES, Optima-4300 DV: Perkin-Elmer, MA, U.S.A.) was employed to determine the atomic ratio of Ti/Zn in the electrode. In order to investigate the electrochemical reactions at the interfaces [34-36], electrochemical impedance spectroscopy (EIS) and open-circuit voltage decay (OCVD) were measured from a potentiostat (CHI 608C: CH

Instrumental Inc., Austin, U.S.A.). The absorption spectra of the unloaded dye molecules were recorded on a UV/Vis spectrophotometer (Lambda 20: Perkin-Elmer, Waltham, U.S.A.), and incident photon-to-current conversion efficiency (IPCE) spectra were measured on an IPCE measurement system (K3100: McScience, Korea).

2.3. Results and Discussion

To clearly identify the mechanisms of the TiO_2-coating layers with various thicknesses, the experiment was performed with extremely long dye-adsorption time (6 h). The most critical reason for the low efficiency of ZnO-based DSSCs is the formation of Zn^{2+}/dye complexes. When ZnO is immersed in acidic dye solution, the dissolved Zn^{2+} ions and deprotonated dyes form Zn^{2+}/dye complexes [22]. These complexes cover the surface as a multilayer form, and change the original morphology of the electrode. Furthermore, Zn^{2+}/dye-complexes can absorb the visible light, and the electron transfer through these complexes is not effective [21]. The Zn^{2+}/dye-complex formation is much severe under the extreme condition (6 h), and the suppressed complex formation by TiO_2-coating layer can be observed more dramatically. To achieve higher efficiency, shorter immersion time (30 min) is also performed, because typical efficiencies of ZnO-based DSSCs exhibit approximately 1.5% - 5.4% [32,37-40].

The ZnO nanoparticle has hexagonal wurtzite structure (JCPDS #36-1451), with no zinc-blende phase (JCPDS #77-0191), and TiO_2 is not detected due to the subnanometer-scale coating (XRD analysis in Fig. 2-1) [41]. The nanocrystallites are able to provide effective light scattering having relatively large surface area, because the submicrometer-sized ZnO spheres are consisted with nanoparticles, as shown in Fig. 2-2 [19,32].

The TiO_2-coating layer on the ZnO surface improves both the open-circuit voltage (V_{oc}) and short-circuit current (J_{sc}) as shown in the *J-V* curves of Fig. 2-3. In particular, the 60-min-coated cell shows an optimum power-conversion efficiency of 1.27%, increased by a factor of three compared with that of the bare cell. As the coating layer becomes thicker, V_{oc} gradually increases while J_{sc} decreases as summarized in Table 2-1.

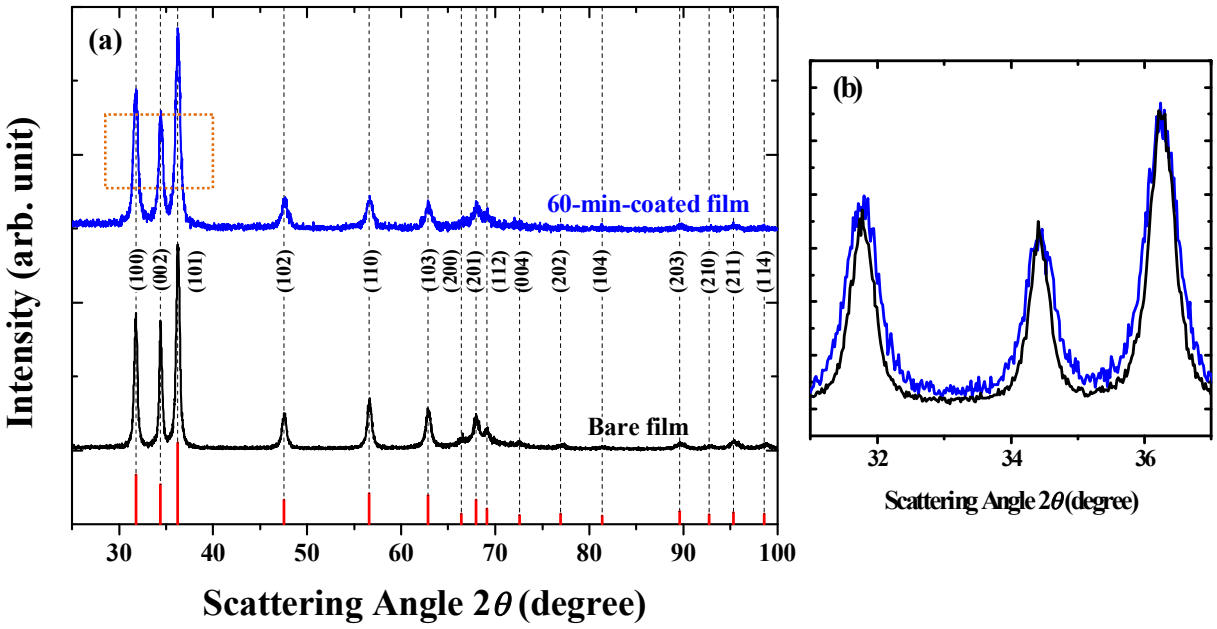

Fig. 2-1. (Color) (a) X-ray diffraction of bare and 60-min-coated film after 450°C annealing. The peak intensities and positions from the hexagonal ZnO (JCPDS #36-1451) are shown as solid lines. (b) a comparison of enlarged part of (100), (002), and (101) peaks.

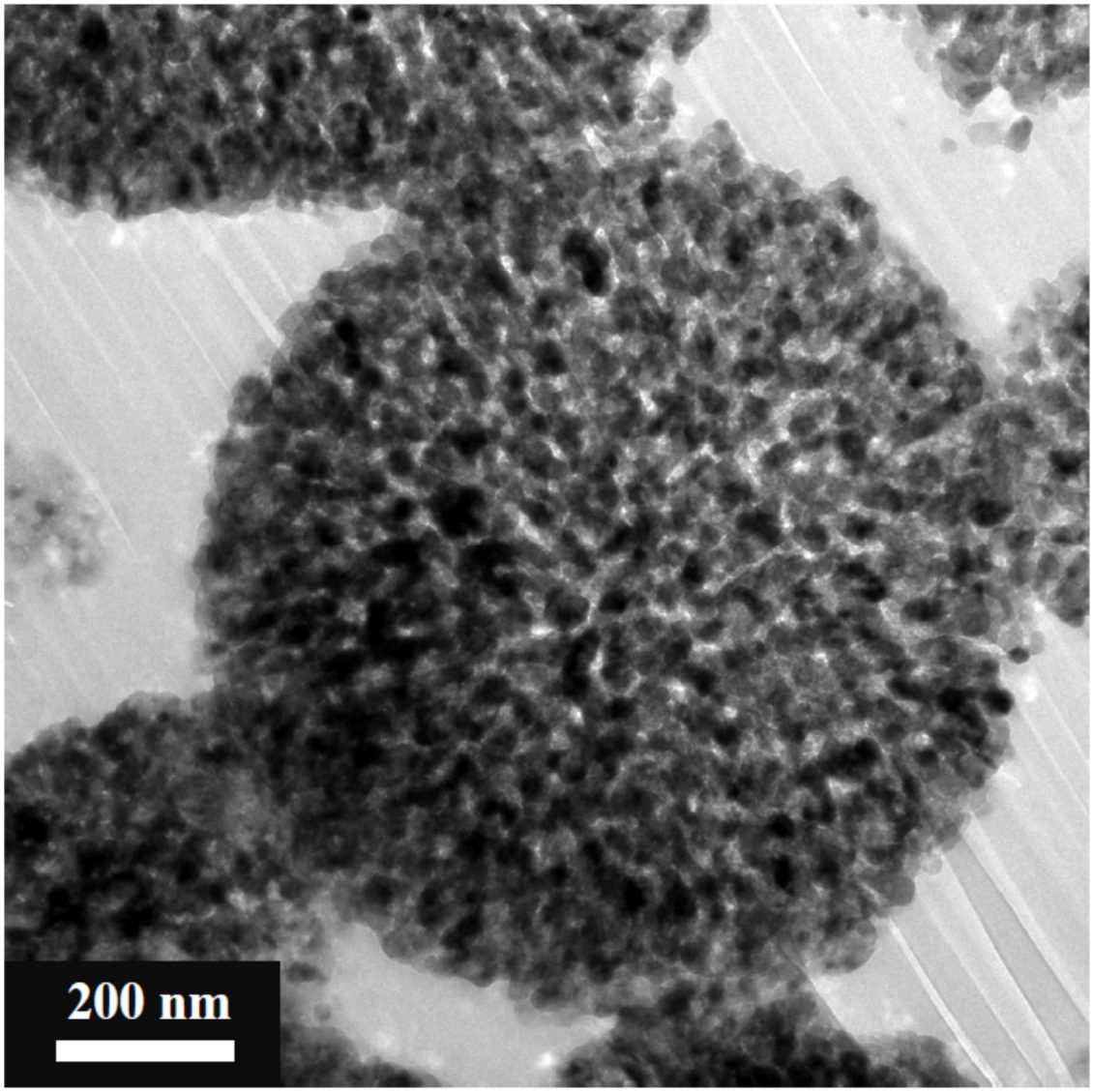

Fig. 2-2. Cross-sectional TEM image of nanoporous ZnO spheres coated with TiO_2 (60 min).

Table 2-1. (Color) Performance of DSSCs consisting of nanoporous ZnO spheres with various TiO_2-coating times (dye-adsorption time: 6 h).

	J_{sc} (mA cm^{-2})	V_{oc} (V)	*FF*	η
Bare	**1.50**	**0.595**	**43.9%**	**0.39%**
30 min	**3.02**	**0.645**	**54.2%**	**1.06%**
60 min	**3.30**	**0.663**	**58.3%**	**1.27%**
120 min	**2.55**	**0.679**	**57.2%**	**0.99%**

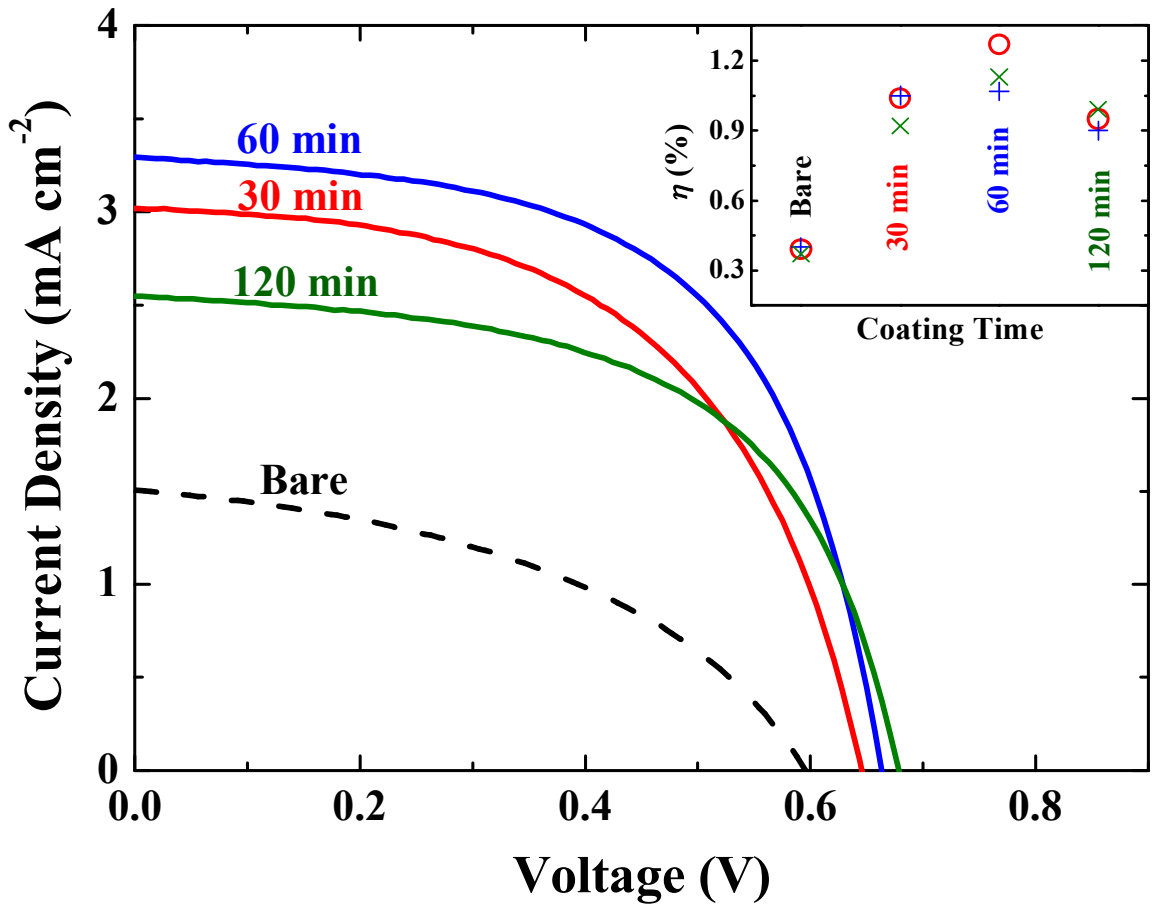

Fig. 2-3. (Color) Photocurrent-voltage curves of DSSCs with various TiO_2-coating times, and the inset shows the corresponding power-conversion efficiency (dye-adsorption time: 6 h).

The interface control using TiO_2 has an effect on nanostructure morphology. The as-synthesized ZnO nanoporous spheres by hydrothermal method are composed of ~10 nm-sized nanoparticles as shown in Fig. 2-4(a) and magnified SEM image. The as-synthesized ZnO nanoporous spheres are annealed at 350°C to remove organic component in paste and improve the crystallinity of ZnO nanoparticles. While undergoing relatively high temperature annealing, ZnO atoms on the surface are diffused to reduce the surface energy. Both the nanoparticle size and the pore size are consequently increased as shown in Fig. 2-4(b) [42]. As 350°C annealing is performed in all samples, with and without TiO_2-coating samples have bigger nanoparticle size than that of as-synthesized ZnO. After TiO_2-coating process, additional annealing of 450°C is carried out on all samples to improve the quality of TiO_2 layer and keep the same experimental conditions. Although the bigger particle size is expected at higher annealing temperature of 450°C, TiO_2 layer on ZnO would prevent the surface diffusion of ZnO atoms; therefore, TiO_2-coated sample is composed of smaller ZnO nanoparticles than without TiO_2-coated sample. When comparing the ZnO nanoparticle size between with (Fig. 2-4(c)) and without (Fig. 2-4(e)) TiO_2-coating samples, size of ZnO nanoparticle is confirmed to be approximately 20 nm and 30 nm by SEM images respectively. The difference of nanostructure morphology is also supported by the larger full-width at half-maximum (FWHM) of the TiO_2-coated film than bare film from XRD diffraction data (Fig. 2-1) [43,44]. The full width half-maximum (FWHM) is the full width of the peak measured at half of the maximum value and can be obtained by fitting each peak using Lorentzian peak function. The FWHM ($\Delta(2\theta)$) has correlation with effective grain size and strain as described below [45]:

$$\Delta k = \frac{2\pi}{\lambda} cos\theta \, \Delta(2\theta)$$

$$\Delta k_{measured} = \Delta k_{grain\ size} + \Delta k_{local\ strain} = \frac{K(2\pi)}{D} + \frac{\Delta d}{d}\frac{4\pi}{\lambda} sin\theta$$

where λ is incident x-ray wavelength, K is shape factor and has a value of 0.9 for spherical-shape particle, D is effective grain size, d is interplanar spacing in the atomic lattice, and θ is the angle between the incident x-ray and the scattering planes. When effective grain size becomes smaller or local strain is larger, the FWHM value becomes larger, because finite grain size or local strain disturbs

the crystal periodicity [46]. Thus, a coated film is considered as compose of smaller grain size than bare film from larger full-width at half-maximum of the coated film as shown in Fig. 2-1(b). After dye loading for 6 h, the bare film (Fig. 2-4(d)) is covered with Zn^{2+}/dye complexes. However, no significant morphological change is observed in the coated film (Fig. 2-4(f)), confirming that the TiO_2 layer efficiently restrains the formation of Zn^{2+}/dye complexes.

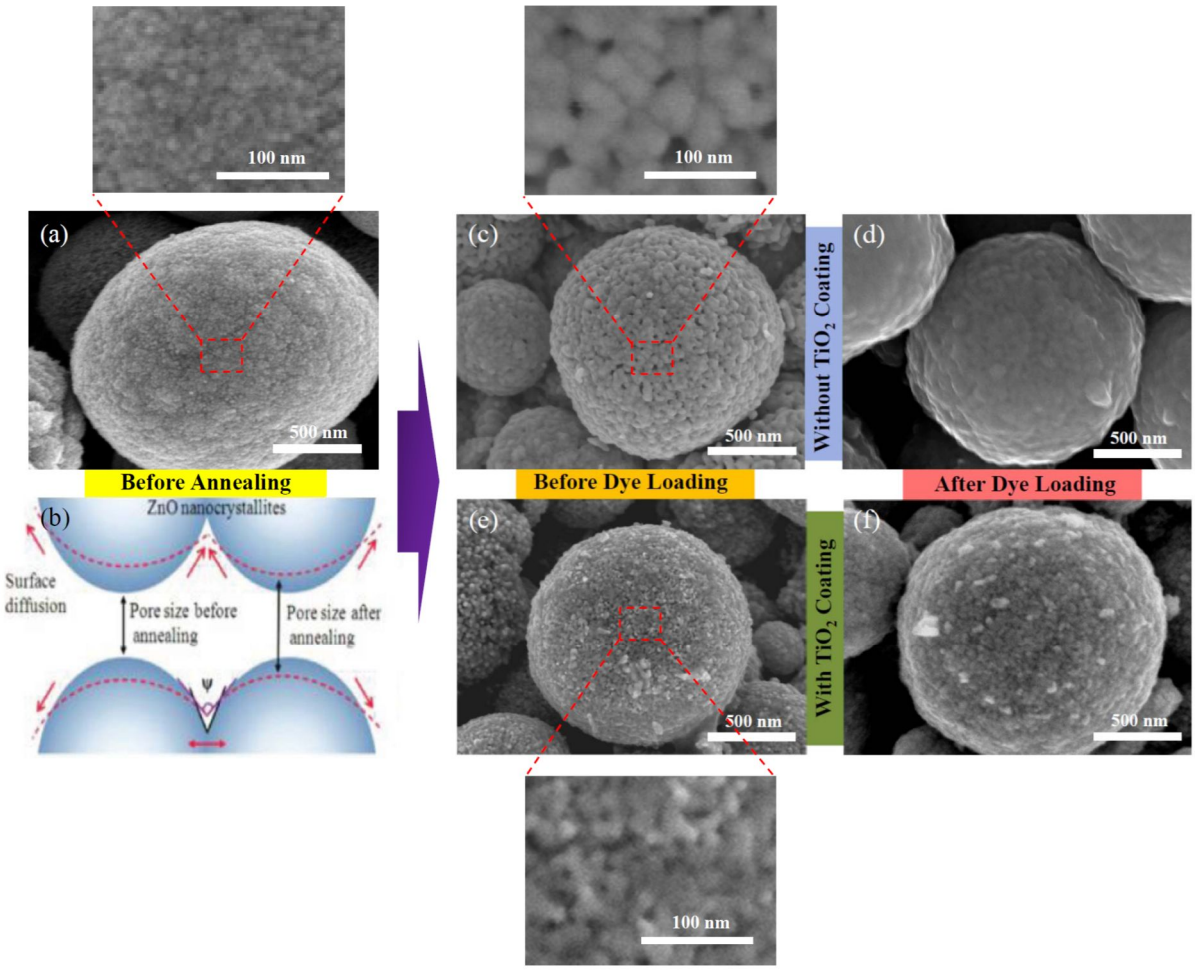

Fig. 2-4. (Color) Plan-view and magnified of FE-SEM images of (a) as-synthesized nanoporous ZnO spheres (b) schematic illustration of surface diffusion from reference [42]. (c-f) with/without TiO_2-coating layer (60 min) followed by 450°C annealing, and before/after dye loading.

As Fig. 2-5 demonstrated, the homogeneous coating of TiO_2 is confirmed from the spatial distribution of Zn and Ti elements throughout the nanopores and TiO_2-growth mechanism is investigated. TiO_2 layer is prepared by hydrolysis and polycondensation reactions of titanium butoxide ($Ti(O(CH_2)_3CH_3)_4$) and the reaction is listed below [47]:

$$\text{hydrolysis: } Ti(OR)_4 + HOH \rightarrow Ti(OR)_3OH + ROH \quad (1)$$

$$\text{water condensation: } Ti(OR)_3OH + Ti(OR)_3OH \rightarrow TiO(OR)_6 + H_2O \quad (2)$$

$$\text{alcohol condensation: } Ti(OR)_4 + Ti(OR)_3OH \rightarrow TiO(OR)_6 + ROH \quad (3)$$

$$\text{overall reaction: } Ti(OR)_4 + 2H_2O \rightarrow TiO_2 + 4ROH \quad (4)$$

In this reaction, R is alkoxides ($(CH_2)_3CH_3)_4$). The hydrolysis reaction of titanium butoxide is so fast that homogeneous nucleation and precipitation of TiO_2 can happen individually, so alcohol based isopropanol is used for solvent without additional water. Therefore, water is needed in hydrolysis reaction and it would come from the adsorbed water molecules on the ZnO surface. The formation of water by water-condensation reaction would become the cause of TiO_2 homogeneous nucleation observed by being whitish solution color at some point during synthesis and nonlinear increase of TiO_2 thickness with time. The linear formula of titanium butoxide is $Ti(OCH_2CH_2CH_2CH_3)_4$ and the expected horizontal and vertical length of the Ti precursor molecule is less than 2 nm, respectively, according to bonding length of C-O is 0.143 nm, C-C is 0.154 nm, C-H is 0.109 nm, and Ti-O is 0.194 nm [48].

To investigate the penetration possibility of a Ti precursor into the core part of nanoporous ZnO spheres, nanostructural feature and pore size of nanoporous ZnO spheres are considered. Nanoporous ZnO spheres are synthesized by gradual temperature rise of solution including Zn precursors from RT to 160°C in autoclave. When the solution temperature reaches 130°C, solution color is changed from turbid to colorless, indicating Zn precursors are completely dissolved. As temperature increases to 160°C, the solution color is changed from transparent to milky white, meaning ZnO nanoparticles aggregate each other and form spherical secondary particles of micron size and this phenomenon is considered as reduction of the surface energy. When synthesis temperature rises more from 160°C to 190°C, ZnO aggregates are disassembled and lost their

spherical shape of micron sized-secondary particles, however, no appreciable differences in the nanoparticle size, shape, and surface area are observed by SEM, XRD, and Brunauer-Emmett-Teller (BET) [32]. In addition, compared surface area measured by BET between ZnO aggregates composed about 12~15 nm nanoparticles (~80 m^2/g) and ZnO nanoparticles (~12 nm: 98 m^2/g and ~20 nm: 90 m^2/g), ZnO aggregates indicate comparable surface area with nanoparticles, though a slight surface area loss would be occurred by aggregation formation [32,42,49-51]. It indicates that nanoporous ZnO spheres are consisted of individual nanoparticles to the inside, suppressing the grain growth between ZnO nanoparticles or closed pore formation spheres in aggregation process. The pores are formed by interstitial voids among the nanoparticles and these pores provide pathway, where a Ti precursor or dye can be penetrated. The pore sizes of ZnO aggregates measured by BET are reported approximately 10 nm, referring the study that uses the similar synthesis methods [52]. When comparing the assumed size of pore and a Ti precursor, Ti precursor molecules are expected to diffuse into ZnO nanoporous spheres. Furthermore, from the comparison of the amount of dye loading of nanoparticles film (1.4×10^{-7} mol/cm^2) and aggregates film (1.38×10^{-7} mol/cm^2), it implies that the ~1.26 nm sized of a N719 dye which has similar size with a Ti precursor can penetrate and adsorbed inside of porous ZnO aggregates [53,54]. Nevertheless, the pore or network can be blocked in TiO_2-coating process and there would exist non-coated ZnO part because coating process is solution process and the narrow parts of inert passage from small pore size are stuck during a Ti precursor diffusion. The formed pores are multidirectional pores not the one-way open pores because they are built from a nanoparticle surrounded by other nanoparticles on every side, therefore, the penetration of a Ti precursor would be possible even if a pore in some place is blocked. In addition, larger FWHM values (Fig. 2-1) support that TiO_2 is coated throughout the nanopores, because the FWHM value indicates the average value of total.

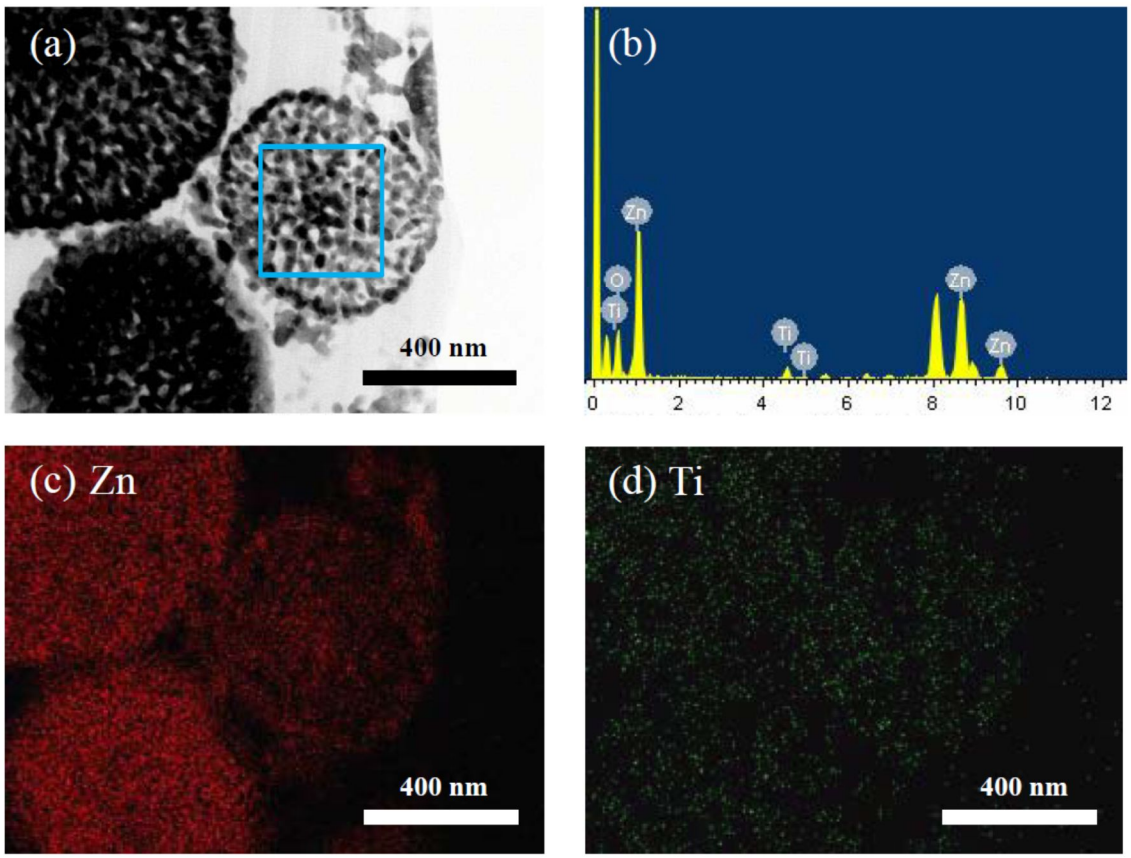

Fig. 2-5. (Color) (a) Cross-sectional TEM image of nanoporous ZnO spheres (60-min-coated film), (b) elemental analysis, and (c and d) EDX mapping of Zn and Ti, respectively.

The realistic possibility of uniform TiO_2 growth on ZnO surface is approached with surface free energy perspective. There are three modes of the thin film growth: Stranski–Krastanov growth (layer-by-layer), Volmer-Weber with islands formation, and layer plus island. The growth modes depend on the difference of surface free energy of substrate (ZnO in this study) and sum of surface free energy of deposited material (TiO_2) and interfacial energy between two materials (ZnO/TiO_2). The surface free energy relies on the size, shaped or exposed direction, and strain energy but it can be neglected on the basis of Yong-Dupre equation and can be defined as below [55]:

$$\Delta\gamma = \gamma_m + \gamma_i - \gamma_s \tag{5}$$

where γ_m, γ_s and γ_i is are material's surface free energy, substrate's surface free energy, and interfacial energy subsequently. In this study, γ_s is surface free energy of ZnO nanoporous spheres, γ_m is surface free energy of coated TiO_2, and γ_i is interfacial energy of newly formed interphase between ZnO and TiO_2. In case when the surface free energy of ZnO (γ_s) is higher than the sum of the surface free energy of TiO_2 (γ_m) and interfacial energy between ZnO and TiO_2 (γ_i), the growth mode will be layer-by-layer ($\Delta\gamma < 0$) because surface covered with TiO_2 is a way to minimize overall surface free energy of system. If the opposite, it will be Volmer-Weber mode, as shown in Fig. 2-6. The surface free energies of ZnO and TiO_2 are investigated by literature survey. A. Navrotsky's group experimentally researched the surface free energy of ZnO and TiO_2 by measuring the surface free enthalpy difference between 20 nm-sized nanoparticle and bulk material when they are dissolved in molten sodium molybate ($3Na_2O\ 4MoO_3$) at 700°C [56,57]. The surface free energy arises from different environment of atoms at the surface compared to those atoms from its interior. Each atom in the bulk is surrounded by same atoms; however, the atoms at the surface have a different energy distribution, such as broken bonding and configuration changes, and etc., from the inside and have a higher excess energy. The difference in energy between atoms located at the surface and in the bulk is the surface free energy [58]. As all systems try to minimize the total energy, the surface free energy is also considered to have a tendency to minimize with minimizing area as small as possible. Thermodynamically at constant temperature, pressure, and composition, the surface free energy is the increase in the Gibbs energy of the system when surface area increases. Thus, it is a function of the

difference between the surface free enthalpy formed by broken bonding and surface free entropy by reduced geometric constrain and increased extra configuration such as vacancy, kink, step, and etc. The surface free entropy is slightly dependent on temperature and measured value vary between 0 and 3 mJ/m^2 K [59]. The reported surface free entropy of ZnO is ~0.02 mJ/m^2 K, which is essentially zero, therefore the surface free energy is considered to be evaluated by surface free enthalpy [60]. The surface free energy is obtained as below equation:

$$\Delta H\,(\text{nano} \rightarrow \text{soln}) = \Delta H\,(\text{bulk} \rightarrow \text{soln}) - A\gamma. \quad (6)$$

Where, ΔH is the surface free enthalpy normalized by mole, A is surface area measured by BET, and γ is surface free energy of nanoparticle. Although the experiment performs in solution not in air, the principle of the surface free enthalpy measurement is the relative comparison of endothermic reaction for bulk and nanomaterial. Thus, the final state condition of solution merely provides the standard of relative comparison, as mentioned below.

$$\Delta H\,(\text{nano} \rightarrow \text{soln}) = H_{dissolved\ in\ solvent} - H_{\text{nano}} \quad (7)$$

$$\Delta H\,(\text{bulk} \rightarrow \text{soln}) = H_{\text{dissolved in solvent}} - H_{\text{bulk}} \quad (8)$$

$$A\gamma = \Delta H\,(\text{bulk} \rightarrow \text{soln}) - \Delta H\,(\text{nano} \rightarrow \text{soln}) = H_{\text{dissolved in solvent}} - H_{\text{bulk}} - (H_{\text{dissolved in solvent}} - H_{\text{nano}}) \quad (9)$$

where ΔH (nano → soln) is the energy needed in endothermic reaction of tens of nanometer particle dissolution in high temperature solvent at 700°C. It is measured by temperature change of solvent when nanoparticles are supplied. ΔH (bulk → soln) is the same signification with the exception of dissolved bulk material. As mentioned above, surface has higher energy then bulk, the energy required for dissolution of nanoparticle is smaller than bulk material and this difference arises from the surface free energy term ($A\gamma$).

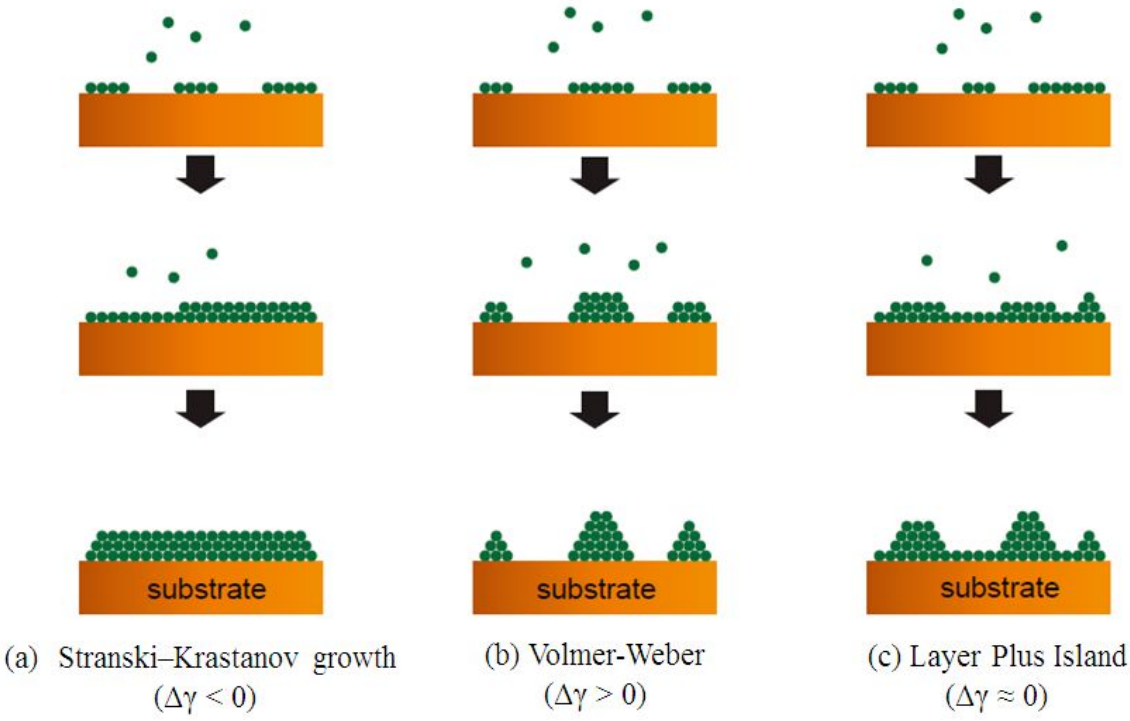

Fig. 2-6. (Color) Schematic figures of growth modes (a) Stranski–Krastanov growth (layer-by-layer), (b) Volmer-Weber, and (c) layer plus island. From Ref. [47].

As a result, surface free energy of TiO_2 is 0.51 J/m^2 and ZnO has 1.31 J/m^2 that is greater than twice of TiO_2 value. These values are in reasonable range when compared with values obtained in other research, which illustrated in Fig. 2-7. The investigated values are calculated by density functional theory considering atom density of each plane and bonding energy or experimentally obtained by calorimetric measurement, and detailed information is specified on the right side of the graph [61-66]. The distribution shows that the difference in ZnO and TiO_2 surface free energy is at least 0.5 J/m^2 up to 1.5 J/m^2.

The interfacial energy between ZnO and TiO_2 is approached from the point of view of a misfit because the interface can be considered to be comparable or smaller than some high angle grain boundary when two materials having different lattice parameters create the interface [67,68]. The interphase interface can be divided on the basis of their crystal structure and lattice parameter into three classes: coherent, semicoherent, and incoherent [59]. A coherent interface occurs between materials having same crystal structure and lattice parameter and it has small interface energy of approximately 200 mJ/m^2, such as a interface energy between $Cu(111)_{fcc}//Si(0001)_{hcp}$. The interface is replaced from coherent to semicoherent interface having misfit dislocations when atomic misfits of interfacial area are sufficient. When a misfit (δ) is under 0.25, it classified as a semicoherent interface and a misfit can be defined as below:

$$\delta = \frac{d_\beta - d_\alpha}{d_\alpha} \tag{10}$$

where d_α is atomic distance of substrate and d_β is atomic distance of deposited film. The semicoherent interfacial energy is composed of structural distortions caused by misfits and chemical contributions by different components, and the value range is 200 to 500 mJ/m^2. When a misfit is more than 0.25, an incoherent interface can be formed and has interfacial energy of 500 to 1000 mJ/m^2. The interface between ZnO and TiO_2 is considered coherent or semicoherent because the atomic distance between Zn-O in wurtzite structure (1.98 Å) and Ti-O in anatase (1.98 and 1.93 Å) are very similar and epitaxial relationship is observed between zone axes of $[110]_{TiO2}$ and $[010]_{ZnO}$ with a twisted angle of 27º as shown in Fig. 2-8. Furthermore, the deposited film would be grown toward direction having the similar distance to maintain continuity and reduce the strain, especially within several atomic layers [69].

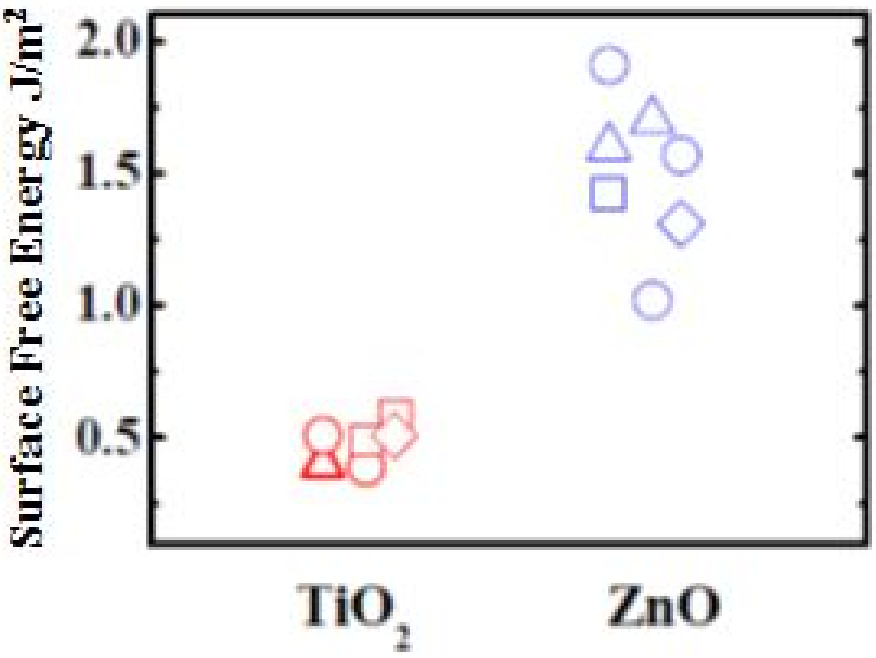

TiO_2

○ A. S. Barnard, *J. Chem. Theory Comput.* (2005)
hydrated anatase (001): 0.51 J/m², (100): 0.39 J/m²
by density functional calculations

△ A. Navrotsky, *Geochem. Trans.* (2003)
TiO_2 anatase: 0.4±0.1 J/m² by calorimetric measurements

□ A. Selloni, *Physical Review B* (2001)
TiO_2 (101): 0.49 J/m², (100): 0.58 J/m² by DFT (PBE)

◇ A. Navrotsky, *J. Mater. Chem.* (2010)
anatase nanoparticle (~20 nm): 0.51 J/m² by calorimetric

ZnO

□ B.-L. Su, *Chem. Mater.* (2007)
hydrated porous ZnO (15 nm, 3 nm): 1.42±0.21 J/m²
by calorimetric measurements

○ G. C. Yi, "semiconductor nanostructures for optoelecronic devices" (springer), ZnO crystal (0011): 1.91 J/m² (1120):1.02 J/m² (1011):1.57 J/m² (1010):1.01 J/m², by theoretical calculation

△ D. Marx, *Physical Review B* (2003)
ZnO (1010): 1.6 J/m², (1120): 1.7 J/m², by DFT (PBE)

◇ A. Navrotsky, *J. Mater. Chem.* (2010)
nanoparticle (~20 nm): 1.31 J/m² by calorimetric measurements

Fig. 2-7. (Color) Literature survey of interface energy of ZnO and TiO_2 [48,54,58-63].

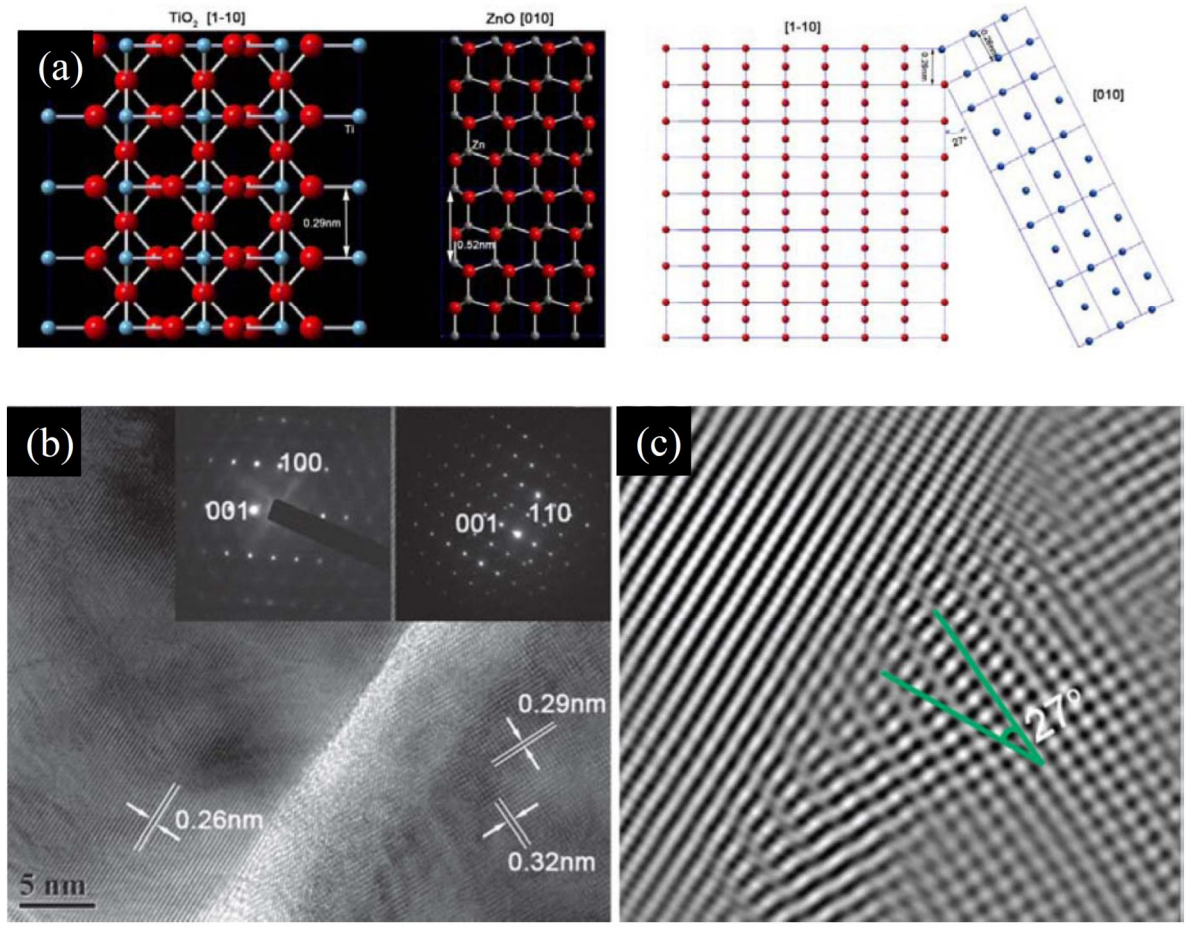

Fig. 2-8. (Color) (a) Structural models and 2D atomic arrangement along $[110]_{TiO2}$ and $[010]_{ZnO}$ axis, respectively, with a twisted angle of 27º (b) HRTEM image, and (c) lattice-fringe-resolved HRTEM Image at TiO_2/ZnO interface. From Ref. [69].

I confirm the possibility of formation of uniform TiO_2 layer on ZnO surface from the perspective of surface free energy and interfacial energy, but principle of energy minimization is not sufficient to predict the growth mode when deposition does not occur under thermodynamic equilibrium conditions. In practice, uniform TiO_2 coating using ALD or sol-gel method on various ZnO nanostructures is reported. Furthermore when they form multilayers alternately, ZnO agglomerates on TiO_2 but TiO_2 builds the relatively uniform layer on ZnO as demonstrated in Fig. 2-9 [70-72]. It is hard to predict the growth mode on the basis of surface free energy alone, it is valuable that the thermodynamically approach to possibility of uniform TiO_2 layer on ZnO is attempted. The way of adding the surfactant which has opposite charge to a Ti precursor or exposure the plane having larger surface energy would be help to increase the possibility of uniform coating.

With the atomic ratios of Ti/Zn measured by ICP-AES, the thicknesses of TiO_2 coating layers are estimated with a simple back-of-an-envelope calculation. Because I confirmed from the EDX analysis that TiO_2 is coated relatively uniformly throughout the ZnO nanopores, I assume that each nanoparticle is covered with a uniform TiO_2 layer. The TiO_2-coating thicknesses are obtained without considering the three-dimensional necking of nanoparticles and all calculated values are estimated in subnanometer as shown in table 2-2. The subnanometer thickness of TiO_2 layer is not regarded as unreasonable values when considering the growth mechanism that each Ti precursor molecules are bonded and condensed one by one. The actual thicknesses are considered to be thicker than the calculated thicknesses in respect that calculation does not take account of surface loss from annealing. Although the atomic ratios of Ti/Zn are also measured by EDX, ICP-AES method is used due to its reliability of quantitative analysis. Most of the generated electron carriers from dye would transfer through ZnO nanoparticles because TiO_2 layer is too thin to transfer electrons effectively, and also ZnO is a preferred electron channel due to the high mobility [4,5].

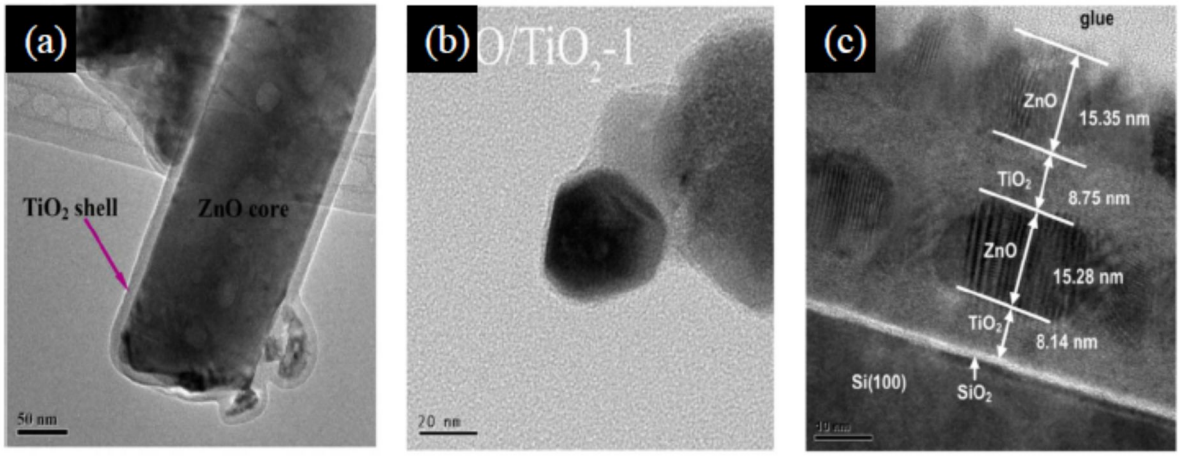

Fig. 2-9. SEM images of (a) TiO_2 shell on ZnO nanowire deposited by APCVD, (b) amorphous TiO_2 coating on ZnO nanoparticle by sol-gel method, and (c) multilayer of ZnO (polycrystalline) and TiO_2 layers (amorphous) by ALD. From Ref. [70-72].

Table 2-2. (Color) Atomic ratios of Ti/Zn in the films, as measured by ICP-AES, and the thicknesses of TiO_2 layer, with the assumption of uniform coating on each nanoparticle.

	Ti/Zn	TiO_2 Thickness
30 min	**0.81%**	**0.04 nm**
60 min	**2.67%**	**0.23 nm**
120 min	**3.63%**	**0.32 nm**

The amount of adsorbed dye was carried out by desorbing the dye from the ZnO films into 1 M NaOH solution and then measured using the ultraviolet-visible absorption spectra of the resultant solution as shown in Fig. 2-10. The adsorption amount of dye molecules on ZnO surface was calculated by Beer-Lambert law:

$$A = \varepsilon c \ell . \tag{11}$$

Where A is absorption, ε is molar absorption coefficient (m^2/mol), c is concentration (mol/l), and l is path length (cm) of measured sample [73]. While the dye loading of all the coated films is higher than that of the bare film, and the 60-min-coated film shows the optimum value. The increase in dye loading is attributed to the suppression of Zn^{2+}/dye-complex formation at the outer surface of ZnO sphere, which can block the dye diffusion into the nanoporous sphere. In the 120-min-coated film, the amount of dye is slightly decreased. A possible reason is the surface area loss due to the coating on the nanoporous connections among ZnO nanoparticles.

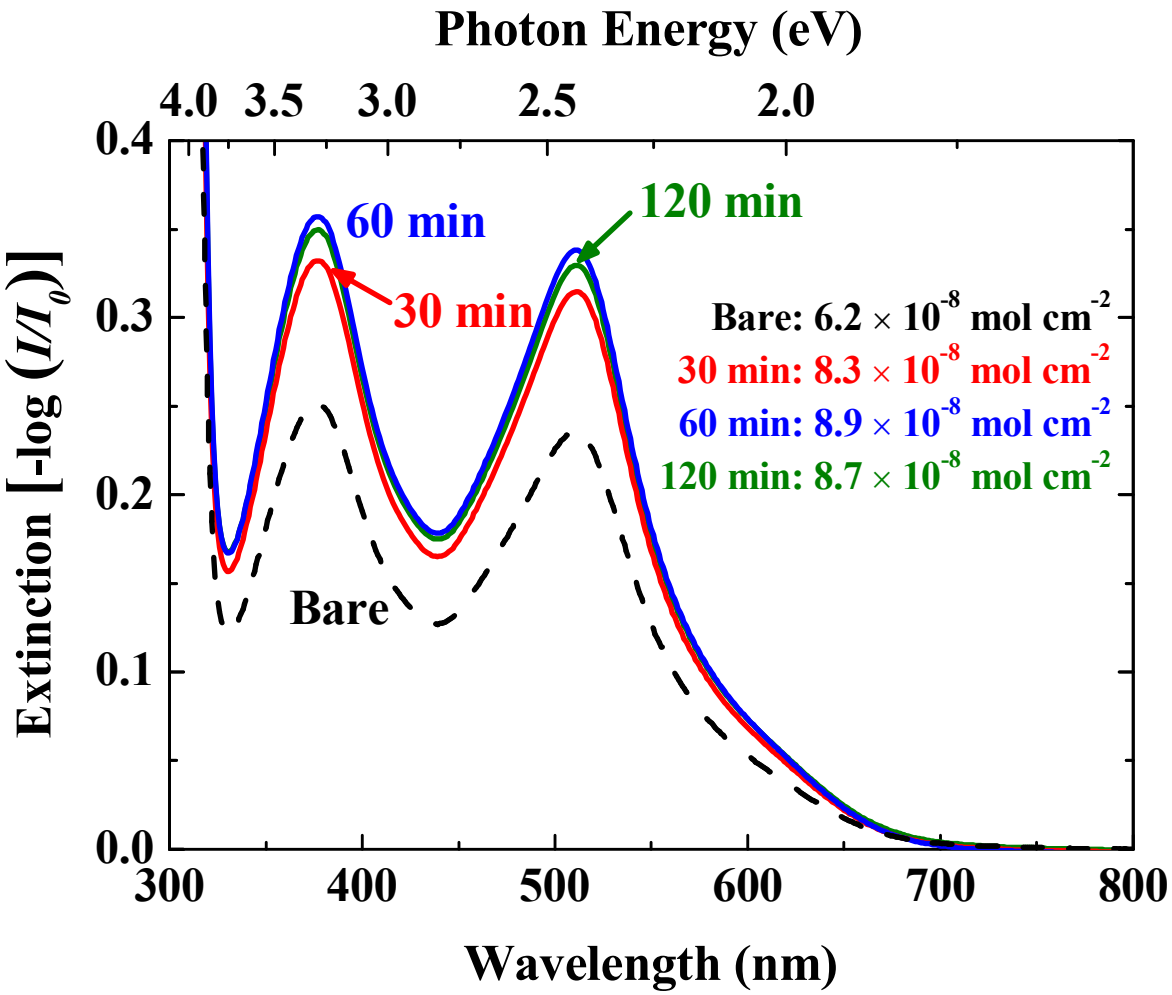

Fig. 2-10. (Color) UV-Vis absorption spectra of N719 desorbed from DSSCs in 1 M NaOH solution.

Impedance analysis was performed at the open-circuit condition under AM 1.5 [74-76], and the resistance (between ~10^0 and ~10^3 Hz) increases with the thickness of the coating layer (Fig. 2-11). This indicates that the TiO_2-coating layer suppresses back electron transfer, and consequentially improves V_{oc} [77,78]. In contrast, thicker coating suppresses forward electron injection, resulting in a decreased current density [79-82]. The bare cell shows the highest resistance due to the formation of resistive Zn^{2+}/dye complexes.

Reduction of charge recombination was also observed (Fig. 2-12) [83-85]. The decay response of the coated cell is slower than that of the bare cell, indicating recombination is effectively reduced. The electron-carrier lifetime (τ) is obtained from [83]:

$$\tau = -\frac{k_B T}{e}\left(\frac{dV_{oc}}{dt}\right)^{-1}, \quad (12)$$

where $k_B T$ is the thermal energy, e is the elementary charge, and t is time (Fig. 2-8(b)). The electron-carrier lifetime of the coated cell is approximately one order of magnitude higher in comparison with the bare cell.

The TiO_2-coated cells show higher IPCE values than the bare cell in the whole visible region due to the reduction of recombination by TiO_2 coating, as shown in Fig. 2-13. Even in the lower wavelength region (below ~390 nm) where light is mainly absorbed by ZnO, the IPCE of the bare cell is still lower than that of the coated cell because of the formation of Zn^{2+}/dye complexes while the degree of enhancement among the coated cells becomes insignificant. The bandgap of ZnO nanoparticle aggregate is expected to be similar to that of the bulk (~3.2 eV), because the size of nanoparticle is much larger than the exciton diameter of ZnO (~5.6 nm) [86]. The IPCE value dropped to zero at wavelength around 300 nm due to the absorption of FTO [87].

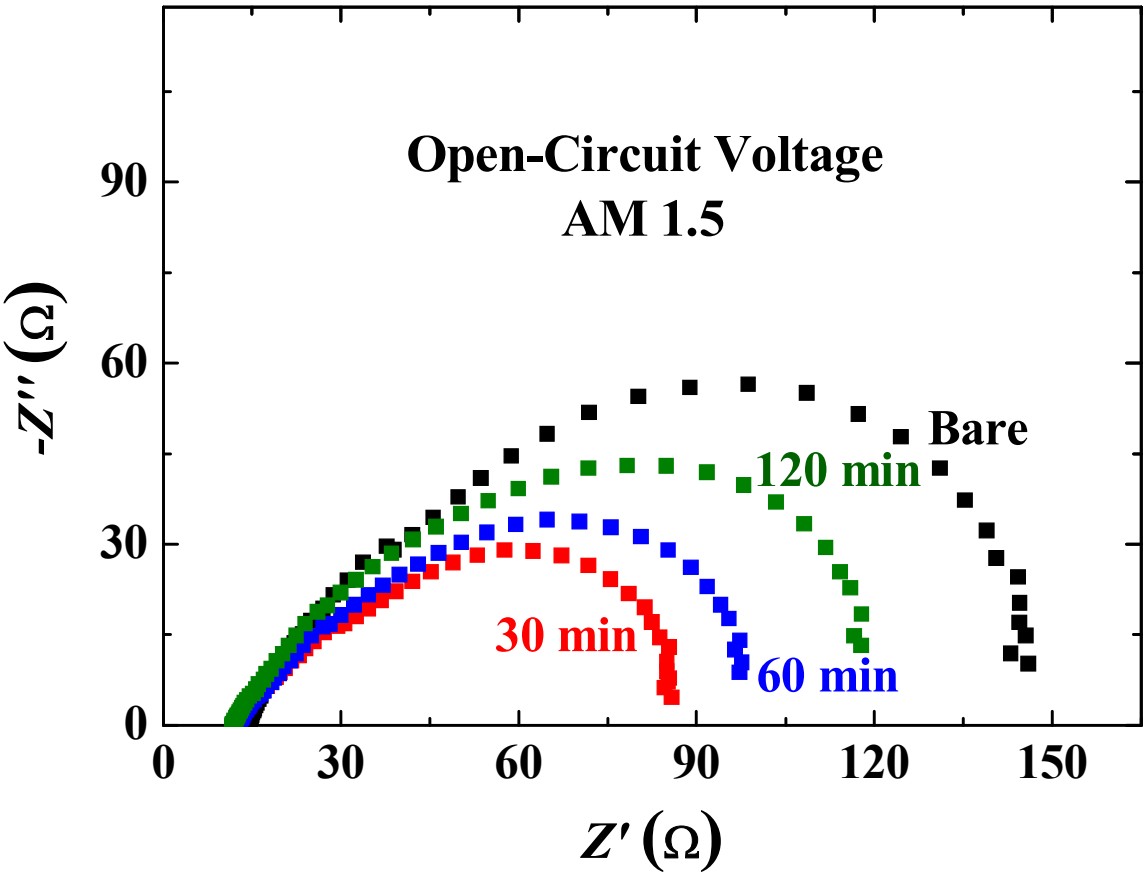

Fig. 2-11. (Color) Nyquist plots with different coating times.

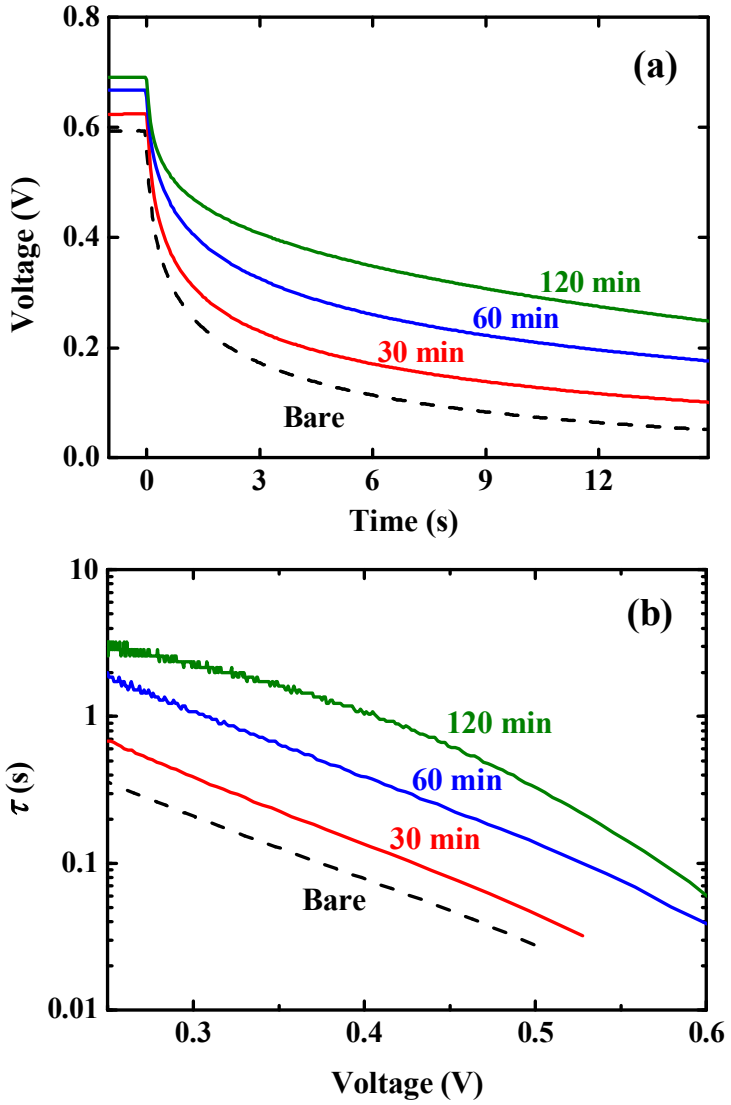

Fig. 2-12. (Color) (a) Experimental decay results of V_{oc} for the bare and coated cells. (b) Electron lifetime from Eq. (12) as a function of voltage.

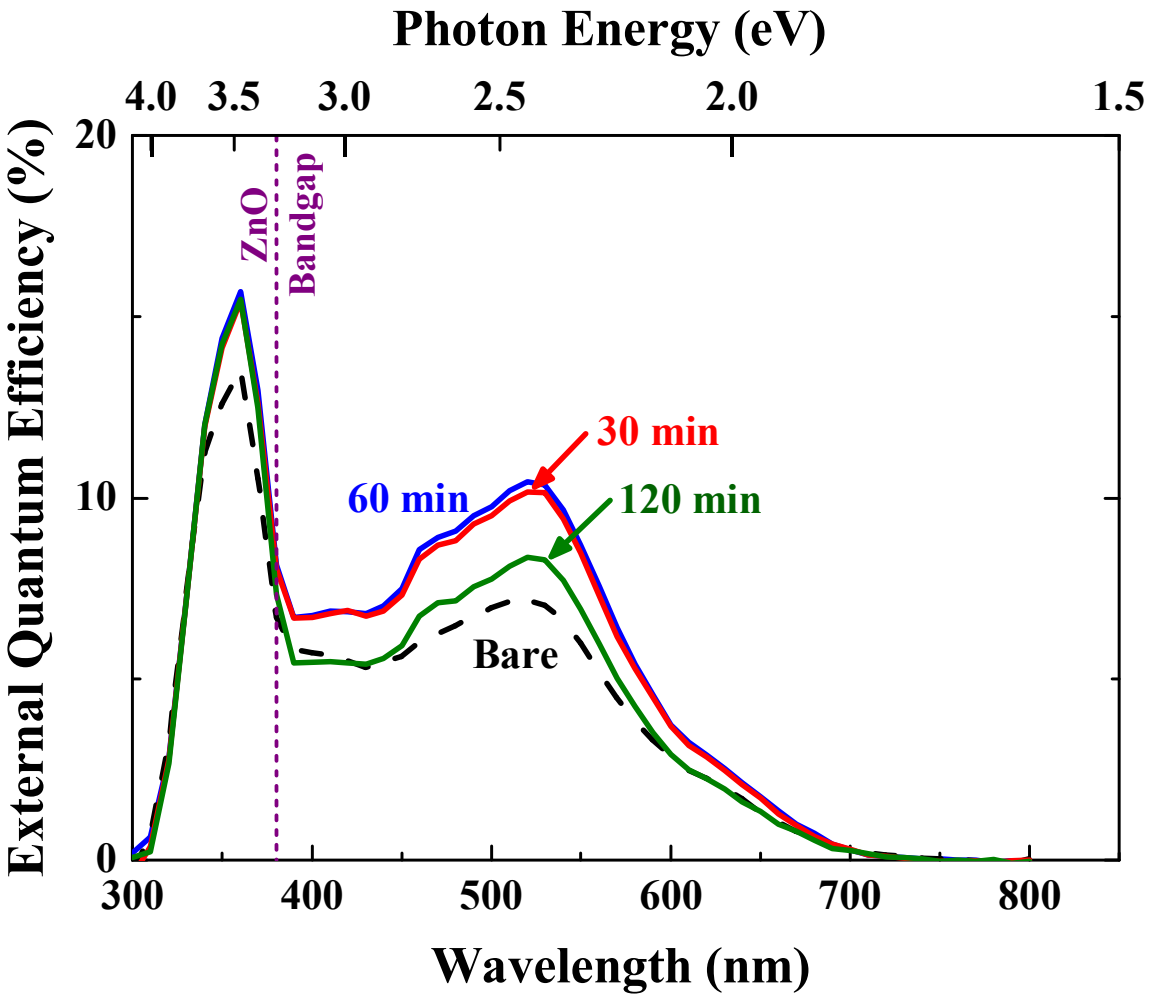

Fig. 2-13. (Color) Incident photon-to-current conversion efficiency (IPCE) spectra of bare and coated cells.

The shorter dye-adsorption time (30 min) is also performed for higher efficiency, and the corresponding photocurrent density-voltage (*J-V*) characteristics are presented in Fig. 2-14. These results indicate similar tendency with that of the longer dye-immersion time (6 h) that V_{oc} increases while J_{sc} decreases, as the coating-layer thickness increases, as shown in table 2-3. The optimum power-conversion efficiency of 2.54% is obtained in the 60-min-coated cell, which is ~26% higher than that of the bare cell (1.87%).

The interface stability of TiO_2-coated cell is investigated for two weeks, which shown in Fig. 2-15. In first several days, both V_{oc} and fill factor (*FF*) increase while J_{sc} decreases, resulting in the 15% decrease in efficiency, however, all values remain relatively constant after several days, indicating good stability of the TiO_2-coated cell. The similar tendency of stability is also reported in TiO_2-based DSSCs [88,89]. The reason of decreased efficiency is not verified clearly, but most widely accepted theory is that thiocyanate (SCN^-) ligand of N719 dye is exchanged into iodide in electrolyte [90]. A. Hagfelt's group reported that the exchange of SCN ligand into iodide occurs when the dye is regenerated by redox reaction of electrolyte mediator repeatedly as the equation below:

$$Ru(dcbpy)_2(SCN)_2^{2-} + I_3^- \rightarrow Ru(dcbpy)_2I_2^{2-} + I_2SCN \quad (13)$$

where Ru is ruthenium metal and dcbpy is bis(2,20-bipyridyl-4,40-dicarboxylato) in N719 dye. The exchange reaction is observed by resonance Raman scattering with various electrolyte component conditions. When both iodide and iodine are not included in electrolyte, all Raman lines of the dye such as SCN at 2103 cm^{-1}, bcdpy at 699 cm^{-1} and 1549 cm^{-1} are well indicated. When same concentration of iodide and iodine with commercially used electrolyte added, the intensity of SCN Raman line at 2104 cm^{-1} is markedly decreased expect nothing else. Furthermore, Z. Zou's group measured the absorbance of the dye after 1000 h cell operation and the blue shift of absorbance onset is confirmed [89]. The ligand exchange of SCN with iodide decreases the dye regeneration and efficient light absorption which mentioned as above, and those issues lead current reduction over time. Otherwise, V_{oc} can be increased by reduced tri-iodide ion (I_3^-) which acts recombination site of electrons in metal oxide conduction band.

Table 2-3. (Color) Short-circuit current, open-circuit voltage, fill factor, and power-conversion efficiency of the DSSCs with various TiO_2-coating times (dye-adsorption time: 30 min).

	J_{sc} (mA cm^{-2})	V_{oc} (V)	*FF*	η
Bare	**5.44**	**0.601**	**57.2%**	**1.87%**
30 min	**6.64**	**0.605**	**58.7%**	**2.36%**
60 min	**6.77**	**0.627**	**59.9%**	**2.54%**
120 min	**4.63**	**0.635**	**60.4%**	**1.78%**

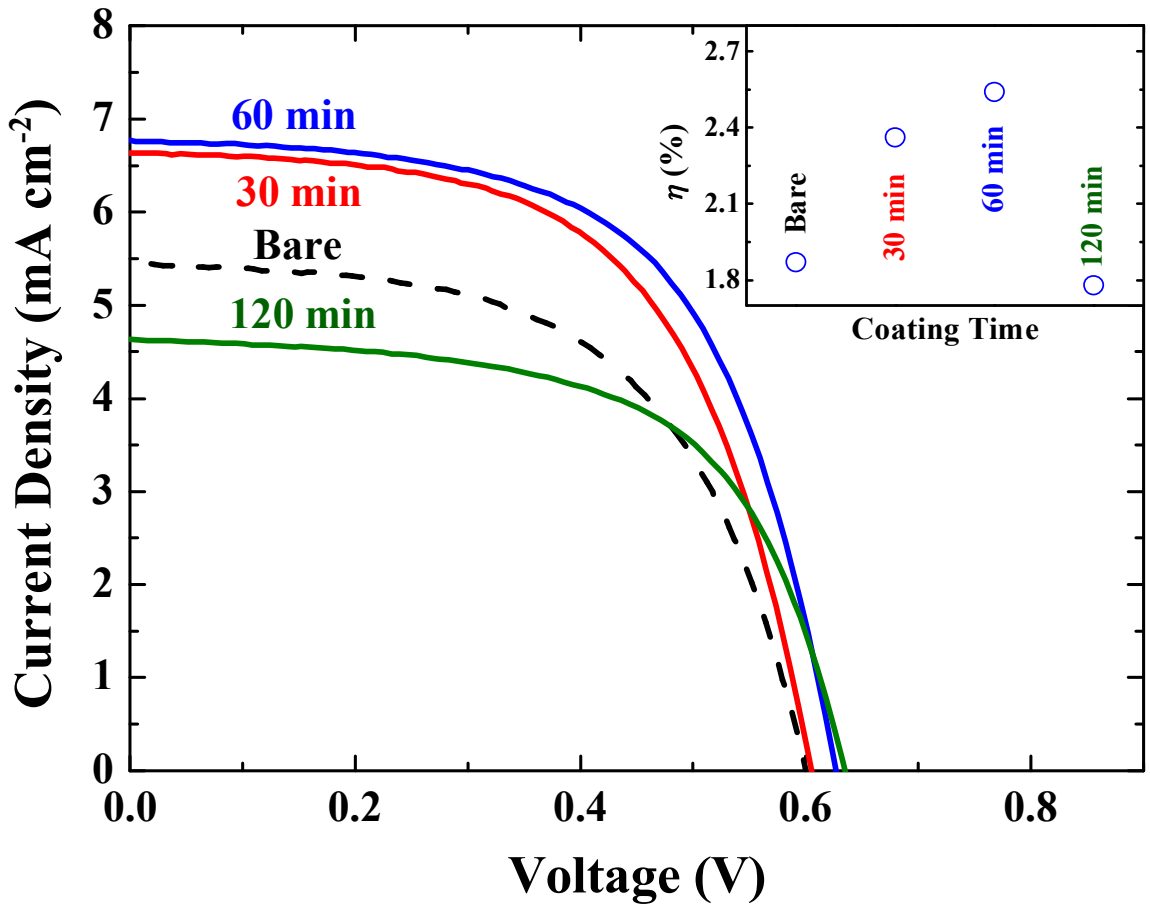

Fig. 2-14. (Color) Photocurrent density-voltage characteristics of the TiO_2-coated ZnO-based DSSCs (dye-adsorption time: 30 min), and the inset shows the power-conversion efficiency of DSSCs with respect to the TiO_2-coating time.

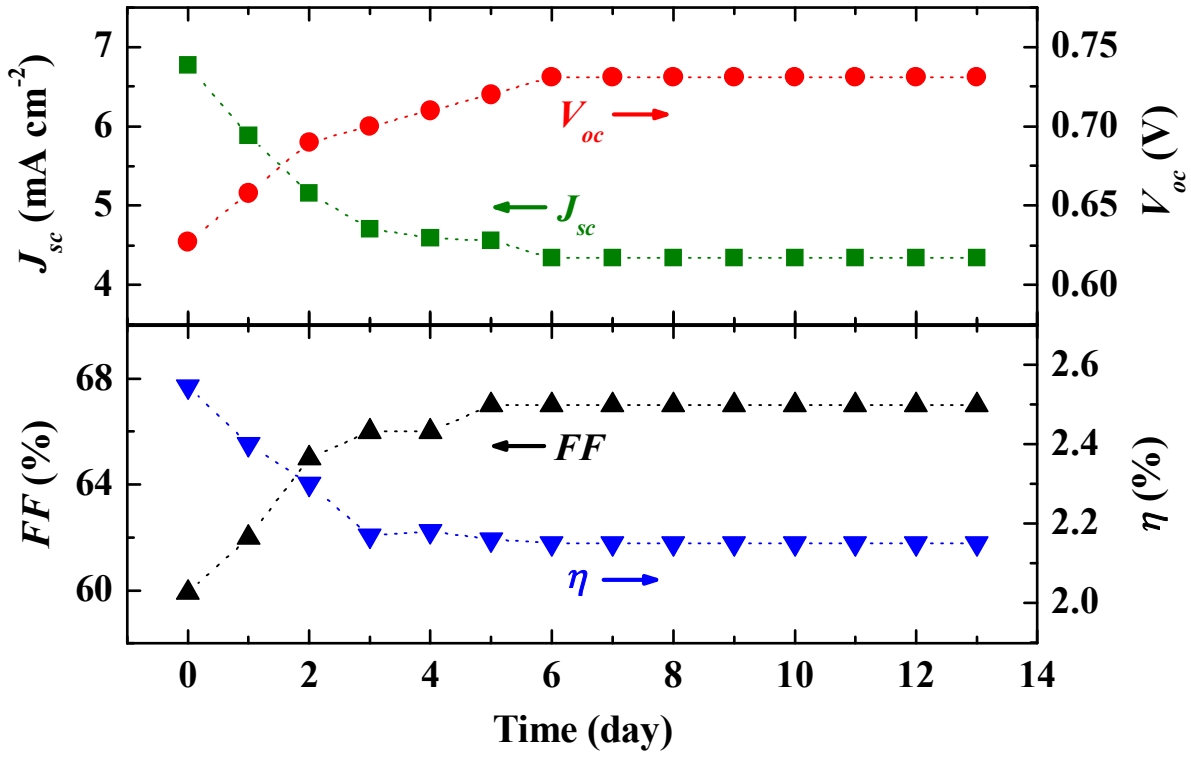

Fig. 2-15. (Color) The changes of short-circuit current, open-circuit voltage, fill factor, and power-conversion efficiency of the 60-min-coated cell for two weeks (dye-adsorption time: 30 min).

I calculate that the amount of reduced I_3^- and the ligand exchanged dye which leads to increased V_{oc} of approximately 0.1 V, with assumption that the reduced concentration of tri-iodide ions is the only reason of increase in V_{oc}. V_{oc} value is defined as below equation [91]:

$$V_{oc} = \frac{k_B T}{qu\alpha} \ln\left(\frac{I_{inj}}{n_0^{u\alpha} k_{et} [I_3^-]^m}\right), \quad (14)$$

where $k_B T$ is the thermal energy, q is the elementary charge, I_{inj} is the current resulting from injection, n_{cb} is the electron concentration at the conduction band of metal oxide in dark, k_{et} is the rate constant for the back transfer of electron, m is order of the rate of reaction for I_3^- ($m \approx 1.9$), u is order of the rate of reaction for electrons, α is electron-transfer coefficient ($u\alpha \approx 0.7$), and $[I_3^-]$ is I_3^- concentration in electrolyte. The V_{oc} increase occurs in the same cell system, the values of I_{inj}, n_{cb}, and k_{et} are roughly considered to be same between before and after light exposure. As a result, 75% decrease of I_3^- concentration causes the V_{oc} incensement of 0.1 V. This is enormous amount of decrease even if increase of V_{oc} is considered to be only affected by I_3^- concentration in electrolyte. The other studies employing electrolytes of different iodine concentration indicate similar amount of iodide concentration change of 76% for the V_{oc} incensement of 0.1 V [91,92].

To reduce the ligand exchange, development of the thiocyanate-free ruthenium sensitizer is most necessary and many groups have been tried to search a solution as shown in Fig. 2-16. M. Gratzel's group reported the ruthenium-based dye replacing the SCN ligand with a cyclometallated 2,4-difluorophenylpyridine, named the complex YE05, and shows promising result of high efficiency of 10% [93]. A new cyclometalated ruthenium complex T66, [Ru(6'-phenyl-4'-thiophen-2-yl-[2,2']bipyridinyl-4-carboxylic acid)(4,4',4''-tricarboxy- 2,2':6',2''-terpyridine)]Cl, is investigated by T. H. Ghaddar's group in order to engineer new ruthenium dyes having strong light absorption [94].

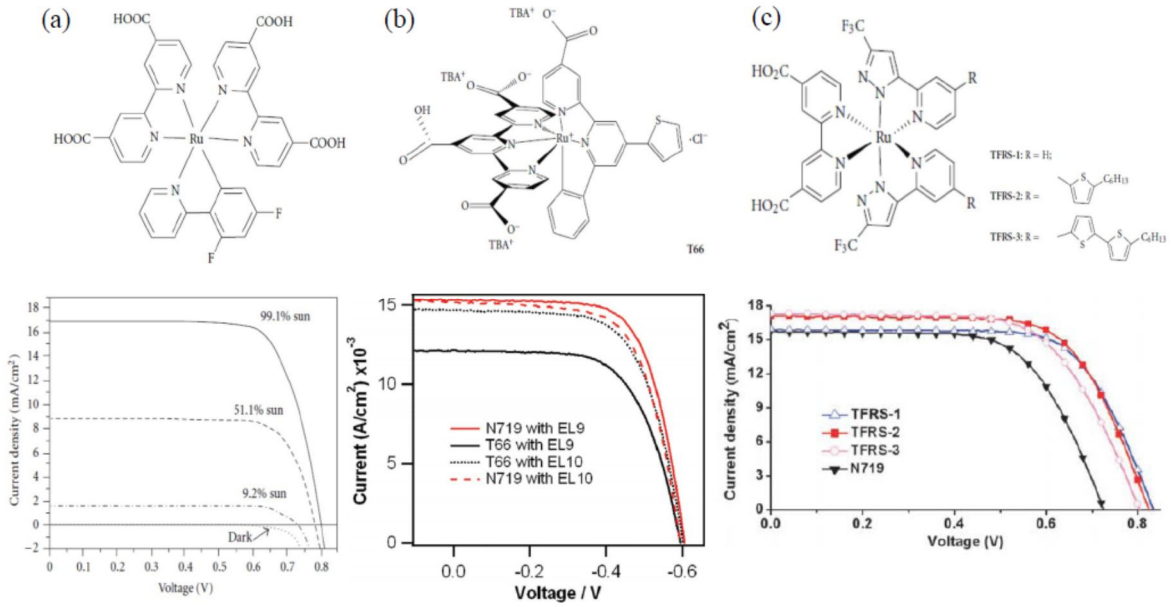

Fig. 2-16. (Color) Molecular structures and current-potential curves of (a) YE05, (b) T66 and (c) TFRS-1-3 dyes. From Ref. [58,65,66].

And also a new thiocyanate-free ruthenium dye, which are assembled using both 4,4′-carboxy-2,2′-bypyridine and 2-pyridyl pyrazolate ancillaries, called TFRS-1-3, is developed showing the high efficiency of 9.5%. Although many attempts to replace the thiocyanata donor ligands have been tried, it still shows the lower efficiencies than thiocyanate ruthenium sensitizer which has outstanding properties of broad range of visible light absorption and relatively long-lived at excited state. Nevertheless, some results of high efficiencies of thiocyanate-free ruthenium dye indicate that the ability of effective dye regeneration and potential possibility of improvement. Unfortunately, influence of new developed thiocyanate dye on cell stability is not sufficiently researched, so it should be performed and fundamental cause of ligand exchange is also investigated.

Schematic representations illustrate the effect of the TiO_2-coating layer (Fig. 2-17). This coating layer not only reduces the recombination and formation of Zn^{2+}/dye complexes, but also preserves the relatively large surface area. These results directly influence the improved V_{oc}, J_{sc}, and *FF* compared with the bare cell.

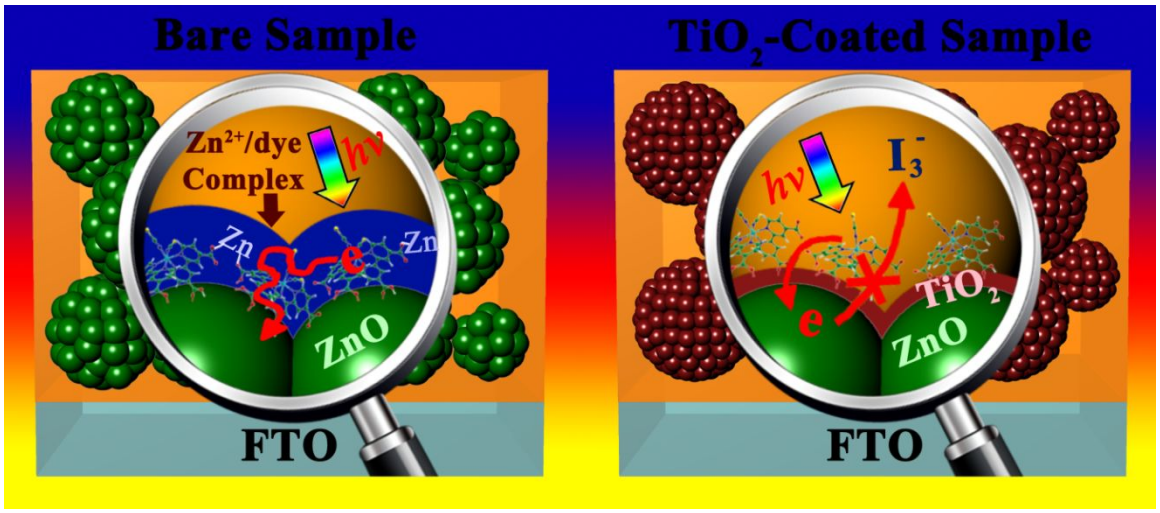

Fig. 2-17. (Color) Schematic figures for the effect of TiO_2-coating layer on the performance of ZnO-based dye-sensitized solar cells.

2.4. Conclusion

In this chapter, I reduced the interface recombination which is one of severe problems to be solved in metal oxide of DSSCs through TiO_2 coating on ZnO electrode. The surface coating of nanostructured metal oxide with other metal oxide is an easy and low-cost technique among interface control methods and it has strong points that take both advantages of inner and outer metal oxide materials. Because the inner material transports electrons through their network and determines cell voltage from differences between its Fermi level and redox potential of electrolyte, ZnO that has fast mobility and higher position of conduction band is chosen for nanostructured material. On account of the direct contact of outer material with dyes, TiO_2 that has strong acidic stability and fast electron injection property is selected as a coating material. TiO_2 is outstanding choice for surface coating material because ZnO is dissolved in acidic environment and forms a complex with a dye that cannot transport electrons effectively when it covers the ZnO surface. The stability against acidic environment is much improved by surface coating with TiO_2 and it is proved from preservation of established porous ZnO nanostructures after extreme dye immersion time of 6 h.

While this experiment, the most curious points for me were the possibility of TiO_2 coating to the inside of porous nanostructure and uniform coating of TiO_2 on ZnO through the simple dipping method. To investigate the doubtful points, I should figure out whether nanoporous ZnO spheres maintain their porous structure into the core part. From the formation process of nanoporous ZnO spheres, I found that the nanoporous ZnO spheres are composed of each nanoparticle not the form closed pores through grain growth of nanoparticles. Nanoporous ZnO spheres keep their nanoparticle shapes or sizes although micron-sized secondary aggregates collapse when synthesis temperature is much higher than that of the aggregates formation. This is also supported in my study from grain or particle size from XRD and TEM analysis. When compared the sizes of expected pore and a Ti precursor, penetration and diffusion of Ti precursors into core part of porous structure are expected; however, I leave to be desired that more accurate pore size or surface area can be obtained if BET measurement is additionally conducted in my experimental system.

I think TEM is the most obvious and visible analysis to investigate the coating thickness or growth morphology of TiO_2 on ZnO. Therefore, I tried TEM analysis with a sample cut into thin slice using FIB to investigate middle of micron sized ZnO spheres not the only nanoparticles situated at outer part. But it is hard to observe the TiO_2 on ZnO by TEM and the reasons might be that TiO_2 is too thin to detect or hard to focus because TiO_2 is on the spherical shape of ZnO, or removed from strong gallium ion beam. Although TEM analysis is specialized for local part not the entire part, I leave regret that cannot observe the TiO_2-coating layer directly and I look forward to precise observation of the TiO_2 layer with samples that is coated longer time than 1 h, for instance 2 h or more.

To investigate the possibility of uniform TiO_2 coating on ZnO, I approached with surface free energy perspective and confirm the possibility of layer-by-layer growth of TiO_2 from comparison of energy values of surface free energy and interphase interfacial energy. Although this approach is based on thermodynamic equilibrium conditions, I think it is worthful because thermodynamically possibility is the most basic step for possibility of realization. And I also convinced that this approach is right direction from practical results of uniform TiO_2 layer on ZnO [66-70].

Also, another interesting result is increased V_{oc} and *FF* of the cell as time goes on. Many studies about interface control or morphology change of metal oxide focus on the efficiency enhancement. I think the ultimate objective of all DSSC studies is practical use on the roof, operation stability is also important without degradation for 10 to 20 years. Although I measure the stability of the cell for two weeks short term, it shows decreased efficiency with 15% and increased V_{oc} and *FF*. I think decreased efficiency with increased V_{oc} means something happened during cell working, not simply cell degradation from extended exposure to sun light. The exchange of SCN ligand of the dye with iodide in electrolyte is the most generally accepted reason according to literature survey. It is very surprising that about 75% of tri-iodide in electrolyte is decreased even if the value is obtained from a simple assumption. It indicates that things to be improved in a research area of dye or electrolyte are also inexhaustible to obtain the higher efficiency and use for 20 years.

2.5. References

1. B. O'Regan and M. Grätzel, "A Low-Cost, High-Efficiency Solar Cell Based on Dye-Sensitized Colloidal TiO_2 Films," *Nature* **353**, 737(1991).
2. J. M. Kroon, N. J. Bakker, H. J. P. Smit, P. Liska, K. R. Thampi, P. Wang, S. M. Zakeeruddin, M. Grätzel, A. Hinsch, S. Hore, U. Würfel, R. Sastrawan, J. R. Durrant, E. Palomares, H. Pettersson, T. Gruszecki, J. Walter, K. Skupien, and G. E. Tulloch, "Nanocrystalline Dye-Sensitized Solar Cells Having Maximum Performance,"*Prog. Photovoltaics* **15(1)**, 1 (2007).
3. A. Yella, H. W. Lee, H. N. Tsao, C. Yi, A. K. Chandiran, M. K. Nazeeruddin, E. W. G. Diau, C. Y. Yeh, S. M. Zakeeruddin, and M. Grätzel, "Porphyrin-Sensitized Solar Cells with Cobalt (II/III)-Based Redox Electrolyte Exceed 12 Percent Efficiency," *Science* **334**, 629 (2011).
4. E. M. Kaidashev, M. Lorenz, H. Wenckstern, A. Rahm, H. C. Semmelhack, K. H. Han, G. Benndorf, C. Bundesmann, H. Hochmuth, and M. Grundmann, "High Electron Mobility of Epitaxial ZnO Thin Films on *c*-Plane Sapphire Grown by Multistep Pulsed-Laser Deposition," *Appl. Phys. Lett.* **82**, 3901 (2003).
5. E. Hendry, F. Wang, J. Shan, T. F. Heinz, and M. Bonn, "Electron Transport in TiO_2 Probed by THz Time-Domain Spectroscopy," *Phys. Rev. B* **69**, 081101 (2004).
6. H. Tang, K. Prasad, R. Sanjinès, P. E. Schmid, and F. Lévy, "Electrical and Optical Properties of TiO_2 Anatase Thin Films," *J. Appl. Phys.* **75**, 2042 (1994).
7. K. Keis, L. Vayssieres, H. Rensmo, S. E. Lindquist, and A. Hagfeldt, "Photoelectrochemical Properties of Nano- to Microstructured ZnO Electrodes," *J. Electrochem. Soc.* **148**, A149 (2001).
8. S. M. Prokes, J. L. Gole, X. B. Chen, C. Burda, and W. E. Carlos, "Defect-Related Optical Behavior in Surface Modified TiO_2 Nanostructures, " *Adv. Funct. Mater.* **15**, 161 (2005).
9. E. Meulenkamp, "Synthesis and Growth of ZnO Nanoparticles," *J. Phys. Chem. B* **102**, 5566 (1998).
10. S. Kar, A. Dev, and S. Chaudhuri, "Simple Solvothermal Route To Synthesize ZnO Nanosheets, Nanonails, and Well-Aligned Nanorod Arrays," *J. Phys. Chem. B* **110**, 17848 (2006).

11. Q. C. Li, V. Kumar, Y. Li, H. T. Zhang, T. J. Marks, and R. P. H. Chang, "Fabrication of ZnO Nanorods and Nanotubes in Aqueous Solutions," *Chem. Mater.* **17**, 1001 (2005).

12. X. D. Wang, Y. Ding, C. J. Summers, and Z. L. Wang, "Large-Scale Synthesis of Six-Nanometer-Wide ZnO Nanobelts," *J. Phys. Chem. B* **108**, 8773 (2004).

13. M. Fu, J. Zhou, Q. F. Xiao, B. Li, R. L. Zong, W. Chen, and J. Zhang, "ZnO Nanosheets with Ordered Pore Periodicity via Colloidal Crystal Template Assisted Electrochemical Deposition," *Adv. Mater.* **18**, 1001 (2006).

14. Z. L. Wang, "Zinc Oxide Nanostructures: Growth, Properties and Applications," *J. Phys. Condens. Matter* **16**, R829 (2004).

15. M. Vafaee and M. S. Ghamsari, "Preparation and Characterization of ZnO Nanoparticles by a Novel Sol–Gel Route," *Mater. Lett.* **61**, 3265 (2007).

16. P. D. Yang, H. Q. Yan, S. Mao, R. Russo, J. Johnson, R. Saykally, N. Morris, J. Pham, R. R. He, and H. J. Choi, "Controlled Growth of ZnO Nanowires and Their Optical Properties," *Adv. Funct. Mater.* **12**, 323 (2002).

17. K. Nonomura, T. Yoshida, D. Schlettwein, and H. Minoura, "One-Step Electrochemical Synthesis of ZnO/$Ru(dcbpy)_2(NCS)_2$ Hybrid Thin Films and Their Photoelectrochemical Properties," *Electrochim. Acta* **48**, 3071 (2003).

18. H. H. Wang and C. S. Xie, "Controlled Fabrication of Nanostructured ZnO Particles and Porous Thin Films via a Modified Chemical Bath Deposition Method," *J. Cryst. Growth* **291**, 187 (2006).

19. N. Memarian, I. Concina, A. Braga, S. M. Rozati, A. Vomiero, and G. Sberveglieri, "Hierarchically Assembled ZnO Nanocrystallites for High-Efficiency Dye-Sensitized Solar Cells," *Angew. Chem. Int. Ed.* **50**, 12317 (2011).

20. N. A. Anderson, X. Ai, and T. J. Lian, "Electron Injection Dynamics from Ru Polypyridyl Complexes to ZnO Nanocrystalline Thin Films," *J. Phys. Chem. B* **107**, 14414 (2003).

21. K. Keis, J. Lindgren, S. E. Lindquist, and A. Hagfeldt, "Studies of the Adsorption Process of Ru Complexes in Nanoporous ZnO Electrodes," *Langmuir* **16**, 4688 (2000).

22. H. Horiuchi, R. Katoh, K. Hara, M. Yanagida, S. Murata, H. Arakawa, and M. Tachiya, "Electron Injection Efficiency from Excited N3 into Nanocrystalline ZnO Films: Effect of (N3-Zn^{2+}) Aggregate Formation," *J. Phys. Chem. B* **107**, 2570 (2003).

23. J. C. Guo, C. X. She, and T. Q. Lian, "Effect of Insulating Oxide Overlayers on Electron Injection Dynamics in Dye-Sensitized Nanocrystalline Thin Films," J. *Phys. Chem. C* **111**, 8979 (2007).

24. E. Palomares, J. N. Clifford, S. A. Haque, T. Lutz, and J. R. Durrant, "Control of Charge Recombination Dynamics in Dye Sensitized Solar Cells by the Use of Conformally Deposited Metal Oxide Blocking Layers," *J. Am. Chem. Soc.* **125**, 475 (2003).

25. S. Wu, H. W. Han, Q. D. Tai, J. Zhang, S. Xu, C. H. Zhou, Y. Yang, H. Hu, B. L. Chen, B. Sebo, and X. Z. Zhao, "Enhancement in Dye-Sensitized Solar Cells Based on MgO-Coated TiO_2 Electrodes by Reactive DC Magnetron Sputtering," *Nanotechnology* **19**, 215704 (2008).

26. S. G. Chen, S. Chappel, Y. Diamant, and A. Zaban, "Preparation of Nb_2O_5 Coated TiO_2 Nanoporous Electrodes and Their Application in Dye-Sensitized Solar Cells," *Chem. Mater.***13**, 4629 (2001).

27. Y.-J. Shin, J.-H. Lee, J.-H. Park, and N.-G. Park, "Enhanced Photovoltaic Properties of SiO_2-treated ZnO Nanocrystalline Electrode for Dye-sensitized Solar Cell," *Chem. Lett.* **36**, 1506 (2007).

28. D. B. Menzies, Q. Dai, L. Bourgeois, R. A. Caruso, Y. B. Cheng, G. P. Simon, and L. Spiccia, "Modification of Mesoporous TiO_2 Electrodes by Surface Treatment with Titanium(IV), Indium(III) and Zirconium(IV) Oxide Precursors: Preparation, Characterization and Photovoltaic Performance in Dye-Sensitized Nanocrystalline Solar Cells," *Nanotechnology* **18**, 125608 (2007).

29. K. Park, Q. Zhang, B. B. Garcia, X. Zhou, Y.-H. Jeong, and G. Cao, "Effect of an Ultrathin TiO_2 Layer Coated on Submicrometer-Sized ZnO Nanocrystallite Aggregates by Atomic Layer Deposition on the Performance of Dye-Sensitized Solar Cells," *Adv. Mater.* **22**, 1 (2010).

30. P. T. Ishwara, B. N. Illy, M. P. Ryan, B. C. O'Regan, J. R. Durrant and J. Nelson, "Control of Photocurrent Generation in Polymer/ZnO Nanorod Solar Cells by Using a Solution-Processed

TiO_2 Overlayer," *J. Phys. Chem. Lett.* **1**, 708 (2008).

31. N. Sakai, N. Kawashima, and T. N. Murakami, "Effect of $TiCl_4$ Treatment on Porous ZnO Photoelectrodes for Dye-sensitized Solar Cells," *Chem. Lett.* **40**, 162 (2011).
32. Q. Zhang, T. P. Chou, B. Russo, S. A. Jenekhe, and G. Cao, "Aggregation of ZnO Nanocrystallites for High Conversion Efficiency in Dye-Sensitized Solar Cells," *Angew. Chem. Int. Ed.* **47**, 2402 (2008).
33. H. Li, Z. Xie, Y. Zhang, and J. Wang, "The Effects of Ethyl Cellulose on PV Performance of DSSC Made of Nanostructured ZnO Pastes," *Thin Solid Films* **518**, E68 (2010).
34. Y. Park, B. Lee, C. Kim, J. Kim, S. Nam, Y. Oh, and B. Park, "Modification of Gold Catalysis with Aluminum Phosphate for Oxygen-Reduction Reaction," *J. Phys. Chem. C* **114**, 3688 (2010).
35. B. Kim, C. Kim, T. G. Kim, D. Ahn, and B. Park, "The Effect of AlPO-Coating Layer on the Electrochemical Properties in LiCoO Thin Films," *J. Electrochem. Soc.* **153**, A1773 (2006).
36. J. Cho, Y. W. Kim, B. Kim, J. G. Lee, and B. Park, "A Breakthrough in the Safety of Lithium Secondary Batteries by Coating the Cathode Material with $AlPO_4$ Nanoparticles," *Angew. Chem. Int. Ed.* **42**, 1618 (2003).
37. A. B. F. Martinson, J. W. Elam, J. T. Hupp, and M. J. Pellin, "ZnO Nanotube Based Dye-Sensitized Solar Cell," *Nano Lett.* **7**, 2183 (2007).
38. M. Saito and S. Fujihara, "Large Photocurrent Generation in Dye-Sensitized ZnO Solar Cells," *Energy Environ. Sci.* **1**, 280 (2008).
39. S. B. Ambadea, R. S. Mane, S. H. Han, S. H. Lee, M. M. Sung, and O. S. Joo, "Indoline-Dye Immobilized ZnO Nanoparticles for Whopping 5.44% Light Conversion Efficiency," *J. Photochem. Photobiol. A* **222**, 366 (2011).
40. S. Yodyingyong, Q. Zhang, K. Park, C. S. Dandeneau, X. Zhou, D. Triampo, and G. Cao, "ZnO Nanoparticles and Nanowire Array Hybrid Photoanodes for Dye-Sensitized Solar Cells," *Appl. Phys. Lett.* **96**, 073115 (2010).
41. C. Suryanarayana and M. G. Norton, *X-Ray Diffraction: A Practical Approach*, New York, (1998).

42. K. Park, Q. Zhang, B. B. Garcia, and G. Cao, "Effect of Annealing Temperature on TiO_2-ZnO Core−Shell Aggregate Photoelectrodes of Dye-Sensitized Solar Cells," *J. Phys. Chem. C* **115**, 4927 **(**2011).

43. T. Moon, S. Hwang, D. Jung, D. Son, C. Kim, J. Kim, M. Kang, and B. Park, "Hydroxyl-Quenching Effects on the Photoluminescence Properties of SnO_2:Eu^{3+} Nanoparticles," *J. Phys. Chem. C* **111**, 4164 (2007).

44. J. L. Gole, S. M. Prokes, and O. J. Glembocki, "Efficient Room-Temperature Conversion of Anatase to Rutile TiO_2 Induced by High-Spin Ion Doping," *J. Phys. Chem. C* **112**, 1782 (2008).

45. B. D. Cullity and S. R. Stock, "Elements of X-Ray Diffraction", Prentice-Hall Inc. 3rd edition (2001).

46. R. Jenkins and R. L. Snyder, "Introduction to X-ray Powder Diffractometry", John Wiley & Sons Inc. (1996).

47. C. Su, B.-Y. Hong, and C.-M. Tseng, "Sol-Gel Preparation and Photocatalysis of Titanium Dioxide," Catalysis Today 96, 119 (2004).

48. S.-W. Zhang, "Tribology of Elastomers," *Elsvier* (2004).

49. Q. Zhang, T. P. Chou, B. Russo, S. A. Jenekhe, and G. Cao, "Polydisperse Aggregates of ZnO Nanocrystallites: A Method for Energy-Conversion-Efficiency Enhancement in Dye-Sensitized Solar Cells," *Adv. Funct. Mater*. **18**, 1654 (2008).

50. S. D. Athar and H. Asilian, "Catalytic Oxidation of Carbon Monoxide Using Copper-Zinc Mixed Oxide Nanoparticles Supported on Diatomite," *J Health Scope*. **1**, 52 (2012).

51. S. Kaluza, M. K. Schrőter, R. N. d'Alnoncourt, T. Reinecke, and M. Muhler, "High Surface Area ZnO Nanoparticles via a Novel Continuous Precipitation Route," *Adv. Funct. Mater*. **18**, 3670 (2008).

52. Yan-Zhen Zheng, Jia-Xing Zhao,Shi-Qing Bi, and Xia Tao, Meilan Huang, and Jian-Feng Chen, "Dual Interfacial Modifications of Hierarchically Structured Iodine-Doped ZnO Photoanodes for High-efficiency dye-sensitized solar cells," *Electrochim. Acta* **157**, 258 (2015).

53. R. Gao, Z. Liang, J. Tian, Q. Zhang, L. Wang, and G. Cao, "ZnO Nanocrystallite Aggregates Synthesized Through Interface Precipitation for Dye-Sensitized Solar Cells," *Nano Energy* **2**, 40 (2013).

54. K. Kakiuchi, E. Hosono, and S. Fujihara, "Enhanced Photoelectrochemical Performance of ZnO Electrodes Sensitized with N-719," *J. Photochem. Photobiol. A* **179**, 81 (2006).

55. C. C. Weigand "Zinc Oxide Nanostructures and Thin Films Grown by Plused Laser Deposition," *Ph.D. Thesis* (Norwegian univ.) (2012).

56. T.-J. Park, A. A. Levchenko, H. Zhou, S. S. Wong, and A. Navrotsky, "Shape-Dependent Surface Energetics of Nanocrystalline TiO_2," *J. Mater. Chem.* **20**, 8639 (2010).

57. J. W. Martin, R. D. Doherty, and B. Cantor, "Stability of Microstructure in Metallic Systems: second edition," Cambridge, UK (1997)

58. P. Zhang, F. Xu, A. Navrotsky, J. S. Lee, S. Kim, and J. Liu, "Surface Enthalpies of Nanophase ZnO with Different Morphologies," *Chem. Mater.* **19**, 5687 (2007).

59. D. A. Porter, "Phase Transformations in Metals and Alloys," *CRC Press* 3rd.

60. C. Ma, Q. Shi, B. F. Woodfield, and A. Navrotsky, "Low Temperature Heat Capacity of Bulk and Nanophase ZnO and $Zn_{1-x}Co_xO$ Wurtzite Phases," *J. Chem. Thermo.* **60**, 191 (2013).

61. F. Xu, P. Zhang, A. Navrotsky, Z.-Y. Yuan, T.-Z. Ren, M. Halasa, and B.-L. Su, "Hierarchically Assembled Porous ZnO Nanoparticles: Synthesis, Surface Energy, and Photocatalytic Activity," *Chem. Mater.* **19**, 23 (2007).

62. A. A. Levchenko, G. Li, J. Boerio-Goates, B. F. Woodfield, and A. Navrotsky, "TiO_2 Stability Landscape: Polymorphism, Surface Energy, and Bound Water Energetics," *Chem. Mater.* **18**, 6324 (2006).

63. M. Lazzeri, A. Vittadini, and A. Selloni, "Structure and Energetics of Stoichiometric TiO_2 Anatase Surfaces," *Phys. Rev. B* **63**, 155409 (2002).

64. B. Meyer and D. Marx, "Density-Functional Study of the Structure and Stability of ZnO Surfaces," *Phys. Rev. B* **67**, 035403 (2003).

65. G. C. Yi, "Semiconductor Nanostructures for Optoelecronic Devices," *springer*.

66. A. S. Barnard, P. Zapol, and L. A. Curtiss, "Modeling the Morphology and Phase Stability of TiO_2 Nanocrystals in Water," *J. Chem. Theory Comput.* **1**, 107 (2005).

67. E. S. Machlin, "Aspects of Thermodynamics and Kinetics Relevant to Materials Science," *Elsevier.*

68. A. R. Miedema and F. J. A. den Broeder, "On the Interfacial Energy in Solid-Liquid and Solid-Solid Metal Combinations" *Z. Metallkd.* **70**, 14 (1979)

69. F. Gu, L. Gai, W. Shao, C. Li, and L. Schmidt-Mende, "Heteroepitaxial Growth of ZnO Branches Selectively on TiO_2 Nanorodtips with Improved Light Harvesting Performance," *Chem. Commun.* 47, 8400 (2011).

70. A. Irannejad, K. Janghorban, O. K. Tan, H. Huang, C. K. Lim, P. Y. Tan, X. Fang, C.S. Chua, S. Maleksaeedi, S. M. H. Hejazi, M. M. Shahjamali, and M. Ghaffari, "Effect of the TiO_2 Shell Thickness on the Dye-Sensitized Solar Cells with ZnO-TiO_2 Core-Shell Nanorod Electrodes," *Electrochim. Acta* **58**, 19 (2011).

71. I.-L. Hsiao and Y.-J. Huang, "Titanium Oxide Shell Coatings Decrease the Cytotoxicity of ZnO Nanoparticles," *Chem. Res. Toxicol.* **24(3)**, 303 (2011).

72. Y.-Z. Gu, H.-L. Lu, Y. Geng, Z.-Y. Ye, Y. Zhang, Q.-Q. Sun, S.-J. Ding, and D. W. Zhang, "Optical and Microstructural Properties of ZnO/TiO_2 Nanolaminates Prepared by Atomic Layer Deposition," *Nanoscale Res Lett.* **8(1)**, 107 (2013).

73. T. P. Chou, Q. Zhang, and G. Cao "Effects of Dye Loading Conditions on the Energy Conversion Efficiency of ZnO and TiO_2 Dye-Sensitized Solar Cells," *J. Phys. Chem. C* **111**, 18804 (2007).

74. B. Yoo, K. J. Kim, S. Y. Bang, M. J. Ko, K. Kim, and N. G. Park, "Chemically Deposited Blocking Layers on FTO Substrates: Effect of Precursor Concentration on Photovoltaic Performance of Dye-Sensitized Solar Cells," *J. Electroanal. Chem.* **638**, 161 (2010).

75. H. Choi, C. Nahm, J. Kim, J. Moon, S. Nam, C. Kim, D.-R. Jung, and B. Park, "The Effect of $TiCl_4$-Treated TiO_2 Compact Layer on the Performance of Dye-Sensitized Solar Cell," *Curr. Appl. Phys.* **12**, 737 (2012).

76. J. Kim, H. Choi, C. Nahm, C. Kim, S. Nam, S. Kang, D.-R. Jung, J. I. Kim, J. Kang, and B. Park, "The Role of a $TiCl_4$ Treatment on the Performance of CdS Quantum-Dot-Sensitized Solar Cells," *J. Power Sources* **220**, 108 (2012).

77. C. H. Lin, S. Chattopadhyay, C. W. Hsu, M. H. Wu, W. C. Chen, C. T. Wu, S. C. Tseng, J. S. Hwang, J. H. Lee, C. W. Chen, C. H. Chen, L. C. Chen, and K. H. Chen, "Enhanced Charge Separation by Sieve-Layer Mediation in High-Efficiency Inorganic-Organic Solar Cells," *Adv. Mater.* **21**, 759 (2009).

78. L. Larina, D. Shin, J. H. Kim, and B. T. Ahn, "Alignment of Energy Levels at the ZnS/Cu(In,Ga)Se_2 Interface," *Energy Environ. Sci.* **4**, 3487 (2011).

79. S. W. Boettcher, E. L. Warren, M. C. Putnam, E. A. Santori, D. Turner-Evans, M. D. Kelzenberg, M. G. Walter, J. R. McKone, B. S. Brunschwig, H. A. Atwater, and N. S. Lewis, "Photoelectrochemical Hydrogen Evolution Using Si Microwire Arrays," *J. Am. Chem. Soc.* **133**, 1216 (2011).

80. A. Irannejad, K. Janghorban, O. K. Tan, H. Huang, C. K. Lim, P. Y. Tan, X. Fang, C. S. Chua, S. Maleksaeedi, S. M. H. Hejazi, M. M. Shahjamali, and M. Ghaffari, "Effect of the TiO_2 Shell Thickness on the Dye-Sensitized Solar Cells with ZnO–TiO_2 Core-Shell Nanorod Electrodes," *Electrochim. Acta* **58**, 19 (2011).

81. M. Law, L. E. Greene, A. Radenovic, T. Kuykendall, J. Liphardt, and P. Yang, "ZnO−Al_2O_3 and ZnO−TiO_2 Core−Shell Nanowire Dye-Sensitized Solar Cells," *J. Phys. Chem. B* **110**, 22652 (2006).

82. A. Mihi, C. Zhang, and P. V. Braun, "Transfer of Preformed Three-Dimensional Photonic Crystals onto Dye-Sensitized Solar Cells," *Angew. Chem. Int. Ed.* **50**, 5712 (2011).

83. A. Zaban, M. Greenshtein, and J. Bisquert, "Determination of the Electron Lifetime in Nanocrystalline Dye Solar Cells by Open-Circuit Voltage Decay Measurements," *ChemPhysChem* **4**, 864 (2003).

84. J. Bisquert, A. Zaban, M. Greenshtein, and I. Mora-Seró, "Determination of Rate Constants for Charge Transfer and the Distribution of Semiconductor and Electrolyte Electronic Energy Levels

in Dye-Sensitized Solar Cells by Open-Circuit Photovoltage Decay Method," *J. Am. Chem. Soc.* **126**, 13550 (2004).

85. J. Kim, H. Choi, C. Nahm, J. Moon, C. Kim, S. Nam, D.-R. Jung, and B. Park, "The Effect of a Blocking Layer on the Photovoltaic Performance in CdS Quantum-Dot-Sensitized Solar Cells," *J. Power Sources* **196**, 10526 (2011).
86. R. Viswanatha, S. Sapra, B. Satpati, P. V. Satyam, B. N. Dev, and D. D. Sarma, "Understanding the Quantum Size Effects in ZnO Nanocrystals," *J. Mater. Chem.* **14**, 661 (2004).
87. X. Z. Guo, Y. D. Zhang, Y. H. Qin, Y. H. Luo, D. M. Li, Y. T. Pang, and Q. B. Meng, "Hybrid Tandem Solar Cell for Concurrently Converting Light and Heat Energy with Utilization of Full Solar Spectrum," *J. Power Sources* **195**, 7684 (2010).
88. M. Toivola, J. Halme, L. Peltokorpi, and P. Lund, "Investigation of Temperature and Aging Effects inNanostructured Dye Solar Cells Studied by ElectrochemicalImpedance Spectroscopy," *Journal of Photoenergy* 786429 (2009).
89. G. Xue, Y. Guo, T. Yu, J. Guan, X. Yu, J. Zhang, J. Liu, and Z. Zou, "Degradation Mechanisms Investigation for Long-term Thermal Stability of Dye-Sensitized Solar Cells," *Int. J. Electrochem. Sci.* **7**, 1496 (2012).
90. H. Greijer, J. Lindgren, and A. Hagfeldt. "Resonance Raman Scattering of a Dye-Sensitized Solar Cell: Mechanism of Thiocyanato Ligand Exchange," *J. Phys. Chem. B* **105**, 6314 (2001).
91. S. Y. Huang, G. Schlichthorl, A. J. Nozik, M. Gratzel, and A. J. Frank, "Charge Recombination in Dye-Sensitized Nanocrystalline TiO_2 Solar Cells," *J. Phys. Chem. B* **101(14)**, 2676 (1997).
92. C. Wu, Y. Gong, S. Han, T. Jin, B. Chi, J. Pua, L. Jian, "Electrochemical Characterization of a Novel Iodine-Free Electrolyte for Dye-Sensitized Solar Cell," *Electrochim. Acta* **71**, 33 (2012).
93. H. Kisserwan and T. H. Ghaddar, "Enhancement of Photocurrent in Dye Sensitized Solar Cells Incorporating a Cyclometalated Ruthenium Complex with Cuprous Iodide as an Electrolyte Additive," *Dalton Transactions* **40**, 3877 (2011).
94. K. L.Wu, H. C. Hsu, and K. Chen, "Development of Thiocyanate-Free, Charge-Neutral Ru(II) Sensitizers for Dye-Sensitized Solar Cells," *Chem. Commun.* **46**, 5124 (2010).

Chapter 3.

* Improving Scattering Layer through Mixture of Nanoporous Spheres and Nanoparticles in ZnO-Based Dye-Sensitized Solar Cells

3.1. Introduction

Dye-sensitized solar cells (DSSCs) have shown promising potential as an alternative to Si thin-film solar cells because of low fabrication cost and relatively high efficiency [1,2]. Efficient utilization of sunlight is greatly important in photovoltaic systems for high efficiency. Therefore, there have been many studies on the scattering layer to fully utilize incident light inside solar cells by using different morphology and size of scatterers in TiO_2-based DSSCs [3-10]. Despite of the advantages of ZnO such as higher carrier mobility and fabrication easiness for various nanostructures, studies were limited on scattering layer for ZnO-based DSSCs [11-15].

Among various nanostructures, hundred-nanometer-sized nanoporous spheres provide both effective light scattering and large surface area [16]. X. Tao's group and W. Que's group have reported on the scattering layer consisting of nanoporous spheres [17,18]. While they have shown improvements on the scattering effect, large voids between spheres leave the possibility of providing more available surface area where dye can be attached, and better charge transport by improved percolation of large-sized spheres should be achieved.

In this paper, I report the improvements of scattering layers using a mixture of nanoparticles and nanoporous spheres. Nanoporous spheres act as effective light scatterers with the large surface area, and nanoparticles favor both efficient charge transport and an additional surface area.

---

*The work presented in Chapter. 3 was published in *Nanoscale Res. Lett.* **9**, 295 (2014) entitled,

"Improving Scattering Layer through Mixture of Nanoporous Spheres and Nanoparticles in ZnO-Based Dye-Sensitized Solar Cells"

Chohui Kim, Hongsik Choi, Jae Ik Kim, Sangheon Lee, Jinhyun Kim, Woojin Lee, Taehyun Hwang, Suji Kang, Taeho Moon,* and Byungwoo Park*

3.2. Experimental Section

The ZnO nanoporous spheres were synthesized by using zinc acetate dihydrate (0.01 M, $Zn(CH_3COO)_2 \cdot 2H_2O$: Sigma-Aldrich) and diethylene glycol ($(HOCH_2CH_2)_2O$: Sigma-Aldrich) in an oil bath at 160°C for 6 h with vigorous stirring at 500 rpm [16]. A reflux condenser was used to prevent the solvent from boiling away. After washing centrifuged ZnO nanoporous spheres powders with anhydrous ethanol two times, ZnO nanoporous spheres (NS) and ZnO nanoparticle (NP) (721085: Sigma-Aldrich) were mixed to the weight ratios of NP to NS of 10:0, 7:3, 5:5, 3:7, and 0:10. Anhydrous ethanol was used for solvent and 0.5 g of cellulose ($(C_6H_{10}O_5)_n$: Aldrich) was added at each mixing condition. The paste stirred on a hot plate at 150 rpm and 40°C for one day.

To fabricate bilayer-structured electrodes, a only ZnO nanoparticles (NP:NS = 10:0) paste was first spread on a fluorine-doped tin oxide substrate (FTO, TEC 8: Pilkington) covered with dense TiO_2-blocking layer by sputtering. The deposition was performed using TiO_2 target with an operating pressure of 3 mTorr, rf power of 100 W, and deposition time of 30 min at RT under Ar atmosphere. The bottom layer was deposited by doctor-blade method using one layer of punched Scotch tape and dried on hot plate at 60°C for 10 min. After solvent evaporation, the mixed pastes with various ratios of NS and NP were spread on top of the nanoparticle film by the same method mentioned above. The upper mixed layer was also fabricated with one layer of punched Scotch tape and bigger size than bottom layer to construct the uniform bilayer structure. The active area was 0.28 cm^2 and the as-deposited films were subsequently annealed at 350°C for 1 h.

The films were sensitized with 0.5 mM of N719 dye ($RuL_2(NCS)_2$:2TBA, L = 2,2'-bipyridyl-4,4'-dicarboxylic acid, TBA = tetrabutylammonium: Solaronix) dissolved in anhydrous ethanol for 30 min at RT. The sensitized electrode was washed with anhydrous ethanol and platinized counter electrode were sealed with thermoplastic foil (25 μm: DuPont, U.S.A.) on a hot plate at 100°C. When thermoplastic foil is transparent, pressure was applied between electrodes and cool down the cell to RT after adhesion. The gap between the two electrodes was filled with an iodide-based redox electrolyte (AN-50: Solaronix, Switzerland) with micropipette.

X-ray diffraction (XRD, M18XHF-SRA: Mac Science, Japan) was employed to analyze the

crystal structure of ZnO electrodes, and field-emission scanning electron microscopy (FE-SEM, SU70: Hitachi, Japan) was used to observe the morphology of bilayer-structured electrodes. The electrochemical properties were analyzed by a solar cell measurement system (K3000: McScience, Korea) under a solar simulator (Xenon lamp, air mass (AM) 1.5, 100 mW cm^{-2}). The extinction and diffused reflectance spectra were recorded on a UV/Vis spectrophotometer (Cary 5000: Agilent Technologies), and incident photon-to-current conversion efficiency (IPCE) spectra were measured by an IPCE measurement system (K3100: McScience, Korea). Electrochemical impedance spectra (EIS) were taken by using a potentiostat (CHI 608C: CH Instrumental Inc., Austin, U.S.A.) to analyze the kinetic parameters in the DSSCs [19-21].

3.3. Results and Discussion

Crystalline structures and grain sizes of ZnO nanoparticles and nanoporous spheres were analyzed by XRD (Fig. 3-1). The diffraction confirms the crystalline ZnO having hexagonal wurtzite structure (JCPDS #36-1451). From Williamson-Hall plots [22-24], synthesized ZnO nanoporous spheres are composed of ~35-nm-sized grains, while the grain size of the commercial ZnO nanoparticles is ~55 nm.

The ZnO-bilayer electrodes were sequentially prepared by the bottom layer made with only ZnO nanoparticles and the top-scattering layer fabricated with various mixing ratios of nanoparticles and nanoporous spheres. As shown in Fig. 3-2, the plan-view SEM images of the scattering layers indicate that the nanoparticles and nanoporous spheres are mixed uniformly, not aggregated separately. The diameter of nanoporous-sphere is approximately 150 - 500 nm, with the average size of ~300 nm. As the ratio of nanoporous spheres increases, void spaces in the film get larger. The cross-sectional SEM images show bilayer structures consisting of the nanoparticle bottom layer and mixed scattering upper layer, without any crushes at the interface. The average thickness of the bilayer films is approximately 5.5 μm, and the deviation is less than 10 percent. The poor connectivity among the ZnO nanoporous spheres with the decreased nanoparticle ratio is consistent with the plan-view SEM images.

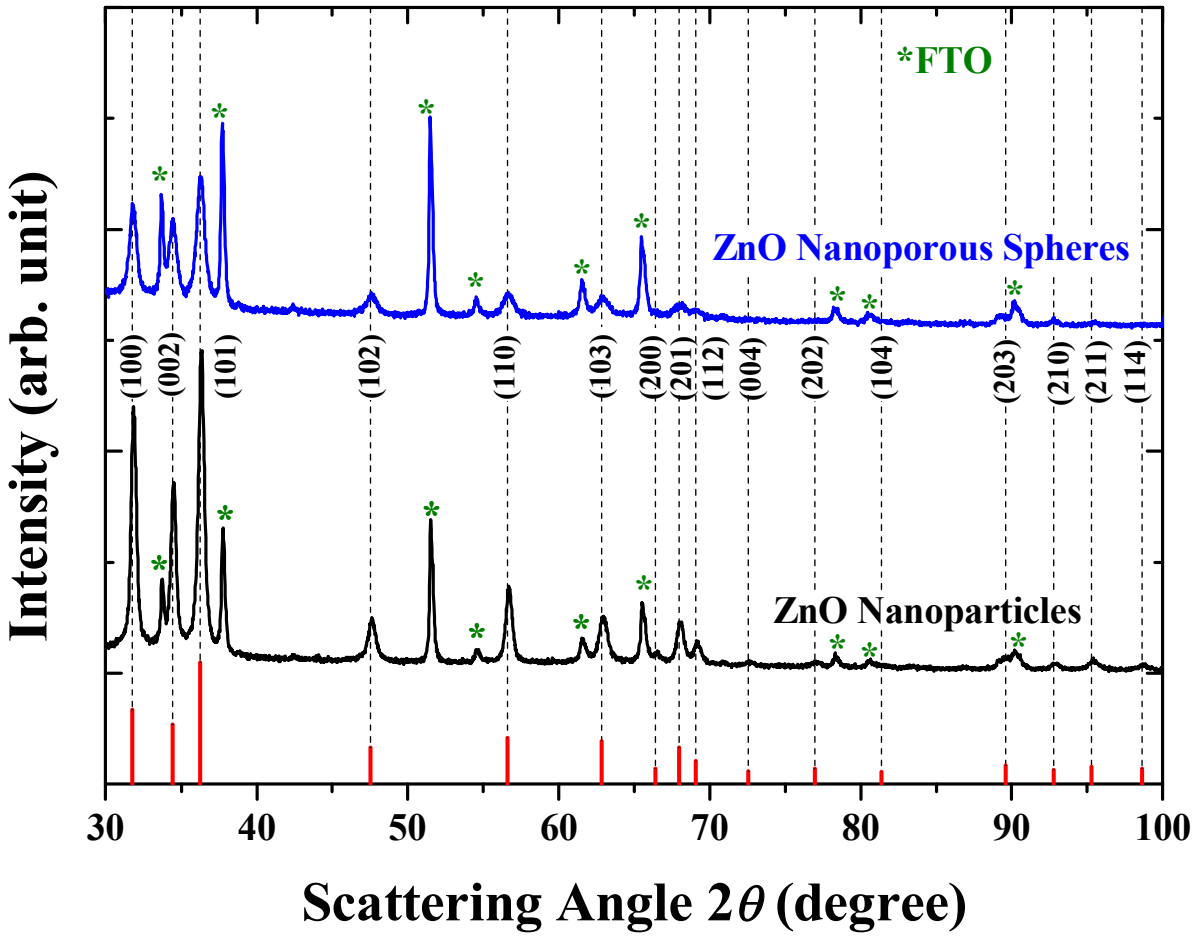

Fig. 3-1. (Color) X-ray diffraction of the ZnO films consisting of only nanoparticles or nanoporous spheres. The peak intensities and positions from the hexagonal ZnO (JCPDS #36-1451) are shown as solid lines.

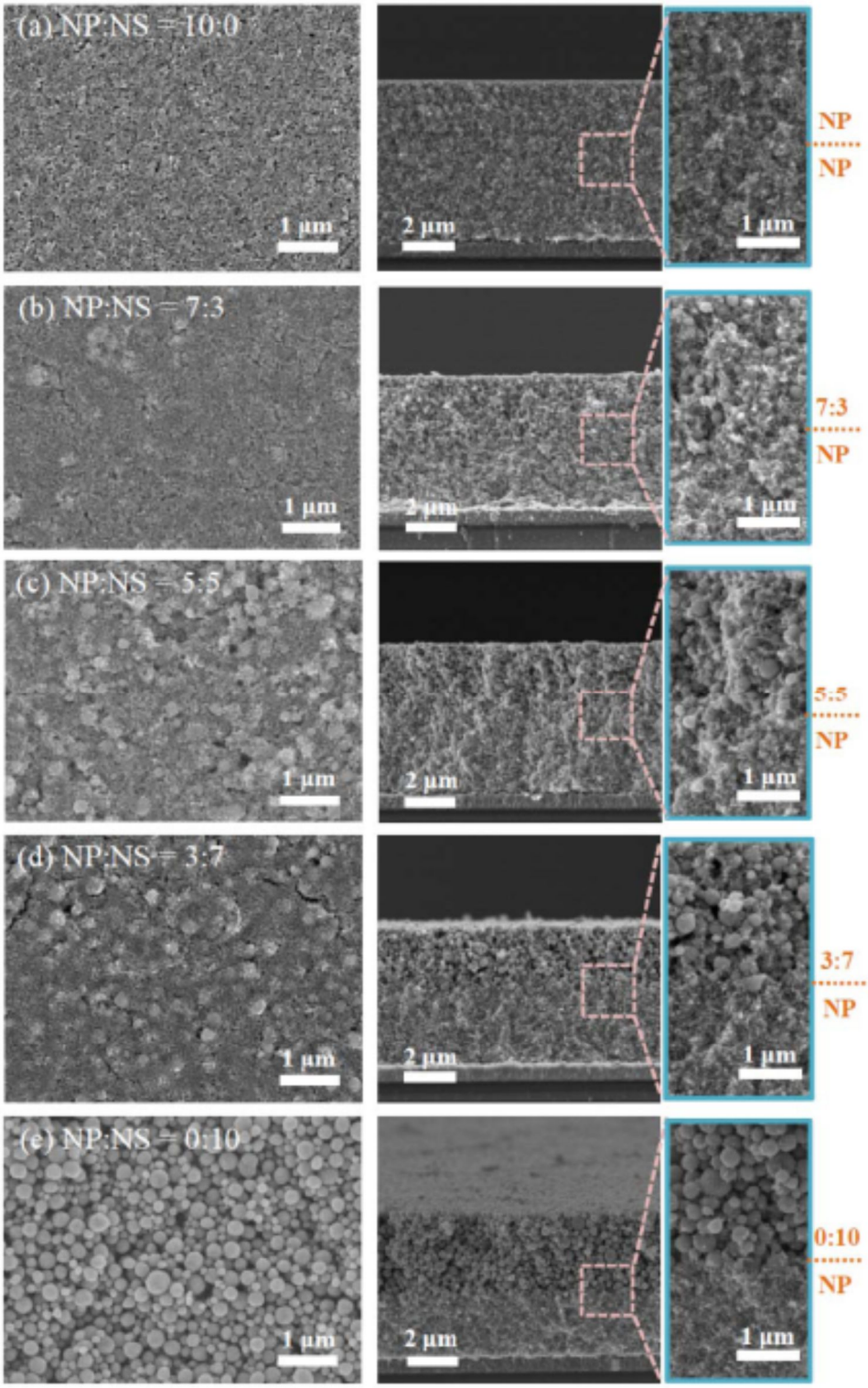

Fig. 3-2. (Color) Plan-view and cross-sectional SEM images of the ZnO-bilayer electrodes. The weight ratios of nanoparticle (NP) to nanoporous sphere (NS) for the top layers are (a) 10:0, (b) 7:3, (c) 5:5, (d) 3:7, and (e) 0:10, respectively. Blue labeled boxes are higher magnification for the bilayer interface.

To investigate the optical properties of the mixed scattering layer, the diffused reflectance of the bilayer films (without dye) were measured (Fig. 3-3(a)) [25,26]. With the increased nanoporous-sphere ratio, the diffused reflectance increases, indicating the better light-scattering ability of nanoporous spheres due to the comparable size to the visible light wavelength [27,28]. The optical images also confirm the scattering effect by the nanoporous spheres. Without dye, the film which consists of only nanoparticles has the weak scattering effect, and the green color of background transmitted clearly through the whole film. With the increase ratio of nanoporous spheres, the color of film is getting unclear and the color changes to totally white when the ratio reaches to NP:NS = 0:10. After dye adsorption, as the amount of nanoporous spheres increases, the color of the film is changed from transparent red to opacity pink. This observation shows the efficient scattering effect of the mixed bilayer obviously.

Furthermore, after dye adsorption, the NP:NS = 3:7 film shows the highest extinction (Fig. 3-3(b)). Especially when NP:NS = 3:7 film is compared to the NP:NS = 0:10 film, the higher extinction near the dye-absorption peak is more clear [29]. The results indicate an optimum condition for the surface area between void filling by nanoparticles and primary nanoporous spheres. The notable change in the curve shape for the NP:NS = 0:10 film (Figs. 3-3(a) and (b)) means that light scattering plays a role considerably for the adsorbed dye molecules [30].

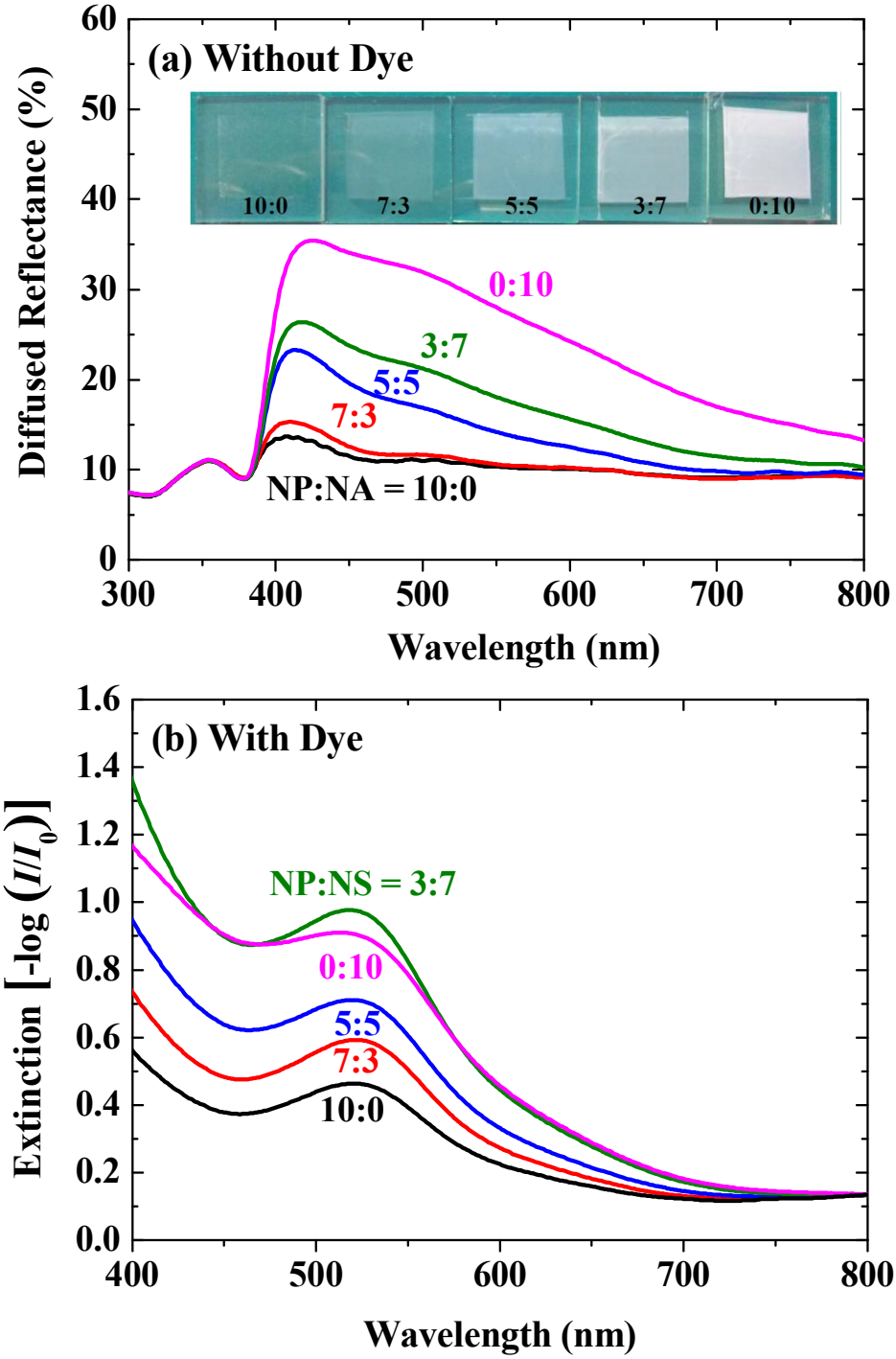

Fig. 3-3. (Color) (a) Diffused reflectance spectra and optical images of the ZnO-bilayer electrodes before dye loading with various mixing ratios. (b) Extinction spectra with dye loading.

The solar-cell performance of the DSSCs fabricated with the various ZnO-bilayer electrodes was investigated (Fig. 3-4(a)), and the parameters for each cell were summarized in Table 3-1. The mixed scattering layer improves the both short-circuit current (J_{sc}) and fill factor (FF), compared to the nanoparticle layer. In particular, the optimum power-conversion efficiency (η) of 2.91% is obtained at the ratio of NP:NS = 3:7, and the trend of η is generally consistent with that of J_{sc}. The J_{sc} value of NP:NS = 5:5 is higher than that of NP:NS = 0:10, however, this shows the opposite tendency with extinction data. The extinction data (Fig. 3-3(b)) represents higher value in NP:NS = 0:10 than in NP:NS = 5:5, and this means NP:NS = 0:10 absorbs the more light due to the efficient scattering effect of nanoporous spheres. Nevertheless, the reason of the higher J_{sc} value of NP:NS = 5:5 would be the shorten electron path length due to the added nanoparticles between nanoporous spheres, resulted in the fast electron transport. Although NP:NS = 0:10 has more efficient scattering effect, recombination caused by relatively long electron path gives rise to reduction of J_{sc}. And also lower resistance value of the charge transport (R_{ct}) in impedance data (Fig. 3-5) supports that NP:NS = 5:5 has the fast electron transport.

The open-circuit voltage (V_{oc}) values are not notably changed among the cells except for the NP:NS = 3:7. From the general trend of parameters, I cautiously consider that the value for the open-circuit voltage in NP:NS = 3:7 is out of the tendency. I consider about different nanomorphologies of porous spheres synthesized from the limited number of samples. Open-circuit voltage is represented as [31]:

$$V_{OC} \approx \frac{nkT}{e} \cdot \frac{J_{SC}}{J_0}, \quad (1)$$

from the general one-diode model [31], and between two conditions of the NP:NS = 5:5 and 3:7, the difference in J_{sc} (i.e., ln J_{sc}) is not enough to impact on V_{oc}. Also, the change of V_{oc} may result from the difference of reverse saturation current J_0. I have synthesized nanoporous ZnO spheres by hydrothermal method [16], and the nanostructural quality of porous ZnO spheres may vary from batch-to-batch, thus resulting in the difference of band offset, charge-transfer mobilities, porosities, and etc. [32,33].

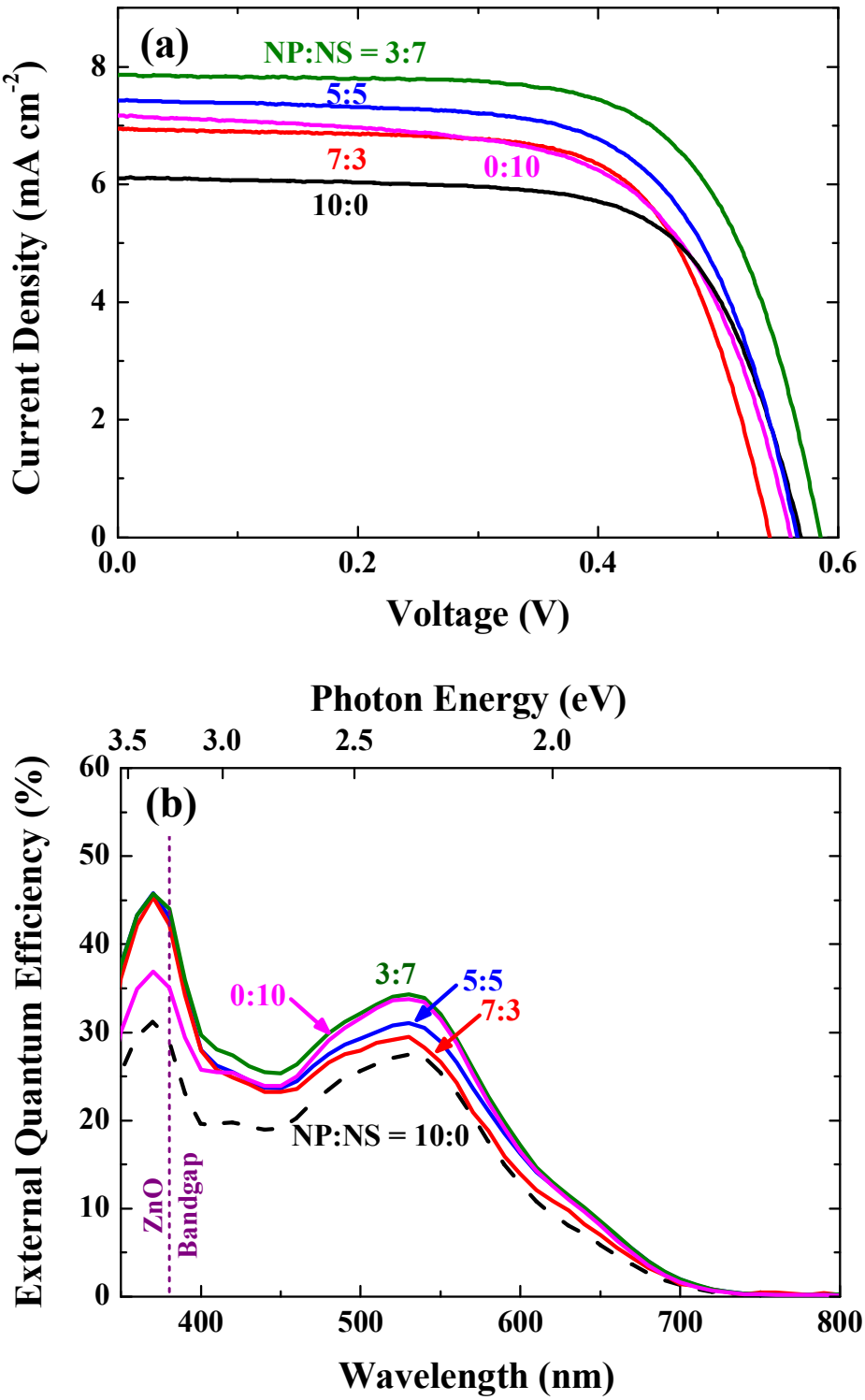

Fig. 3-4. (Color) (a) Photocurrent-voltage curves of the DSSCs with various mixing ratios. (b) Incident photon-to-current conversion efficiency (IPCE) spectra.

Table 3-1. (Color) Characteristics of photocurrent-voltage curves and charge-transfer resistances (R_{ct}) for ZnO/electrolyte interfaces, with various mixing ratios of nanoparticles (NP) and nanoporous spheres (NS) for the bilayer electrodes in the DSSCs.

NP:NS	J_{sc} (mA cm^{-2})	V_{oc} (V)	*FF*	η (%)	R_{ct} (Ω)
10:0	**5.98 ± 0.25**	**0.56 ± 0.01**	**0.67 ± 0.01**	**2.25 ± 0.15**	**30.7 ± 0.3**
7:3	**6.64 ± 0.30**	**0.55 ± 0.01**	**0.65 ± 0.02**	**2.36 ± 0.17**	**33.1 ± 0.2**
5:5	**7.45 ± 0.13**	**0.56 ± 0.01**	**0.68 ± 0.03**	**2.81 ± 0.14**	**29.8 ± 0.2**
3:7	**7.47 ± 0.24**	**0.58 ± 0.01**	**0.67 ± 0.01**	**2.91 ± 0.13**	**31.6 ± 0.2**
0:10	**7.28 ± 0.18**	**0.56 ± 0.01**	**0.64 ± 0.02**	**2.60 ± 0.09**	**34.5 ± 0.3**

In order to characterize the light-harvesting effects of cells with various mixing ratios, I carried out IPCE measurements, shown in Fig. 3-4(b). If charge-collection probabilities are similar among the cells, quantum efficiency depends on the light trapping inside the solar cell [34-37]. The different values among the cells in the long wavelength range of 600 - 800 nm is not significant, especially when the cells establish a certain degree of the scattering effect as nanoporous spheres added. Nevertheless, the NP:NS = 3:7 cell exhibits the highest IPCE values and this IPCE trend is consistent with the extinction data (Fig. 3-3(b)). Therefore, the enhanced light-harvesting capability (i.e., J_{sc}) by the mixed scattering layer is attributed to efficient light scattering and increased surface area.

Impedance analyses were performed to understand the electrical properties of the synthesized solar cells [38-41]. Nyquist plots display two semicircles in Fig. 3-5(a), and the larger semicircles in low frequency range ($\sim 10^0$ - $\sim 10^3$ Hz) are related to the charge transport/accumulation at dye-attached ZnO/electrolyte interfaces, and the smaller semicircles in high frequency ($\sim 10^3$ - $\sim 10^5$ Hz) are ascribed to the charge transfer at the interfaces of electrolyte/Pt-counter electrode [42]. The impedance parameters were extracted using the equivalent-circuit model (inset of Fig. 3-5(a)), and the fitting lines are shown as solid lines in the Nyquist and Bode plots. From the charge-transfer resistances (R_{ct}) in Table 3-1, I can see that the proper mixing ratio (e.g., 5:5 or 3:7) exhibits lower values implying more efficient charge-transfer processes across the ZnO/electrolyte interfaces, while the pure nanoporous sphere layer (0:10) shows the highest R_{ct}. The low resistance favors the transport of the electrons injected within ZnO, thus eventually leading to an effective collection of electrons [11]. The better connectivity achieved by the nanoparticles likely facilitate charge transfer by providing electron-transport pathways, thereby resulting in the enhancement of *FF* with less recombination.

Schematic representations illustrate the effect of the mixed scattering layer (Fig. 3-6). This mixed scattering layer of nanoparticles and nanoporous spheres offers the effective scattering ability, and also provides the direct charge transport pathway not by the point contact among big-sized nanoporous spheres.

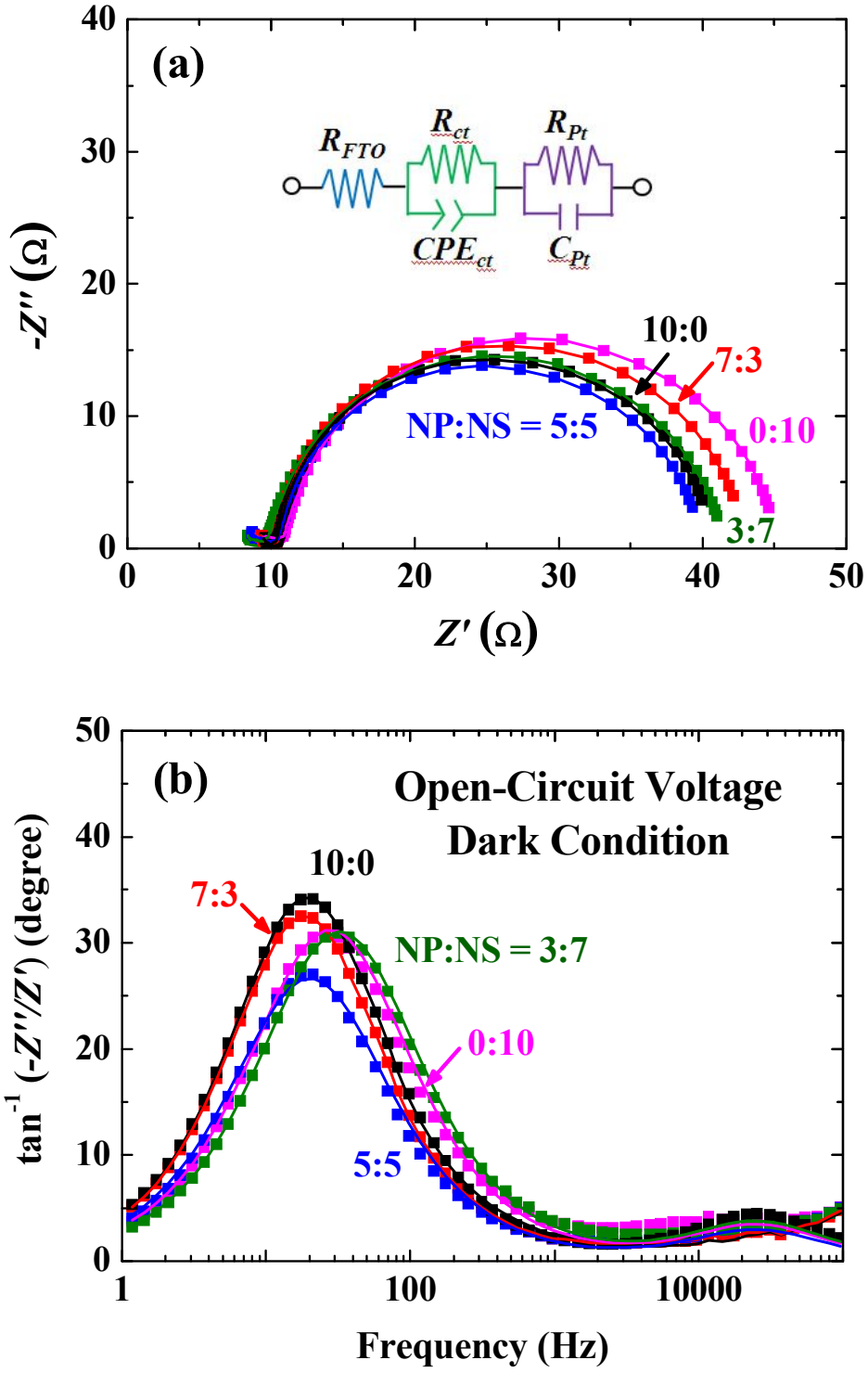

Fig. 3-5. (Color) (a) Nyquist and (b) Bode plots with various mixing ratios of ZnO nanoparticle to nanoporous sphere. Solid lines are the fitting results using the equivalent-circuit model in the inset.

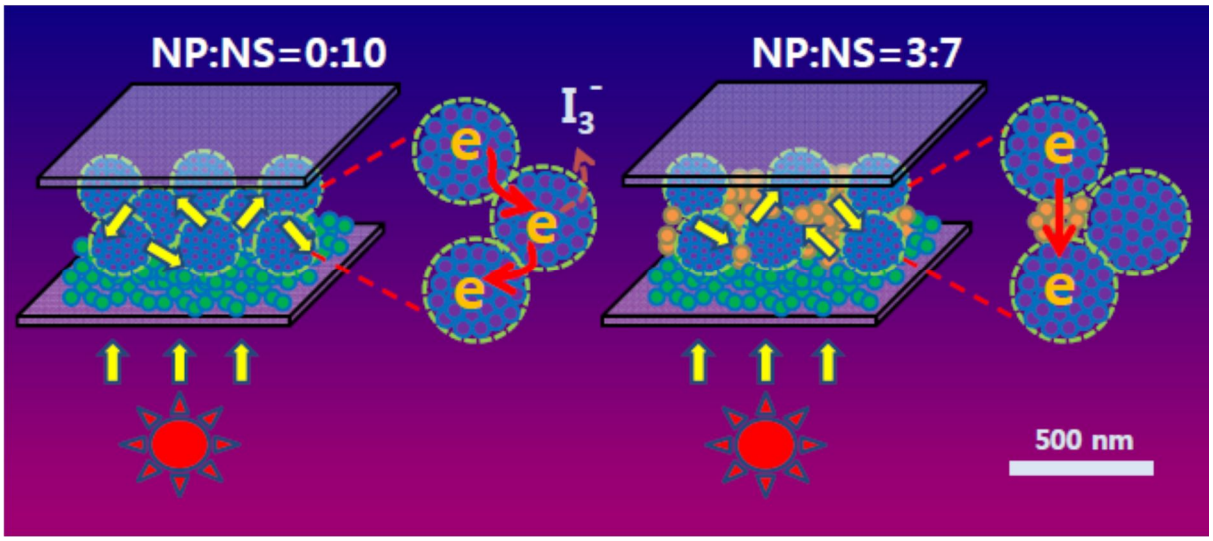

Fig. 3-6. (Color) Schematic figures for the effect of mixed scattering layer with nanoparticle and nanoporous sphere on the performance of ZnO-based dye-sensitized solar cells.

3.4. Conclusion

The efficient use of sun light is the other important issue with interface recombination in metal oxide of DSSCs. The incident light can be used effectively as increase the light-path length passed through the metal oxide film by scattering effect. Efficient scattering effects of various hierarchical nanostructures have been confirmed by many studies [16-18,43-45]. Among the various hierarchical scatterers, nanoporous ZnO spheres with tens-of nanometer particles are employed both in chapter 2 and 3 experiments. Because of very efficient scattering effect of nanoporous ZnO sphere, they would rather reflect the incident light before dye absorbs when ZnO spheres are near the glass where the light is incident. Therefore, proper position of scatters should be designed for using its scattering effect efficiently. This experiment is carried out with the film thickness (~5.5 μm) less than half of film thickness (~12 μm) in chapter 2 due to entirely focus on scattering effect and the promising perspective of DSSCs is that obtains high efficiency in thin metal oxide with sufficient light absorption. Because when film gets thicker than electron diffusion length, recombination exceeds the increased electrons from increased surface area and absorption is not increased proportionally to film thickness, therefore, thicker film drops the voltage eventually with decreased average electron density of the film [46,47]. Since thin film cannot absorb the light sufficiently from the low amount of dye loading, it is very important to use the light efficiently with scattering effect in enough thin metal oxide film to allow transport all the generated electrons to electrode. For these reason, the bottom layer consists of only nanoparticle to supply the large surface area and minimize the light loss and the upper layer composed of nanoporous spheres acts as a scattering layer are designed in thin film of ~5.5 μm. Especially in this study, I plan to optimize the scattering layer. The scatterers should have large size of several hundreds for efficient scattering of visible wavelength; thus, large voids exist between scatterers and electrons transport through the point contact among scatterers. Therefore, the upper layer is made up of the various ratios of mixture of nanoparticle and nanoporous sphere and nanoparticles in the mixture offer the additional surface area by filling the large voids among hundreds-sized nanoporous spheres and facilitate the carrier transport through providing short electron-path length.

Differences in scattering effects among samples are very distinct and easily distinguished with the naked eye from changes of film colors, which are getting whiter. Although the highest efficiency is obtained in NP:NS=3:7, it was found that impact of scattering on the efficiency is great from higher efficiency of film composed of only nanoporous spheres (NP:NS=0:10) than that of only nanoparticle (NP:NS=10:0).

When I plan this experiment, I expected not only the better transport from offering short electron path through adding nanoparticles, but also increasing the surface area. I try to analyze the transport property by impedance, however in measurement frequency region, the recombination at metal oxide/electrolyte interfaces and charge transport through material oxide are mixed. I think more-sophisticated analysis such as transient absorption spectroscopy is needed to investigate effects of added nanoparticles on the electron transport [48,49]. Although added nanoparticles would facilitate the electron transport, electrons should cross the grain boundary of added nanoparticles, not only the nanoporous one. I consider that would be interesting to investigate the transport property with various sized of nanoparticles, especially bigger size one, finding the optimization between surface area and transport property.

This experiment indicates enhanced efficiency through mixed scattering layer of nanoparticles and nanoporous spheres and efficient scattering effect, increased surface area, and better transport have an effect on efficiency enhancement. If the impact of these improvement factors can be quantified through an additional analysis of BET for comparison of surface area and transient absorption spectroscopy for transport property, it is considered to present the standard for more advanced studies in scattering research filed.

3.5. References

1. B. O'Regan, and M. Grätzel, "A Low-Cost, High-Efficiency Solar Cell Based on Dye-Sensitized Colloidal TiO_2 Films," *Nature* **353**, 737 (1991).
2. M. Grätzel, "Solar Eenergy Conversion by Dye-Sensitized Photovoltaic Cells," *Inorg. Chem.* **44**, 6841 (2005).
3. Z. S. Wang, H. Kawauchi, T. Kashima, and H. Arakawa, "Significant Influence of TiO_2 Photoelectrode Morphology on the Energy Conversion Efficiency of N719 Dye-Sensitized Solar Cell," *Coordin. Chem. Rev.* **248**, 13 (2004).
4. C. S. Chou, M. G. Guo, K. H. Liu, and Y. S. Chen, "Preparation of TiO_2 Particles and Their Applications in the Light Scattering Layer of a Dye-Sensitized Solar Cell," *Appl. Energ.* **92**, 224 (2012).
5. X. Sun, Y. Liu, Q. Tai, B. Chen, T. Peng, N. Huang, S. Xu, T. Peng, and X. Z. Zhao, "High Effciency Dye-Sensitized Solar Cells based on a Bi-Layered Photoanode Made of TiO_2 Nanocrystallites and Microspheres with High Thermal Stability," *J. Phys. Chem. C* **116**, 11859 (2012).
6. C. R. Ke, L. C. Chen, and J. M. Ting, "Photoanodes consisting of Mesoporous Anatase TiO_2 Beads with Various Sizes for High-Efficiency Flexible Dye-Sensitized Solar Cells," *J. Phys. Chem. C* **116**, 2600 (2012).
7. D. Sadgostar, F. Tajabadi, and N. Taghavinia, "Mesoporous Submicrometer TiO_2 Hollow Spheres as Scatterers in Dye-Sensitized Solar Cells," *ACS Appl. Mater. Interfaces* **4**, 2964 (2012).
8. S. Jong, H. B. Yang, X. Wang, S. Y. Khoo, C. C. Wong, X. W. Liu, and C. M. Li, "Improved Utilization of Photogenerated Charge Using Fluorine-Doped TiO_2 Hollow Spheres Scattering Layer in Dye-Sensitized Solar Cells," *ACS Appl. Mater. Interfaces* **4**, 3712 (2012).
9. K. S. Hang, J. Y. Kim, H. S. Kim, H. D. Koh, J. S. Lee, and Y. E. Sung, "Influence of Light Scattering Particles in the TiO_2 Photoelectrode for Solid-State Dye-Sensitized Solar Cell," *J. Photoch. Photobio. A* **200**, 294 (2008).

10. H. J. Koo, J. Park, B. Yoo, K. Yoo, K. Kim, and N. G. Park, "Size-Dependent Scattering Efficiency in Dye-Sensitized Solar Cell," *Inorg. Chem.* **361**, 677 (2008).
11. Y. Z. Zheng, X. Tao, L. X. Wang, H. Xu, Q. Hou, W. L. Zhou, and J. F. Chen, "Novel ZnO-Based Film with Double Light-Scattering Layers as Photoelectrodes for Enhanced Efficiency in Dye-Sensitized Solar Cells," *Chem. Mater.* **22**, 928 (2010).
12. S. He, S. Zhang, J. Lu, Y. Zhao, J. Ma, M. Wei, D. G. Evans, and X. Duan, "Enhancement of Visible Light Photocatalysis by Grafting ZnO Nanoplatelets with Exposed (0001) Facets onto a Hierarchical Substrate," *Chem.Commun.* **47**, 10797 (2011).
13. J. Zhang, W. Que, Q. Jia, P. Zhong, Y. Liao, X. Ye, and Y. Ding, "Novel Bilayer Structure ZnO Based Photoanode for Enhancing Conversion Efficiency in Dye-Sensitized Solar Cells," *J. Alloy. Compd.* **509**, 742 (2011).
14. E. M. Kaidashev, M. Lorenz, H. Wenckstern, A. Rahm, H. C. Semmelhack, K. H. Han, G. Benndorf, C. Bundesmann, H. Hochmuth, and M. Grundmann, "High Electron Mobility of Epitaxial ZnO Thin Films on C-Plane Sapphire Grown by Multistep Pulsed-Laser Deposition," *Appl. Phys. Lett.* **82**, 3901 (2003).
15. K. Keis, L. Vayssieres, H. Rensmo, S. E. Lindquist, and A. Hagfeldt, "Photoelectrochemical Properties of Nano- to Microstructured ZnO Electrodes," *J. Electrochem. Soc.* **148**, A149 (2001).
16. Q. Zhang, T. P. Chou, B. Russo, S. A. Jenekhe, and G. Cao, "Aggregation of ZnO Nanocrystallites for High Conversion Efficiency in Dye-Sensitized Solar Cells," *Angew. Chem. Int. Ed.* **47**, 2402 (2008).
17. Y. C. Park, Y. J. Chang, B. G. Kum, E. H. Kong, J. Y. Son, Y. S. Kwon, T. Park, and H. M. Jang, "Size-Tunable Mesoporous Spherical TiO_2 as a Scattering Overlayer in High-Performance Dye-Sensitized Solar Cells," *J. Mater. Chem.* **21**, 9582 (2011).
18. I. G. Yu, Y. J. Kim, H. J. Kim, C. Lee, and W. I. Lee, "Size-Dependent Light-Scattering Effects of Nanoporous TiO_2 Spheres in Dye-Sensitized Solar Cells," *J. Mater. Chem.* **21**, 532 (2011).
19. C. Nahm, H. Choi, J. Kim, S. Byun, S. Kang, T. Hwang, H. H. Park, J. Ko, and B. Park, "A Simple Template-Free 'Sputtering Deposition and Selective Etching' Process for Nanoporous

Thin Films and Its Application to Dye-Sensitized Solar Cells," *Nanotechnology* **24**, 365604 (2013).

20. J. Kim, H. Choi, C. Nahm, J. Moon, C. Kim, S. Nam, D. R. Jung, and B. Park, "The Effect of a Blocking Layer on the Photovoltaic Performance in CdS Quantum-Dot-Sensitized Solar Cells," *J. Power Sources* **196**, 10526 (2011).
21. H. Choi, C. Nahm, J. Kim, J. Moon, S. Nam, C. Kim, D. R. Jung, and B. Park, "The Effect of $TiCl_4$-Treated TiO_2 Compact Layer on the Performance of Dye-Sensitized Solar Cell," *Curr. Appl. Phys.* **12**, 737 (2012).
22. C. Suryanarayana, and M. G. Norton, "X-ray Diffraction: A Practical Approach," New York (1998).
23. J. Kang, S. Nam, Y. Oh, H. Choi, S. Wi, B. Lee, T. Hwang, S. Hong, and B. Park, " Electronic Effect in Methanol Dehydrogenation on Pt Surfaces: Potential Control During Methanol Electrooxidation," *J. Phys. Chem. Lett.* **4**, 2931 (2013).
24. Y. Oh, S. Nam, S. Wi, S. Hong, and B. Park, "Review Paper: Nanoscale Interface Control for High-Performance Li-Ion Batteries," *Electron. Mater. Lett.* **8**, 91 (2012).
25. C. Nahm, H. Choi, J. Kim, D. R .Jung, C. Kim, J. Moon, B. Lee, and B. Park, ".The Effects of 100 nm-Diameter Au Nanoparticles on Dye-Sensitized Solar Cells," *Appl. Phys. Lett.* **99**, 253107 (2011).
26. J. Kim, H. Choi, C. Nahm, and B. Park, "Review Paper: Surface Plasmon Resonance for Photoluminescence and Solar-Cell Applications," *Electron. Mater. Lett.* **8**, 351 (2012).
27. J. Ferber, and J. Luther, "Computer Simulations of Light Scattering and Absorption in Dye-Sensitized Solar Cells," *Sol. Energ. Mat. Sol. C.* **54**, 265 (1998).
28. S. Ito, S. M. Zakeerudiin, R. Humphry-Baker, P. Liska, P. Charvet, P. Comte, M. K. Nazeeruddin, P. Péchy, M. Takata, H. Miura, S. Uchida, and M. Grätzel, " High-Efficiency Organic-Dye-Sensitized Solar Cells Controlled by Nanocrystalline-TiO_2 Electrode Thickness," *Adv. Mater.* **18**, 1202 (2006).
29. J. D. J. Ingle, and S. R. Crouch, "Spectrochemical Analysis," New Jersey (1988).

30. F. E. Gálvez, E. Kemppainen, H. Míguez, and J. Halme, "Effect of Diffuse Light Scattering Designs on the Efficiency of Dye Solar Cells: an Integral Optical and Electrical Description," *J. Phys. Chem. C* **116**, 11426 (2012).

31. J. H. Lee, S. Cho, A. Roy, H. T. Jung, and A. J. Heeger, "Enhanced Diode Characteristics of Organic Solar Cells Using Titanium Suboxide Electron Transport Layer," *Appl. Phys. Lett.* **96**, 163303 (2010).

32. B. C. O'reagan, and J. R. Durrant: Kinetic and Energetic Paradigms for Dye-Sensitized Solar Cells, "Moving from the Ideal to the Real," *Acc. Chem. Res.* **42**, 1799 (2009).

33. D. W. Park, Y. Jeong, J. Lee, J. Lee, and S. H. Moon, "Interfacial Charge-Transfer Loss in Dye-Sensitized Solar Cells," *J. Phys. Chem. C* **117**, 2734 (2013).

34. C. Kim, J. Kim, H. Choi, C. Nahm, S. Kang, S. Lee, B. Lee, and B. Park, " The Effect of TiO_2-Coating Layer on the Performance in Nanoporous ZnO-Based Dye-Sensitized Solar Cells," *J. Power Sources* **232**, 159 (2013).

35. H. Choi, J. Kim, C. Nahm, C. Kim, S. Nam, J. Kang, B. Lee, T. Hwang, S. Kang, D. J. Choi, Y. H. Kim, and B. Park, "The role of ZnO-Coating-Layer Thickness on the Recombination in CdS Quantum-Dot-Sensitized Solar Cells," *Nano Energy* **2**, 1218 (2013).

36. J. Kim, H. Choi, C. Nahm, C. Kim, J. I. Kim, W. Lee, S. Kang, B. Lee, T. Hwang, H. H. Park, and B. Park, "Graded Bandgap Structure for PbS/CdS/ZnS Quantum-Dot-Sensitized Solar Cells with a PbxCd1-xS interlayer," *Appl. Phys. Lett.* **102**, 183901 (2013).

37. Y. Chen, F. Huang, D. Chen, L. Cao, X. L. Zhang, R. A. Caruso, and Y. B. Cheng, "Effect of Mesoporous TiO_2 Bead Diameter in Working Electrodes on the Efficiency of Dye-Sensitized Solar Cells," *ChemSusChem* **4**, 1498 (2011).

38. J. Kim, H. Choi, C. Nahm, C. Kim, S. Nam, S. Kang, J. D. R. ung, J. I. Kim, J. Kang, and B. Park, "The Role of a $TiCl_4$ Treatment on the Performance of CdS Quantum-Dot-Sensitized Solar Cells," *J. Power Sources* **220**, 108 (2012).

39. H. Choi, C. Nahm, J. Kim, C. Kim, S. Kang, T. Hwang, and B. Park, "Review Paper: Toward Highly Efficient Quantum-Dot- and Dye- Sensitized Solar Cells," *Curr. Appl. Phys.* **13**, S2 (2013).

40. M. S. Goes, E. Joanni , E. C. Muniz, R. Savu, T. R. Habeck, P. R. Bueno, and F. Fabregat-Santiago, "Impedance Spectroscopy Analysis of the Effect of TiO_2 Blocking Layers on the Efficiency of Dye Sensitized Solar Cells," *J. Phys. Chem. C* **116**, 12415 (2012).

41. F. Fabregat-Santiago, J. B. Garcia-Belmonte, G. Boschloo, and A. Hagfeldt, "Influence of Electrolyte in Transport and Recombination in Dye-sensitized Solar Cells Studied by Impedance Spectroscopy," *Sol. Energ. Mat. Sol. C.* **87**, 117 (2005).

42. F. Fabregat-Santiago, J. Bisquert, E. Palomares, L. Otero, D. Kuang, S. M. Zakeeruddin, and M. Grätzel, "Correlation Between Photovoltaic Performance and Impedance Spectroscopy of Dye-Sensitized Solar Cells Based on Ionic Liquids," *J. Phys. Chem. C* **111**, 6550 (2007).

43. C. Y. Jiang, X. W. Sun, G. Q. Lo, D. L. Kwong, and J. X. Wang, "Improved Dye-Sensitized Solar Cells with a ZnO-Nanoflower Photoanode," *Appl. Phys. Lett*. **90**, 263501 (2007).

44. W. Yang, J. Li, Y. Wang, F. Zhu, W. Shi, F. Wan, and D. Xu, "A Facile Synthesis of Anatase TiO_2 Nanosheets-Based Hierarchical Spheres with Over 90% {001} Facets for Dye-Sensitized Solar Cells," *Chem. Commun*. **47**, 1809 (2011).

45. H.-J. Koo, Y. J. Kim, Y. H. Lee, W. I. Lee, K. Kim, and N.-G. Park, "Nano-Embossed Hollow Spherical TiO_2 as Bifunctional Material for High-Efficiency Dye-Sensitized Solar Cells," *Adv. Mater*. **20**, 195 (2008).

46. A. Mathewa, G. M. Raoa, and N. Munichandraiah, "Effect of TiO_2 Electrode Thickness on Photovoltaic Properties of Dye Sensitized Solar Cell Based on Randomly Oriented Titania Nanotubes," *Mater. Chem. Phys.* **127**, 95 (2011).

47. M. G. Kang, K. S. Ryu, S. H. Chang, N. G. Park, J. S. Hong, and K.-J. Kim "Dependence of TiO_2 Film Thickness on Photocurrent-Voltage Characteristics of Dye-Sensitized Solar Cells," *Bull. Korean Chem. Soc.* **25**, 742 (2004).

48. A. N. M. Green, E. Palomares,S. A. Haque, J. M. Kroon, and J. R. Durrant, "Charge Transport versus Recombination in Dye-Sensitized Solar Cells Employing Nanocrystalline TiO_2 and SnO_2 Films," *J. Phys. Chem. B* **109**, 12525-12533 (2005).

49. B. C. O'Regan and F. Lenzmann, "Charge Transport and Recombination in a Nanoscale Interpenetrating Network of n-Type and p-Type Semiconductors: Transient Photocurrent and Photovoltage Studies of TiO_2/Dye/CuSCN Photovoltaic Cells," *J. Phys. Chem. B* **108**, 4342-4350 (2004).

Chapter 4. Concluding Remarks

4.1. Concluding Remarks

The effect of TiO_2-coating on the ZnO-based DSSCs performance is systematically investigated with various TiO_2-coating thicknesses (topic 1). The TiO_2 layer plays an important role in the suppression of the formation of Zn^{2+}/dye complexes and the recombination at ZnO/dye/electrolyte interfaces. As a result, the power-conversion efficiency is enhanced by approximately three times. In addition, nanoparticles and nanoporous spheres are mixed with various ratios to improve the utilization of scattering layer in ZnO-based DSSCs (topic 2). Nanoporous spheres play an important role in the scattering effect with the large surface area, but possess disadvantages of large voids and point contacts between spheres. Nanoparticles advance facile carrier transport with the additional surface area, thereby improving the solar cell efficiency by the enhanced short-circuit current (J_{sc}) and fill factor (*FF*). These results imply that not only interface control but also nanostructure optimization are greatly important in metal oxides of DSSCs.

Besides emphasizing the importance of interface control and efficient use of light theoretically, it is experimentally demonstrated. Nevertheless, smaller film thickness of topic 2 (~5.5 μm) than topic 1 film thickness (~12 μm), higher current in topic 2 (7.47 mA/cm^2) than in topic 1 (6.77 mA/cm^2) is obtained, which indicates the increase in surface area by adding nanoparticles to the scattering layer. The increased surface area leads to more recombination; therefore, the average value of V_{oc} in topic 2 (0.56 V) is much lower than that of the topic 1 (0.62 V). Considering the reported diffusion length of nanostructured ZnO film of ~8 μm, the increase in film thickness (≥ ~5.5 μm) is proper direction for efficiency improvement [1]. Although more occurrences of the recombination from increased film thickness can be an issue of concern, the recombination can be effectively reduced by interface control using TiO_2 that is already proven its superior impact in topic 1. Therefore, the collaboration of topic 1 and topic 2 is considered to be better and expected results will be discussed in next chapter in details.

4.2. Future aspects

I consider synergy effects of surface coating and scattering effect based on the factors affecting the efficiency. Due to the limited information in this study, I try to predict theoretically as close approximation as possible to approach quantitatively with precise values. The energy conversion efficiency (η) is determined by the short-circuit current (J_{sc}), open-circuit voltage (V_{oc}), fill factor of the cell (FF), and intensity of the incident light (P_{in}) as given by [2]:

$$\eta = \frac{J_{sc}\, V_{oc}\, FF}{P_{in}}\,. \tag{1}$$

V_{oc} means the potential when the flux of recombining charges becomes equal to that of charge generation and defined as below [3]:

$$V_{oc} = \frac{nkT}{q_e} ln\left(\frac{J_{ph}}{J_0}\right) \tag{2}$$

where n is diode ideality factor, J_{ph} is photo-generated current, and J_0 is saturation current which is typically expressed as [3]:

$$J_0 = n_{e0}\, k_{rec}\, N_A \tag{3}$$

where n_{eo} is the electrons density available for recombination when the device is in the dark, k_{rec} is the recombination rate, N_A is the density of empty redox states available for recombination. From these relations, the main determinants of V_{oc} are regard as photo-generated current (J_{ph}) and recombination rate (k_{rec}). The optimized nanostructured film used in future work is bilayer with scattering layer in topic 2. This scattering layer is composed of mixture of nanoparticles and nanoporous spheres to increase the surface area and facile electron transport. The nanostructured film is coated with TiO_2 to reduce interface recombination between ZnO/electrolyte, and to improve the acidic stability of electrode. The thickness of metal oxide is decided comparable to diffusion length that is thicker than that of topic 2 (~ 5.5 μm), as consider the reported diffusion length of nanostructured ZnO film [1]. Therefore, optimized nanostructured film has larger surface area than those of topic 1 and topic 2. Increased surface area by the addition of nanoparticles in scattering layer and increased film thickness allow to absorb more dyes that increase photo-generated current (J_{ph}). Thus, the higher V_{oc} value than that of topic 2 (~0.56 V) is expected from increased photo-generated current (J_{ph}). Additional

TiO_2-coating layer reduces the recombination rate (k_{rec}) of ZnO and also contributes to increase V_{oc} value. Since the collaboration of topic 1 and topic 2 has the larger surface area than that of topic 1, it leads to more interface recombination. Therefore, V_{oc} of the collaboration of topic 1 and topic 2 is expected to be similar or smaller than that of the topic 1 (~0.62 V) [4,5].

J_{sc} is difference between photo-generated current and lost from recombination and is expressed as below when a cell is under the illumination with the incident photon flux of $I_{photon}(\lambda)$ [3]:

$$J_{sc} = q_e \int_{\lambda_{min}}^{\lambda_{max}} J_{photon}(\lambda)\, \eta_{LHE}\, \eta_{inj}\, \eta_{cc}\, d\lambda \tag{4}$$

where q_e is the electron charge, η_{LHE} is the light harvesting efficiency, η_{inj} is electron injection yield from N719 dye into metal oxide, and η_{cc} is charge collection efficiency at the electrode. The light harvesting efficiency (η_{LHE}) can be enhanced by using absorbers having higher molar absorption coefficient, more amount of dye loading, or increased optical path length with scattering effect. In the optimized nanostructure, the light harvesting efficiency (η_{LHE}) is enhanced by efficient scattering effect of bilayer structure and increased amount of dye loading caused by additional surface area from nanoparticles in mixture and increased film thickness. The electron injection efficiency (η_{inj}) from N719 dye to TiO_2 is reported to be almost 1 [6]. Therefore, TiO_2 coating is considered to enhance the electron injection efficiency (η_{inj}) because faster kinetic property of electron injection from dye to TiO_2 than dye to ZnO [7,8]. The charge collection efficiency (η_{cc}) is related with the mobility and the recombination rate in metal oxide [3]. Not only the reduced recombination by TiO_2 layer, but also shorten electron path-length by added nanoparticles help more charges to reach electrode before recombination, resulting increase of charge collection efficiency (η_{cc}) [9]. All improved points of optimized nanostructure are beneficial to improve J_{sc}, thus most enhanced improvement is expected for J_{sc} value than that of V_{oc} or *FF*.

The fill factor is also important parameter that determines the efficiency, and defined as the ratio of the maximum power from the solar cell to the product of V_{oc} and I_{sc} [2],

$$FF = \frac{V_{max}\, J_{max}}{V_{oc}\, J_{sc}}. \tag{5}$$

As a high *FF* means there is little resistance inside the solar cell itself, in order to get higher *FF,* series resistance (R_s) should be decreased and shunt resistance (R_{sh}) should be increased [2]. The series resistance is composed of resistance attributed to the redox reaction at Pt counter electrode, ion transport within electrolyte, and contact resistance between TCO and metal oxide. The shunt resistance is related to the recombination resistance at metal oxide/dye/electrolyte interfaces. As film thickness is thicker than topic 2 (~5.5 μm) and less porous nanostructured film by TiO_2 coating, the diffusion of ions within electrolyte becomes more difficult [10]. It increases the ion transport resistance so decreased *FF* value than topic 2 (~67%) is expected. On the other hand, shunt resistance will be increased by surface coating with TiO_2 and film thickness is smaller than topic 1 (~12 μm), it will help the *FF* not to be smaller than that of topic 1 (~60%) [11]. Therefore, *FF* value is expected to be increased than topic 1 (~60%) but decreased than topic 2 (~67%). The expected synergy effects are illustrated in Fig. 4-1.

As mentioned above, the collaboration of two factors (topic 1 + topic 2) is expected to have a more improved J_{sc} value than those of topic 1 and 2, when surface treatment with TiO_2 is applied to optimized bilayer structure. Although V_{oc} and *FF* values are found to be in between values obtained from topic 1 and 2, the synergy effects are considered in the film consisting thickness comparable to diffusion length [1]; therefore, the respective film thickness of bottom and upper layer and coating time of TiO_2 should be optimized in newly constructed thick bilayer structure.

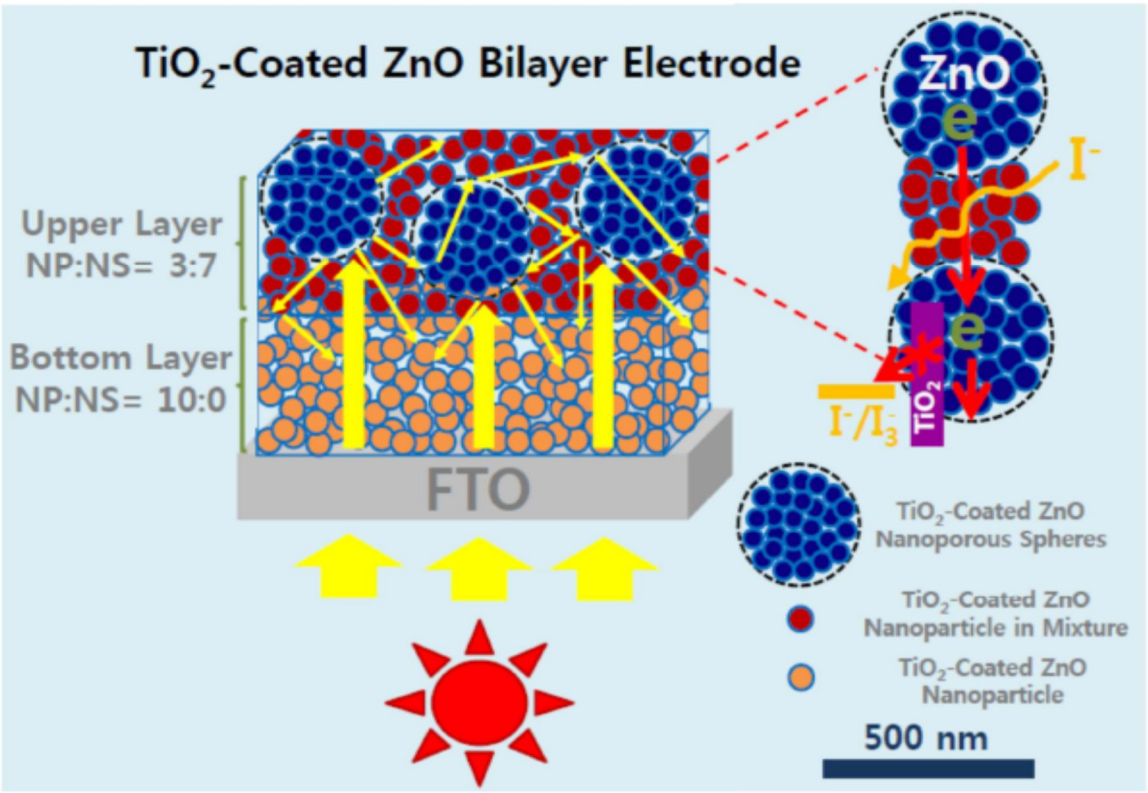

Fig. 4-1. (Color) Schematic figure for the synergy effects of optimized bilayer ZnO electrode coated with TiO_2 in dye-sensitized solar cells.

4.3. References

1. F. Xu, J. Chen, X. Wu, Y. Zhang, Y. Wang, J. Sun, H. Bi, W. Lei, Y. Ni, and L. Sun, "Graphene Scaffolds Enhanced Photogenerated Electron Transport in ZnO Photoanodes for High-Efficiency Dye-Sensitized Solar Cells," *J. Phys. Chem. C* **117**, 8619 (2013).
2. J. Nelson, "The Physic of Solar Cells," Imperial College, UK (2003).
3. S. Zhang, X. Yang, Y. Numata, and L. Han "Highly Efficient Dye-Sensitized Solar Cells: Progress and Future Challenges," *Energy Environ. Sci.* **6**, 1443 (2013)
4. K Zhu, N. Kopidakis, N. R. Neale, J. van de Lagemaat, and A. J. Frank, "Influence of Surface Area on Charge Transport and Recombination in Dye-Sensitized TiO_2 Solar Cells," *J. Phys. Chem. B*, **110**, 25174 (2006).
5. A. Mathewa, G. M. Raoa, and N. Munichandraiah, "Effect of TiO_2 Electrode Thickness on Photovoltaic Properties of Dye Sensitized Solar Cell Based on Randomly Oriented Titania Nanotubes," *Mater. Chem. Phys.* **127**, 95 (2011).
6. S. E. Koops, B. C. O'Regan, P. R. F. Barnes, and J. R. Durrant, "Parameters Influencing the Efficiency of Electron Injection in Dye-Sensitized Solar Cells," *J. Am. Chem. Soc.* **131**, 4808 (2009).
7. N. A. Anderson, X. Ai, and T. Lian, "Electron Injection Dynamics from Ru Polypyridyl Complexes to ZnO Nanocrystalline Thin Films," *J. Phys. Chem. B* **107**, 14414 (2003).
8. A. Hagfeldt, G. Boschloo, L. Sun, L. Kloo, and H. Pettersson, "Dye-Sensitized Solar Cells," *Chem. Rev.* **110**, 6595 (2010).
9. A. B. F. Martison, M. S Góes, F. Fabregat-Santiago, J. Bisquert, M. J. Pellin, and J. T. Hupp, "Evidence for Highly Efficient Charge Collection and Exceptionally Dynamics," *J. Phys. Chem. A* **113**, 4015 (2009).
10. G. Kron, U. Rau, M. Dürr, T. Miteva, G. Nelles, A. Yasuda, and J. H. Werner, "Diffusion Limitations to I_3^-/I^- Electrolyte Transport Through Nanoporous TiO_2 Networks," *Electrochem. Solid-State Lett.* **E11**, 6 (2003).
11. H. Sarmimala and K. Rainer, "Implication of Device Functioning Due to Back Reaction of Electrons via the Conducting Glass Substrate in Dye Sensitized Solar Cells," **87**, 263504 (2005).

국문 초록

염료 감응형 태양전지는, 1991년 스위스의 그레첼 교수님 그룹에 의해, 비교적 높은 효율인 7%의 효율을 보이며 처음 보고되었다. 염료감응형 태양전지는 저렴한 제조단가, 플렉시블 (flexible), 그리고 다양한 색상 구현 등으로 인해 차세대 태양전지의 유망한 후보자로 간주되었지만, 현재까지 효율이 10% 초반대에 머무르고 있다. 염료 감응형 태양전지의 효율을 향상시키기 위해서는, 메인 구성성분인 염료, 산화금속, 그리고 전해질 모두가 개선되어야 한다. 염료의 경우 가시광선 영역의 흡수를 증가시키기 위해, 감소된 밴드갭의 새로운 염료가 개발되어야 한다. 산화금속은 표면 개선을 통해 전해질과의 계면 사이에서 발생하는 재결합을 최소화하고 나노구조 제어를 통해 산란효과를 최적화하여야 한다. 마지막으로 전해질의 경우, 전해질의 산화환원 전위를 낮추어 전지의 전압 손실을 최소화하고 비휘발성 전해질의 개발을 통해 장시간 사용에 대한 안정성을 확보해야 한다.

1장에서는, 염료 감응형 태양전지의 주요 구성성분인 염료, 산화금속, 그리고 전해질의 최근 동향과 나아가야 할 방향에 대해 서술하였다. 특히 이 논문의 주요 목표인 산화금속의 표면 개선과 나노구조 제어의 중요성을 강조하기 위해, 산화 금속에 대한 부분은 더욱 자세하게 다뤄졌다.

2장에서는, 산화 티타늄에 의한 산화 아연의 표면개선이 염료 감응형 태양전지의 효율에 미치는 영향을 다양한 산화 티타늄 코팅시간에 따라 체계적으로 연구하였다. 산화티타늄 코팅층은 효율을 감소시키는 아연 이온/염료 복합체의 형성과 산화 아연 계면에서 발생하는 재결합을 효율적으로 감소시키며, 개방전압 (V_{oc})과 단락 전류 (J_{sc})를 모두 향상시켰다. 결과적으로, 1시간의 산화티타늄 코팅시간에서 가장 높은 효율을 보였으며, 이는 표면개선을 하지 않은 태양전지에 비해 약 3배 증가된 효율향상을 보여주었다.

3장에서는, 산란효과를 극대화 시키기 위한 나노구조 제어 연구가 수행되었다. 효과적인 산란효과 뿐 아니라 넓은 표면적을 가지는 나노다공성 산화아연 입자를 이용하여 산란층을 구성하였다. 하지만 수백나노미터 크기의 나노다공성 산란입자들 사이에는 빈 공간 (voids)이 존재하고 전자 또한 입자들 사이의 점접점 (point contact)에 의해 전달되게 된다. 이러한 단점들을 수십나노미터의 나노입자와의 다양한 혼합 비율을 통해 극복하고 산란층을 최적화하였다. 산란입자와 나노입자의 혼합을 통해 최적화된 산란층은 나노다공성 입자에 의한 산란효과와 첨가된 나노입자에 의해 증가된 표면적과 향상된 전자 전달특성으로 인해 단락 전류 (J_{sc})와 충전율 (FF)이 모두 향상되었다.

마지막 장인 4장에서는, 첫 번째 연구주제인 산화티타늄을 이용한 표면코팅과 두 번째 연구주제인 산란층의 구조제어의 시너지 효과에 대해 이론적으로 고찰되었다. 최적화된 산화아연 나노구조를 산화 티타늄을 이용하여 표면 코팅하였을 때, 증가된 광생성 전류 (J_{ph})와 감소된 재결합 비율 (k_{rec})에 의해 두번째 연구에서 얻어진 개방전압 (~0.56 V)보다 증가된 개방전압이 기대된다. 충전율 (FF)의 경우 향상된 전자전달 특성으로 인해 직렬저항 (series resistance)이 감소되어, 첫번째 연구주제에서 얻어진 충전율 (~60%)보다 증가될 것으로 기대된다. 단락 전류 (J_{sc})는 첫번째 연구 (6.77 mA/cm^2) 그리고 두번째 연구 (7.47 mA/cm^2) 보다 더욱 향상될 것으로 예상되며, 그 이유는 단락전류에 영향을 미치는 모든 인자들 (빛 흡수율 (η_{LHE}), 전자 주입율 (η_{inj}), 캐리어 집진율(η_{cc}))이 추가된 나노입자와 산화 티타늄 표면코팅에 의해 향상될 것이기 때문이다. 이러한 예측된 시너지 결과들을 고려해 보았을 때, 산화금속의 표면제어와 나노구조 제어는 고효율의 염료 감응형 태양전지를 위해서 반드시 필요하다.

주요어: 염료 감응형 태양전지, 산화 아연 전극, 표면 코팅, 나노 구조 제어, 산란 효과.

학번: 2012-30727

A.1. Publications (International)

1. **Chohui Kim**, Jongmin Kim, Hongsik Choi, Changwoo Nahm, Suji Kang, Sungjun Lee, Byungho Lee, and Byungwoo Park,* "TiO_2-Coating Layer on the Performance in Nanoporous ZnO-Based Dye-Sensitized Solar Cells," *J. Power Sources* **232**, 159 (2013).

2. **Chohui Kim**, Hongsik Choi, Jae Ik Kim, Sangheon Lee, Jinhyun Kim, Woojin Lee, Taehyun Hwang, Suji Kang, Taeho Moon, and Byungwoo Park,* "Improving Scattering Layer through Mixture of Nanoporous Spheres and Nanoparticles in ZnO-Based Dye-Sensitized Solar Cells," *Nanoscale Res. Lett.* **9**, 295 (2014).

3. Hongsik Choi, Jongmin Kim, Changwoo Nahm, **Chohui Kim**, Seunghoon Nam, Joonhyeon Kang, Byungho Lee, Taehyun Hwang, Suji Kang, Dong Joo Choi, Young-Ho Kim,* and Byungwoo Park,* "The Role of ZnO-Coating-Layer Thickness on the Recombination in CdS Quantum-Dot-Sensitized Solar Cells" *Nano Energy* **2**, 1218 (2013).

4. Jongmin Kim, Hongsik Choi, Changwoo Nahm, **Chohui Kim**, Jae Ik Kim, Woojin Lee, Suji Kang, Byungho Lee, Taehyun Hwang, Helen Hejin Park, and Byungwoo Park,* "Graded Bandgap Structure for PbS/CdS/ZnS Quantum-Dot-Sensitized Solar Cells with a $Pb_xCd_{1-x}S$ Interlayer," *Appl. Phys. Lett.* **102**, 183901 (2013).

5. Hongsik Choi, Changwoo Nahm, Jongmin Kim, **Chohui Kim**, Suji Kang, Taehyun Hwang, and Byungwoo Park,* "Review Paper: Toward Highly Efficient Quantum-Dot- and Dye-Sensitized Solar Cells," *Curr. Appl. Phys.* **13**, S2 (2013).

6. Jongmin Kim, Hongsik Choi, Changwoo Nahm, **Chohui Kim**, Seunghoon Nam, Suji Kang, Dae-Ryong Jung, Jae Ik Kim, Joonhyeon Kang, and Byungwoo Park,* "The Role of a $TiCl_4$ Treatment on the Performance of CdS Quantum-Dot-Sensitized Solar Cells," *J. Power Sources* **220**, 108 (2012).

7. Hongsik Choi, Changwoo Nahm, Jongmin Kim, Joonhee Moon, Seunghoon Nam, **Chohui Kim**, Dae-Ryong Jung, and Byungwoo Park,* "The Effect of $TiCl_4$-Treated TiO_2 Compact Layer on the Performance of Dye-Sensitized Solar Cell," *Curr. Appl. Phys.* **12**, 737 (2012).

8. Changwoo Nahm, Hongsik Choi, Jongmin Kim, Dae-Ryong Jung, **Chohui Kim**, Joonhee Moon, Byungjoo Lee, and Byungwoo Park,* "The Effects of 100 nm-Diameter Au Nanoparticles on Dye-Sensitized Solar Cells," *Appl. Phys. Lett.* **99**, 253107 (2011).

9. Jongmin Kim, Hongsik Choi, Changwoo Nahm, Joonhee Moon, **Chohui Kim**, Seunghoon Nam, Dae-Ryong Jung, and Byungwoo Park,* "The Effect of a Blocking Layer on the Photovoltaic Performance in CdS Quantum-Dot-Sensitized Solar Cells," *J. Power Sources* **196**, 10526 (2011).

10. Dae-Ryong Jung, Jongmin Kim, Seunghoon Nam, Changwoo Nahm, Hongsik Choi, Jae Ik Kim, Junhee Lee, **Chohui Kim**, and Byungwoo Park,* "Photoluminescence Enhancement in CdS Nanoparticles by Surface-Plasmon Resonance," *Appl. Phys. Lett.* **96**, 211908 (2010).

A.2. Presentations (International)

1. Byungwoo Park, Hongsik Choi, Jae Ik Kim, Seunghoon Nam, Woojin Lee, Sungun Wi, **Chohui Kim**, and Joonhyeon Kang, "Nanoscale Interface Control for Photoluminescence and Solar-Cell Applications," *The 9th Tsinghua University - University of Tokyo - Seoul National University Student Workshop*, Seoul, Korea, October 9-12, (2013).

2. Hongsik Choi, Jongmin Kim, Changwoo Nahm, **Chohui Kim**, Seunghoon Nam, and Byungwoo Park, "Improved Photovoltaic Performance of CdS Quantum-Dot-Sensitized Solar Cell through ZnO Coating," *Materials Research Society (MRS) Fall Meeting*, Boston, MA, November (2012).

3. Sungun Wi, Seunghoon Nam, Yuhong Oh, **Chohui Kim**, Saeromi Hong, and Byungwoo Park, "Graphene/Carbon Double-Coated ZnO Aggregates as High-Rate Electrode Material for Li-Ion Battery," *Materials Research Society (MRS) Fall Meeting*, Boston, MA, November (2012).

4. **Chohui Kim**, Jongmin Kim, Hongsik Choi, Changwoo Nahm, Suji Kang, Sungjun Lee, Byungho Lee, and Byungwoo Park, "Mixture of Nanoporous Spheres and Nanoparticles for High-Efficiency ZnO-Based Dye-Sensitized Solar Cells," *Global Photovoltaic Conference 2012 (GPVC2012)*, Busan, Korea, November 19-21, (2012). **[Oral by C. Kim]**

5. **Chohui Kim**, Jongmin Kim, Hongsik Choi, Changwoo Nahm, Suji Kang, Sungjun Lee, Byungho Lee, and Byungwoo Park, "The Effect of TiO_2-Coating Layer on the Performance in Nanoporous ZnO-Based Dye-Sensitized Solar Cells," *The 13th Korea - Japan Student Symposium (Seoul National University - Tohoku University),* Seoul, Korea, November 7-9, (2012). **[Oral by C. Kim]**

6. Sungun Wi, Seunghoon Nam, Yuhong Oh, **Chohui Kim**, Saeromi Hong, Suji Kang, and Byungwoo Park, "Graphene/Carbon Double-Coated ZnO Aggregates as High-Rate Electrode Material for Li-Ion Battery," *The 13th Korea - Japan Student Symposium (Seoul National University - Tohoku University),* Seoul, Korea, November 7-9, (2012).

7. Byungwoo Park, Jongmin Kim, Changwoo Nahm, Hongsik Choi, Seunghoon Nam, and **Chohui Kim**, "Semiconductor Nanoparticles with Surface Passivation and Surface Plasmon for Luminescence and Solar-Cell Applications," *Materials Science & Technology 2012 (MS&T'12),* Pittsburgh, PA, October (2012).

9. Byungwoo Park, Jongmin Kim, Changwoo Nahm, Hongsik Choi, Seunghoon Nam, and **Chohui Kim**, "Semiconductor Nanoparticles with Surface Passivation and Surface Plasmon for Luminescence and Solar-Cell Application," *International Conference on Electronic Materials and Nanotechnology for Green Environment (ENGE2012)*, Jeju, Korea, September (2012).

10. **Chohui Kim**, Jongmin Kim, Hongsik Choi, Changwoo Nahm, and Byungwoo Park, "Suppression of Charge Recombination in Photoelectrodes of TiO_2-Coated ZnO Aggregates Using Wet-Chemical Processing," *Materials Research Society (MRS) Fall Meeting*, Boston, MA, November (2011). **[Poster by C. Kim]**

11. Jongmin Kim, Hongsik Choi, Changwoo Nahm, Joonhee Moon, **Chohui Kim**, Seunghoon Nam, Dae-Ryong Jung, and Byungwoo Park, "The Effect of a Blocking Layer on the Photovoltaic Performance in CdS Quantum-Dot-Sensitized Solar Cells," *Materials Research Society (MRS) Fall Meeting*, Boston, MA, November (2011).

12. Dae-Ryong Jung, Jongmin Kim, Seunghoon Nam, Changwoo Nahm, Hongsik Choi, Jae Ik Kim, Junhee Lee, **Chohui Kim**, and Byungwoo Park, "Photoluminescence Enhancement in CdS Nanoparticles by Surface-Plasmon Resonance," *Materials Research Society (MRS) Fall Meeting*, Boston, MA, November (2011).

13. Changwoo Nahm, Hongsik Choi, Jongmin Kim, Dae-Ryong Jung, **Chohui Kim**, and Byungwoo Park, "The Effects of 100 nm-Diameter Au Nanoparticles on Dye-Sensitized Solar Cells," *Materials Research Society (MRS) Fall Meeting*, Boston, MA, November (2011).

14. Hongsik Choi, Changwoo Nahm, Jongmin Kim, Joonhee Moon, Seunghoon Nam, **Chohui Kim**, Dae-Ryong Jung, and Byungwoo Park, "The Effect of $TiCl_4$-Treated TiO_2 Compact Layer on the Performance of Dye-Sensitized Solar Cell," *Materials Research Society (MRS) Fall Meeting*, Boston, MA, November (2011).

15. **Chohui Kim**, Jongmin Kim, and Byungwoo Park, "Polydisperse Aggregates of ZnO Nanoparticles for Dye-Sensitized Solar Cells," *The 11th Korea - Japan Student Symposium (Seoul National University - Tohoku University)*, Seoul, Korea, November 8-10, (2010). **[Oral by C. Kim]**

A.3. Presentations (Domestic)

1. Byungwoo Park, Changwoo Nahm, Hongsik Choi, Jae Ik Kim, Seunghoon Nam, and **Chohui Kim**, "Surface Passivation and Surface Plasmon for Luminescence and Solar-Cell Applications," *춘계금속재료학회*, Jeju, Korea, April 25-26, (2013).

2. Byungwoo Park, Changwoo Nahm, Hongsik Choi, Jae Ik Kim, Seunghoon Nam, and **Chohui Kim**, "Surface Passivation and Surface Plasmon for Luminescence and Solar-Cell Applications" *춘계한국전기화학회*, Changwon, Korea, April 11-12, (2013).

3. **Chohui Kim**, Jongmin Kim, Hongsik Choi, Changwoo Nahm, and Byungwoo Park, "The Effect of TiO_2-Coating Layer on the Performance in Nanoporous ZnO-Based Dye-Sensitized Solar Cells," *태양전지 연구회 워크숍 2012*, Daejeon, Korea, February 28-29, (2012). **[Oral by C. Kim]**

4. Jongmin Kim, Hongsik Choi, Changwoo Nahm, Joonhee Moon, **Chohui Kim**, Seunghoon Nam, Dae-Ryong Jung, and Byungwoo Park, "The Effect of Surface Treatment on the Photovoltaic Performance in CdS Quantum-Dot-Sensitized Solar Cells" *태양전지 연구회 워크숍 2012*, Daejeon, Korea, February 28-29, (2012).

5. Changwoo Nahm, Hongsik Choi, Jongmin Kim, Dae-Ryong Jung, **Chohui Kim**, and Byungwoo Park, "The Effects of 100 nm-Diameter Au Nanoparticles on Dye-Sensitized Solar Cells," *태양전지 연구회 워크숍 2012*, Daejeon, Korea, February 28-29, (2012).

6. Hongsik Choi, Changwoo Nahm, Jongmin Kim, Joonhee Moon, Seunghoon Nam, **Chohui Kim**, Dae-Ryong Jung, and Byungwoo Park, "Interface Control for Highly Efficient Dye- and Quantum-Dot- Sensitized Solar Cells," *태양전지 연구회 워크숍 2012*, Daejeon, Korea, February 28-29 (2012).